FACULTY OF ENGINEERING AND ARCHITECTURE

# Air pollution by ships in close proximity to dense populated areas

Jordy Delvaeye
Student number: 01503307

Supervisors: Prof. dr. ir. Evert Lataire, Dr. ir. Manasés Tello Ruiz

Master's dissertation submitted in order to obtain the academic degree of
Master of Science in Electromechanical Engineering

Academic year 2019-2020

GHENT UNIVERSITY

FACULTY OF ENGINEERING AND ARCHITECTURE

# Air pollution by ships in close proximity to dense populated areas

Jordy Delvaeye
Student number: 01503307

Supervisors: Prof. dr. ir. Evert Lataire, Dr. ir. Manasés Tello Ruiz

Master's dissertation submitted in order to obtain the academic degree of
Master of Science in Electromechanical Engineering

Academic year 2019-2020

GHENT UNIVERSITY

# Permission To Use

The author gives permission to make this master dissertation available for consultation and to copy parts of this master dissertation for personal use. In all cases of other use, the copyright terms have to be respected, in particular with regard to the obligation to state explicitly the source when quoting results from this master dissertation.

Jordy Delvaeye
May $27^{th}$ 2020

# Acknowledgements

This Master thesis is the result of a year of hard work and perseverance in order to obtain the academic degree of Master of Science in Electromechanical Engineering: Maritime Technology. I will forever remember this thesis due to the extraordinary circumstances in which it was performed. While the whole world was going through uncertain times with the COVID-19 Crisis of 2020, I tried to give it my best to deliver a work of which I could be proud.

This thesis was never possible without the help of some very special people. First and foremost, I want to thank prof. dr. ir. Evert Lataire for guiding me through this journey and giving me advice, both concerning the thesis and other aspects of my academic and professional career. This professor was one of the main motivators for me to choose for the specialization in Maritime Engineering and deserves my uttermost respect. Besides this, I also want to thank dr. ir. Manasés Tello Ruiz for all the help and advice I received on every aspect of my thesis, whenever I asked for it. The lengthy discussions and meetings were something which I enjoyed, especially in these times of self-isolation. The proof-reading has been of great help and I hope you enjoy the result. I would also like to thank the Flanders Hydraulic Research (FHR) in Antwerp for providing me with the ship and its full scale measurements, as well as the simulations. I would also like to give special thanks to prof. dr. ir. Maxim Candries and prof. dr. ir. Guillaume Delefortie for answering the questions I had about my research topic.

I want to thank all of my friends which I met during the 5 years at the Faculty of Engineering and Architecture at UGent. Besides the never-ending support, we experienced some magnificent times together and I am forever grateful of having the student life that I did together with you. Koenraad Maes deserves special thanks for continuously listening to my frustrations whenever something went wrong with the thesis and for completing these 2 Master years with me in the Maritime Technology classes. I would also like to thank my parents for believing in me and supporting me throughout these 5 tough years. It has not been easy, but I finally made it. Last but certainly not least, I would like to mention my girlfriend Jenna, without whom I would not have been able to finish this last year. The never-ending love and support meant the world to me. Thanks to you, I always had somebody to fall back on when things seemed impossible. Thank you for being in my life. Always.

Jordy Delvaeye
May $27^{th}$ 2020

# Air pollution by ships in close proximity to dense populated areas

Jordy Delvaeye
Master's dissertation submitted in order to obtain the academic degree of
Master of Science in Electromechanical Engineering
Supervisors: Prof. dr. ir. Evert Lataire, Dr. ir. Manasés Tello Ruiz
Faculty of Engineering and Architecture (FEA)
Ghent University
Academic year 2019-2020
Department of Civil Engineering
Research group of Maritime Technology

## Abstract

The maritime shipping sector is responsible for 2.6% of the global $CO_2$ emissions, which are assumed to increase by 150-250% in business-as-usual scenarios. This critical scenario has boosted research and investment regarding technological measures to reduce harmful emissions. This dissertation investigates the problem of emissions caused by a ship and presents the results of a case study performed on a bulk carrier sailing along the channel Ghent-Terneuzen. In addition, the air pollutants over a specific part of this trajectory were compared with a similar situation in deep and unrestricted water. The present study is based on a model developed with a reversed-calculation procedure of the propeller engine interaction. Results show a significant increase when sailing in shallow and confined water, with ratios of 1.89 for $CO_2$ and $SO_2$ emissions and even higher for others. Moreover, the ship's efficiency takes a serious drop as well, going from an average of 21.3% in deep water to an average of 16-18% in shallow water, with a minimum of 11.7%. Additionally, the effect of using HFO instead of MDO resulted in a slightly higher efficiency, while also emitting more harmful pollutants.

## Keywords

*Maritime Transport, Greenhouse Gases, Shipping and Environment, Shallow and Confined Water, Propeller-Engine Interaction*

# Air Pollution by Ships in Close Proximity to Dense Populated Areas

Jordy Delvaeye

Supervisor(s): Prof. dr. ir. Evert Lataire, Dr. ir. Manasés Tello Ruiz

*Abstract*— **The maritime shipping sector is responsible for 2.6% of the global $CO_2$ emissions, which are assumed to increase by 150-250% in business-as-usual scenarios. This critical scenario has boosted research and investment regarding technological measures to reduce harmful emissions. This dissertation investigates the problem of emissions caused by a ship and presents the results of a case study performed on a bulk carrier sailing along the channel Ghent-Terneuzen. In addition, the air pollutants over a specific part of this trajectory were compared with a similar situation in deep and unrestricted water. The present study is based on a model developed with a reversed-calculation procedure of the propeller engine interaction. Results show a significant increase when sailing in shallow and confined water, with ratios of 1.89 for $CO_2$ and $SO_2$ emissions and even higher for others. Moreover, the ship's efficiency takes a serious drop as well, going from an average of 21.3% in deep water to an average of 16-18% in shallow water, with a minimum of 11.7%. Additionally, the effect of using HFO instead of MDO resulted in a slightly higher efficiency, while also emitting more harmful pollutants.**

*Keywords*—**Maritime Transport, Greenhouse Gases, Shipping and Environment, Shallow and Confined Water, Propeller-Engine Interaction**

## I. Introduction

The use of ships as maritime transport of goods represents more than 90% of the world's trade. According to the latest data released by the International Maritime Organisation (IMO), the shipping sector was responsible for 2.6% of the global carbon emissions in 2012 [1]. Due to the large influence in the trade market, the maritime sector is under a lot of pressure to reduce its emissions of harmful pollutants as fast as possible.

In the literature, different technological and operational measures are presented which might reduce the ship's emissions. According to Bouman et al. [2], these measures can be split up in 4 large categories:

- Power and propulsion, which handles all measures directly related to the engine and propeller. This includes scrubbers, exhaust gas recirculation, but also propulsion efficiency measures such as the use of a nozzle.
- Alternative fuels and energy sources, with examples such as LNG, hydrogen, wind and solar energy.
- Hull design, which discusses the structural part of the ship, ranging from the use of lightweight materials to hydrodynamic shapes to reduce the frictional resistance while sailing.
- Operational measures, which may be implemented to reduce fuel consumption without posing any large modifications or investment costs. Examples are slow steaming and weather routeing.

When ships sail along inland waterways to arrive at ports and harbours, their emissions have a direct effect on the environment and pose a serious threat to the human health. In this dissertation, a case study is conducted on a bulk carrier sailing along the channel Ghent-Terneuzen, in order to assess the emissions of this ship in shallow and confined water. These are then compared to a similar situation in deep and unrestricted water, in order to correctly define the impact of shallow water on the ship's emissions of harmful pollutants. Afterwards, some additional cases are calculated to discern the difference between the usage of different bunker fuels.

## II. Propeller-Engine Interaction

The mathematical model is developed based on a reversed-calculation procedure, taking into account the effect of shallow and confined water. The model is programmed in *Matlab*-code. Besides the emissions, the efficiency and fuel consumption are also important factors to investigate. The inputs necessary for this model are the vessel speed, engine rotational speed and the propeller thrust.

The model starts at the $K_T - K_Q$ propeller diagram, showing the advance number $J$ on the horizontal axis and the thrust and torque coefficients $K_T$ and $K_Q$ on the vertical axis. With the help of this diagram, the propeller torque $Q_P$ can be obtained. The delivered power at the propeller is then given by:

$$P_D = Q_P \cdot 2 \cdot \pi \cdot n \tag{1}$$

Another important factor at the propeller is the propulsive efficiency, consisting of 3 terms:

$$\eta_D = \eta_{prop} \cdot \eta_{hull} \cdot \eta_{rot} \tag{2}$$

Where $\eta_{prop}$ is the propeller efficiency, $\eta_{hull}$ is the hull efficiency which depends on the wake fraction and thrust deduction factor and $\eta_{rot}$ is the rotative efficiency.

The brake power available at the output of the engine, is calculated as:

$$P_B = \frac{P_D}{\eta_{shaft}} \tag{3}$$

$\eta_{shaft}$ is the shaft efficiency, consisting of three parts:

- $\eta_{gearbox}$, the gearbox efficiency;
- $\eta_{bearings}$, the efficiency left after loss due to bearings;
- $\eta_{length}$, an efficiency factor depending on the shaft length.

An important assumption which is made here is the constant rotational speed of the shaft, such that the rotational acceleration $\dot{n} = 0$ and the engine torque equals the propeller torque. This follows from the equation of motion:

$$2 \cdot \pi \cdot I_{pp} \cdot \dot{n} = Q_E - Q_P \tag{4}$$

This implies a large simplification of the model, neglecting any accelerations of the ship in order to proceed.

Arriving at the engine, the fuel consumption needs to be calculated. This depends on the brake specific fuel consumption $BSFC$, which can be provided by the engine manufacturer as a function of engine load [3].

$$\dot{m}_{fuel} = BSFC \cdot P_B/3600 \tag{5}$$

The effective engine efficiency will be calculated as well since it is an important part of the total ship efficiency:

$$\eta_{eff} = \frac{W_{eff}}{m_{fuel} \cdot LHV} \tag{6}$$

With $W_{eff}$ and $m_{fuel}$ the effective work and fuel mass over one engine cycle, respectively. $LHV$ can be defined as the lower heating value of the fuel.

The emissions can be calculated with the help of an emissions factor. This factor relates the emissions to the fuel consumption of the ship, dependent on the type of fuel used. The fuels considered here are the standard bunker fuels: heavy fuel oil (HFO) and marine diesel oil (MDO). The harmful pollutants of which the emissions are discussed in this dissertation are $CO_2, CO, CH_4, NO_x, SO_2$ and PM. The emissions factors $EF_i$ used in this dissertation were determined in the IMO's $3^{rd}$ Greenhouse Gas study [1] and given in Table I. The emissions rates $\dot{EM}_i$ and masses $EM_i$ may be calculated as:

$$\dot{EM}_i = \dot{m}_{fuel} \cdot EF_i \tag{7}$$

$$EM_i = m_{fuel} \cdot EF_i \tag{8}$$

Finally, the total ship efficiency can be calculated, by multiplying the separate efficiencies of the propeller, shaft line and engine.

$$\eta_{tot} = \eta_D \cdot \eta_{shaft} \cdot \eta_{eff} \tag{9}$$

TABLE I: Emissions factors for different types of greenhouse gas emissions.

| Emission factor [g/g fuel] | Fuel type | |
|---|---|---|
| | HFO | MDO |
| $CO_2$ | 3.114 | 3.206 |
| $CO$ | 0.00277 | 0.00277 |
| $CH_4$ | 0.00006 | 0.00006 |
| $NO_x$ | 0.0903 | 0.0961 |
| $PM$ | 0.00728 | 0.00097 |
| $SO_2$ | 0.025 | 0.010 |

## III. Case Study

The trajectory of a bulk carrier sailing along the channel Ghent-Terneuzen was simulated with the help of a fast-time track captive simulation provided by Flanders Hydraulics Research (FHR) [4]. This simulation is based on full-scale measurements of the conditions of this bulk carrier when following the same trajectory, while even taking weather conditions into account. The simulations start when the vessel is leaving the lock in Terneuzen and stop near berthing site 5350 1 hour and 55 minutes later.
The main characteristics of the ship are given in Table II. Due to the lack of engine data, an engine was selected with the design procedure by MAN B&W [5]. The selected characteristics are also specified in Table II. For the propeller, a B4-70 Wageningen propeller was used with a pitch-over-diameter ratio $P/D$ of 0.61.

TABLE II: Basic ship, engine and propeller parameters.

| **Type** | Bulk carrier |
|---|---|
| **Service speed** | $14.5\ kn$ |
| $\mathbf{L_{oa}}$ | $230\ m$ |
| **B** | $37\ m$ |
| **D** | $20.5\ m$ |
| **T** | $12.5\ m$ |
| **DWT** | $91,913\ t$ |
| **Engine Characteristics** | |
| **Type** | G50ME-C9.5 |
| **Piston diameter D** | $0.5\ m$ |
| **Stroke s** | $2.5\ m$ |
| **Cylinders** | 9 |
| **SMCR** | $15,480\ kW$ |
| **100% engine speed** | $100\ rpm$ |
| $\mathbf{L_1MEP}$ | $21\ bar$ |
| **Propeller Characteristics** | |
| **Diameter [m]** | 8 |
| **# blades** | 4 |
| **Propeller efficiency** | 0.591 |
| **Pitch-Diameter ratio P/D** | 0.619 |
| **Propeller Thrust [kN]** | 1,095.88 |

At an average engine load of 13.5% and an average rotational engine speed of $51\ rpm$, the bulk carrier followed the trajectory along the channel. As an input, the simulation required the channel bathymetry. The average water depth varies between 13.5 and $15\ m$. With the draft $T$ of the ship equal to $12.5\ m$, this may be classified as very shallow water [6]. The ship's fuel consumption and emissions along this trajectory were calculated with the help of the mathematical model. In order to assess the gravity of these emissions in shallow and confined water, this case was compared to the same bulk carrier sailing at the same engine load and rotational engine speed in deep and unrestricted water. Since no data was available for this case, the ship is assumed to sail at a constant engine load of 13.5% and a constant engine speed of $51\ rpm$. The effects of wind and waves were neglected. As an extra output, the ship's efficiency will be compared to observe the effect of shallow water.

## IV. Results and Discussion

### A. Bulk carrier on channel Gent-Terneuzen

The mathematical model described in Section II is used on the case study of Section III to obtain the results here. To sim-

plify, all the plots in this section are calculated when sailing with MDO as a fuel.

The total ship efficiency $\eta_{tot}$, starting fom the fuel tank and ending at the propeller thrust, is one of the most important parameters of this case study. This ship efficiency, plotted in Figure 1, consists of 3 parts: the propulsive efficiency $\eta_D$, the shaft line efficiency $\eta_{shaft}$ and the effective engine efficiency $\eta_{eff}$. The shaft line efficiency $\eta_{shaft}$ is taken constant at 98% and independent of the type of sailing area. The propulsive efficiency and effective engine efficiency are plotted in Figure 1 as well.

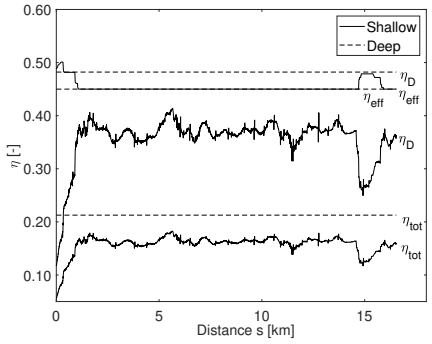


Fig. 1: Effective engine, propulsive and total ship efficiencies when sailing along the channel Gent-Terneuzen and in open sea.

While the effective engine efficiency $\eta_{eff}$ of Figure 1 mainly depends on the engine load and can thus attain a plot absent of many fluctuations, the propulsive efficiency $\eta_D$ and thus also the total ship efficiency $\eta_{tot}$ is a function of the wake fraction $w$ and thrust deduction factor $t$. These factors change throughout the trajectory depending on the dept-to-draft ratio $\frac{h}{T}$ as proven by [7]. The peak at the start of the measurements is due to the high engine load when leaving the lock at a very low speed, as the ship has to accelerate. After the acceleration, a constant vessel speed of $51\ rpm$ is attained for a long time.
After almost $15\ km$, the engine speed was increased to $64\ rpm$ for a short period of time, which is visible from the temporary increase in effective engine efficiency $\eta_{eff}$. Besides this, the propulsive efficiency $\eta_D$ takes a drop, which translates itself into the total ship efficiency $\eta_{tot}$. The explanation here is fairly simple: after $15\ km$ the ship needs to cross a bridge at the city Zelzate. Due to the narrow passage here, the ship has to increase its manoeuvrability by increasing the propeller speed. On the other hand, the blockage increases to a local maximum due to the narrowing of the canal and a decrease in water depth, while the $\frac{h}{T}$-ratio is quite low. These severe detrimental conditions cause the effects on the efficiencies. Once the bridge has been passed, the ship regains its initial engine speed of $51\ rpm$. Besides this, several smaller fluctuations occur as well due to bends and other bridges along the trajectory.

Figure 2 plots the fuel consumption rate of the vessel and the $CO_2$ mass rate. The other emissions, i.e. $CO, CH_4, NO_x, SO_2$ and $PM$, all have a similar plot, which takes the form of the effective engine efficiency $\eta_{eff}$ of Figure 1. This confirms the

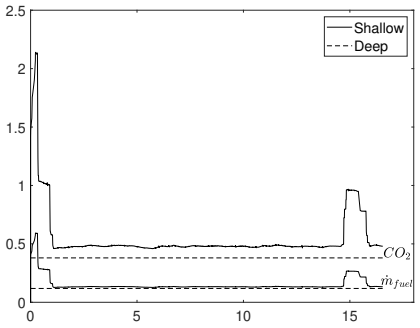


Fig. 2: $CO_2$ emissions rate and fuel consumption when sailing along the channel Ghent-Terneuzen and in open sea.

fact that the emissions are mainly dependent on the engine load and rotational speed. Contrary to the effective engine efficiency $\eta_{eff}$, small fluctuations are still visible during the constant engine speed part of the trajectory, due to the ever-changing propeller thrust related to the $\frac{h}{T}$-ratio. Again a severe increase may be noticed when sailing past the bridge at Zelzate, which almost solely comes from the increased engine load due to the extra manoeuvrability necessary.

### A.1 Comparison with open water

In order to assess the influence of shallow and confined water, this case study is compared to a similar case in deep and unrestricted water. The same bulk carrier is sailing at a constant engine load and engine rotational speed, which is taken equal to the average of the shallow water values. This causes the rest of the parameters along the trajectory to be constant as well. The values for deep water are plotted in Figure 1 and 2.

The total ship efficiency in deep and unrestricted water takes a constant value of 21.3%. This is noticeably higher than the average of 16-18% of shallow and confined water. When sailing past the bridge of Zelzate, the difference increases even more with a minimum value of 11.71%. The comparison with deep water confirms that this is due to the propulsive efficiency which takes a steep drop in shallow water.

The comparison of the emissions and fuel consumption produces similar results, with each time an increased emission rate and fuel consumption rate in shallow and confined water, with the largest difference when passing the bridge of Zelzate. When the total mass of harmful pollutants over the trajectory are compared for the 2 cases, the results are significant. Due to the shallow and confined waterway, some of the pollutants released along the trajectory are even more than doubled compared to the case of deep and unrestricted water. The difference between these two cases is defined as a ratio in Table III.

TABLE III

| **Pollutant** | $CO_2$ | $CO$ | $CH_4$ | $NO_x$ | $PM$ | $SO_2$ |
|---|---|---|---|---|---|---|
| **Factor** | 1.89 | 2.46 | 2.57 | 1.84 | 1.96 | 1.89 |

### B. MDO vs. HFO

A second case study consisted of comparing the emissions when using MDO and HFO as a fuel, both in deep and unrestricted water as in shallow and confined water. These had similar findings, that HFO is more harmful to the environment. This originates mainly from the higher sulphur content in HFO. The effective engine efficiency is slightly higher for HFO as well, in the order of 2-3%, due to the lower heating value of HFO which is lower. The most significant finding from this study occurs at the $NO_x$-emissions. As the ship is compared to the case of shallow and confined water, the engine rotational speed is lowered to $51\ rpm$ at an engine load of 13.5% for deep water as well. When comparing the average $NO_x$ emissions with the Tier limit implied by IMO [8], the emissions in deep and unrestricted water for MDO surpass even the Tier I limit ($17\ g/kWh$ for engine speed $< 130\ rpm$) with $17.5\ g/kWh$. In shallow and confined water the situation is even worse with a $NO_x$ emission rate of $18.93\ g/kWh$. When the emissions are measured at a nominal load of 90%, the Tier II limit is easily satisfied.

## V. Conclusion

This dissertation tried to give an answer on the impact of sailing in shallow and confined water near densely populated areas.
With the help of a mathematical model, a case study was evaluated where the ship's efficiency, fuel consumption and emissions along the channel Ghent-Terneuzen were compared with a similar situation sailing in deep and unrestricted water at the same engine load. Both in fuel consumption and emissions significant increases were noticed. All graphs followed the same path with a large increase near the end of the trajectory. This originated from an increase in engine rotational speed due to the increased manoeuvrability necessary when passing the bridge at Zelzate. Besides this, the efficiency also experienced a serious drop to a minimum value of 11.7%, which may be accounted to the low $\frac{h}{T}$-ratio and increased local blockage at the bridge.
When comparing the difference between HFO and MDO as a fuel, similar conclusions could be drawn, independently of shallow or deep water. HFO was overall more harmful than MDO, and even in deep and unrestricted water, MDO did not comply to a Tier I $NO_x$ limit at the low load of 13.5%. These results only worsened for the shallow and confined water case.
The increased detrimental situation near densely populated areas that was discovered in this dissertation may prove as a starting point towards further research on this important topic. Extra research could involve the use of LNG as a fuel or the effect of cold ironing while berthing near densely populated areas. Whatever the case, the maritime sector should keep transitioning towards a cleaner and healthier shipping industry.


## Acknowledgements

The author would like to thank the generous help, comments and suggestions of his supervisors Prof. dr. ir. Evert Lataire and Dr. ir. Manasés Tello Ruiz. They were a great help towards completing this dissertation. Besides them, the author also thanks the Flanders Hydraulic Research for providing the ship, full scale measurements and the simulations for this case study.


## Nomenclature

| | |
|---|---|
| $BSFC$ | The brake specific fuel consumption [g/kWh] |
| $EM_i$ | The emissions mass of pollutant i [g] |
| $LHV$ | The lower heating value of the fuel [MJ/kg] |
| $P_D$ | The power available at the propeller [W] |
| $Q_P$ | The torque developed at the propeller [kNm] |
| $T$ | The ship's draft [m] |
| $W_{eff}$ | The effective work over one engine cycle [kJ] |
| $\dot{EM}_i$ | The emissions rate of pollutant i [g/s] |
| $\dot{m}_{fuel}$ | The fuel consumption rate [g/s] |
| $\eta_{eff}$ | The effective engine efficiency [-] |
| $\eta_{shaft}$ | The shaft line efficiency [-] |
| $h$ | The water depth [m] |
| $m_{fuel}$ | The fuel mass (used over one engine cycle) [g] |
| $n$ | The rotational speed of the propeller/engine [rev/s] |
| $\eta_D$ | The propulsive efficiency or quasi-propulsive coefficient [-] |
| HFO | Heavy Fuel Oil |
| IMO | International Maritime Organization |
| MDO | Marine Diesel Oil |

## References


[1] T.W.P. Smith et al., "Third IMO greenhous gas study 2014," IMO, 2014.

[2] E. Bouman, E. Lindstad, A. Rialland, and A. Stromman, "State-of-the-art technologies, measures, and potential for reducing GHG emissions from shipping - A review," *Transportation Research Part D 52*, pp. 408–421, 2017.

[3] (2020). CEAS Engine Calculations, [Online]. Available: `https://marine.man-es.com/two-stroke/ceas` (visited on March 30, 2020).

[4] E. Lataire, M. Vantorre, M. Candries, K. Eloot, J. Verwilligen, G. Delefortrie, C. Chen, and M. Mansuy, "Systematic techniques for fairway evaluation based on ship manoeuvring simulations," *34th PIANC-World Congress Panama City*, 2018.

[5] MAN B&W, "Propulsion Trends in Bulk Carriers," *MAN Diesel & Turbo*, 2019.

[6] "Capability of ship manoeuvring simulation models for approach channels and fairways in harbours: Report of working group no. 20 of permanent technical committee ii, supplement to pianc bulletin, no. 77.," PIANC, 1992.

[7] H. Yasukawa, "Computation of effective rudder forces of a ship in shallow water," *Symposium of forces acting on a manoeuvring vessel*, pp. 125–133, 1998.

[8] IMO. (2019). Nitrogen Oxides ($NO_x$ - Regulation 13), [Online]. Available: `http://www.imo.org/en/OurWork/Environment/PollutionPrevention/AirPollution/Pages/Nitrogen-oxides-(NOx)-%E2%80%93-Regulation-13.aspx` (visited on November 18, 2019).

# Contents

# List of Figures

# List of Tables

# Nomenclature

| | | |
|---|---|---|
| $CH_4$ | Methane | |
| $CO_2$ | Carbon dioxide | |
| $C_B$ | The block coefficient | [-] |
| $C_T$ | Dimensionless total resistance Coefficient | [-] |
| $C_a$ | The air resistance coefficient | [-] |
| $D$ | The propeller diameter | [m] |
| $D_b$ | The bore diameter of the engine | [m] |
| $EF_i$ | The emission factor used for emission type i | [g/g fuel] |
| $EM_i$ | The mass of emission type i | [g/s] |
| $F_n$ | The Froude number | [-] |
| $Fr_h$ | The Froude depth number | [-] |
| $I_{pp}$ | The moment of inertia of the shaft line | $[kg \cdot m^2]$ |
| $J$ | The advance coefficient | [-] |
| $K_Q$ | The torque coefficient | [-] |
| $K_T$ | The thrust coefficient | [-] |
| $LHV$ | The lower heating value of the fuel | [MJ/kg] |
| $NO_x$ | Nitrous oxides | |
| $P_B$ | The brake power, available as engine output | [W] |
| $P_D$ | The power available at the propeller | [W] |
| $P_S$ | Shaft power | [W] |
| $P_e$ | Effective engine power | [W] |
| $Q_E$ | The engine torque | [Nm] |

| | | |
|---|---|---|
| $Q_P$ | The torque developed at the propeller | [Nm] |
| $R_A$ | Air resistance | [N] |
| $R_T$ | Total resistance | [N] |
| $R_V$ | Viscous friction resistance | [N] |
| $R_W$ | Wave-making resistance | [N] |
| $S$ | The wetted surface area | [$m^2$] |
| $SO_x$ | Sulphur oxides | |
| $T$ | The draft of the vessel | [m] |
| $T_C$ | The cold source temperature for the Carnot efficiency | [K] |
| $T_H$ | The hot source temperature for the Carnot efficiency | [K] |
| $T_P$ | The thrust developed by the propeller | [N] |
| $V$ | The vessel speed | [m/s] |
| $V_A$ | The advance speed | [m/s] |
| $V_s$ | The swept volume of one cylinder | [$m^3$] |
| $V_{ref}$ | The reference vessel speed | [m/s] |
| $W_{eff}$ | The effective work available at the crankshaft after one cycle | [J] |
| $E\dot{M}_i$ | The rate of emissions for emission type i | [g/s] |
| $\dot{n}$ | The rotational acceleration | [$rev/s^2$] |
| $\chi$ | The number of crankshaft rotations for one complete engine cycle | [-] |
| $\eta_{bearings}$ | The efficiency left after loss due to bearings | [-] |
| $\eta_{eff}$ | The effective engine efficiency | [-] |
| $\eta_{gearbox}$ | The gearbox efficiency | [-] |
| $\eta_{hull}$ | The hull efficiency | [-] |
| $\eta_{length}$ | The efficiency depending on the length of the shaft | [-] |
| $\eta_{mech}$ | The mechanical efficiency of the engine | [-] |
| $\eta_{prop}$ | The propeller efficiency | [-] |
| $\eta_{rot}$ | The rotative efficiency | [-] |
| $\eta_{shaft}$ | The shaft efficiency | [-] |

| | | |
|---|---|---|
| $\eta_{tot}$ | The total ship efficiency | [-] |
| $\lambda$ | The wave length | [m] |
| $\omega$ | The angular frequency | [rad/s] |
| $\rho$ | The fluid density | [kg/m$^3$] |
| $\rho_a$ | The air density | [kg/m$^3$] |
| $a$ | A parameter used in the wake fraction calculation | [-] |
| $b$ | A parameter used in the wake fraction calculation | [-] |
| $bmep$ | The brake mean effective pressure, at the engine crankshaft | [Pa] |
| $c_w$ | The phase velocity of a wave | [m/s] |
| $h$ | The water depth of the vessel | [m] |
| $l$ | The travel distance of the vessel | [m] |
| $m_{fuel}$ | The fuel mass | [g] |
| $n$ | The rotational speed of the propeller/engine | [rev/s] |
| $n_c$ | The number of cylinders | [-] |
| $p_e$ | Mean effective pressure | [Pa] |
| $s$ | The stroke length of the engine | [m] |
| $t$ | The thrust deduction factor | [-] |
| $w$ | The wake fraction | [-] |
| $w_\infty$ | The wake fraction developed in deep water | [-] |
| $\dot{mf_{uel}}$ | The fuel mass rate | [g/s] |
| $\eta_D$ | The propulsive efficiency or quasi-propulsive coefficient | [-] |
| SFOC | Specific fuel oil consumption | []g/kWh] |
| BSFC | Brake specific fuel consumption | [g/kWh] |
| CFD | Computational fluid dynamics | |
| CO | Carbon monoxide | |
| DWT | Deadweight tonnage | [kg] |
| ECA | Emission control area | |
| EEDI | Energy efficiency design index | |

| | | |
|---|---|---|
| EEOI | Energy efficiency operational ondicator | |
| EGR | Exhaust gas recirculation | |
| EPA | Environmental Protection Agency | |
| FHR | Flanders Hydraulic Research | |
| GHG | Greenhouse gas | |
| HFO | Heavy fuel oil | |
| ICE | Internal combustion engine | |
| IMO | International Maritime Organization | |
| k | The form factor | [-] |
| LNG | Liquefied natural gas | |
| MCR | Maximum continuous rating | |
| MDO | Marine diesel oil | |
| MEP | Mean effective pressure | |
| MEPC | Marine Environment Protection Committee | |
| MGO | Marine gas oil | |
| MP | MCR point for propulsion | |
| NCR | Normal continuous rating | |
| PD | Propeller design point | |
| PIANC | Permanent International Association of Navigation Congresses | |
| PM | Particulate matter | |
| PV | Photovoltaïc | |
| REGR | Reformed exhaust gas recirculation | |
| SCR | Selective catalytic reduction | |
| SEEMP | Ship energy efficiency management plan | |
| SMCR | Specified maximum continuous rating | |
| SMR | Small modular reactor | |
| SP | Service rating for propulsion | |
| SVO | Straight vegetable oil | |

UKC Under keel clearance

ULSFO Ultra-low sulphur fuel oil

WHRS Waste heat recovery system

# Chapter I

# Introduction

In 2012, the maritime shipping sector emitted 938 Mt $CO_2$ according to the $3^{rd}$ greenhouse gas (GHG) study of the International Maritime Organization (IMO) [1]. This accounts for 2.6% of the $CO_2$ emissions of the global industry. These emissions are assumed to increase by 150-250 % in 2050 in business-as-usual scenarios, assuming that the world trade through shipping keeps increasing as it has done during the past decades. This path is a likely option because shipping transport is the most economical way of transporting large amounts of goods over long distances. Additionally, the fuel consumption per tonne-km of ships is much lower compared to transport by rail, road and air. In spite of these advantages, air pollution remains a major problem. With climate change being treated as the biggest threat of the $21^{st}$ century, all industries, including the maritime sector, are facing the challenge of significantly reducing their GHG emissions in order to limit the effect on the current global warming. This can be achieved by completely removing the emission of GHG emissions on the one hand, or by using negative emission technologies to balance some unavoidable positive emissions. Most of the technologies currently available aim at the reduction of the fuel consumption per travelled mile, or the use of completely alternative energy sources. The use of negative emissions technologies is currently not working at a large scale, which only increases the need of decarbonizing the complete industry as soon as possible [2]. The IMO has recently conducted a $4^{th}$ GHG study from 2012 to 2018 and is expected to publish its report in Autumn 2020. Based on this report, an intermediary progression result will decide if more stringent regulations are necessary, or if the shipping sector is sailing in the right direction. Figure 1 presents several pathways on how the emissions of $CO_2$ by the shipping sector could increase or decrease over the coming decades, depending on the implementation of the reducing measures.

The IMO has adopted several regulations and policies to reduce these emissions globally. The energy efficiency design index (EEDI) is one of these measures, aiming at a more energy efficient use by establishing mandatory minimum performance levels. Additionally the IMO has also proposed guidelines such as the energy efficiency operational indicator (EEOI) and the ship energy efficiency management plan (SEEMP) for voluntary use to assist shipowners and operators to tackle the efficiency and performance of their fleet with regard to $CO_2$ emissions. Besides $CO_2$, the air pollutant emissions by ships contain other harmful substances as well, including sulphur oxides ($SO_x$), nitrous oxides ($NO_x$), and particulate matter (PM). These are not only harmful to the environment, but also to the human health. By implementing regulations such as Emission Control Areas (ECA) and the Global Sulphur Cap 2020, the IMO is also trying to reduce these pollutants as much as possible. Together with the implementation of several technologi-

cal and operational measures, it tries to achieve its ambitious goal of reducing the GHG emissions by at least 50% by 2050 (compared to 2008). The measures to counteract and reduce these emissions almost always require a large investment, making the shipowners and operators quite inventive with ways to avoid the regulations, or implementing only the bare minimum to comply. Besides an environmental shift, an economical shift will need to happen as well to achieve the IMO's objective in 2050.

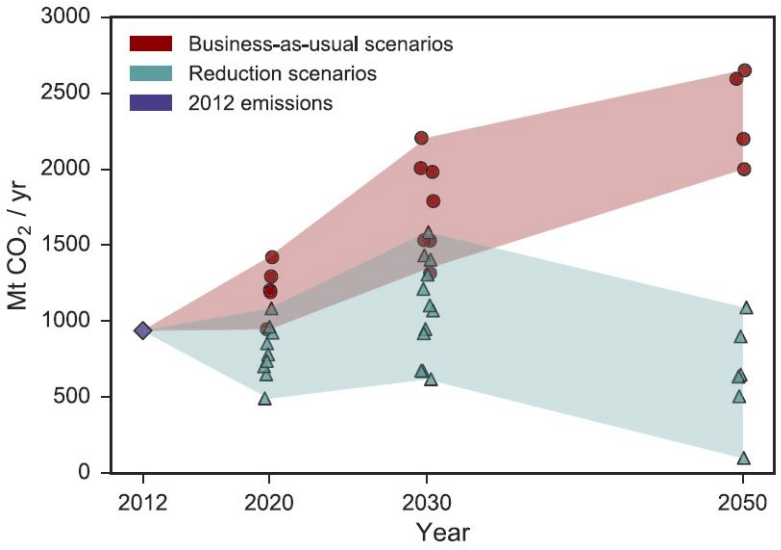


**Figure 1.** *Annual $CO_2$ emissions from the global shipping fleet, distinguished by business-as-usual and reduction scenario pathways [3].*

## 1 Problem Statement

Large ports and harbours established all over the world receive thousands of ships a year which spend a considerable time just hotelling or berthing in these areas. Besides this, some of these harbours are situated inland and are only accessible through various rivers and channels. The large seagoing ships which account for most of the transported goods are designed for achieving an optimal performance during their voyage at sea, which is mostly a deep and unrestricted stretch of water. On the contrary, rivers and channels frequently have a limited depth and are restricted by land at both sides. When a ship wants to call to a port, this will result in an inefficient situation for which the ship is not designed. This may be defined as sailing in shallow and confined water. Due to this undesirable situation, the ship will be forced to sail at a reduced speed, as well as a reduced engine load. The reduced engine load will cause the marine diesel engine with which most of these ships are equipped to be less fuel efficient, as this machine is designed to be used preferably at the nominal load. Besides this, the propeller of the ship will also be affected to some extent by the limitations of the waterway. As if this is not bad enough, ports and harbours are considered essential parts of metropolises and will thus be situated close to these large cities. Just as humans have been doing since forever, cities and towns will also be located along rivers and channels. The frequent passing of large ships which are potentially sailing at a very inefficient operation point may cause severe health threats towards the people living in the densely populated areas near these ports.

Although many studies have already calculated and measured the emissions of ships at sea, few have actually dedicated their resources towards this situation in shallow and confined water near densely populated areas. In order to produce a strong signal to change this, this dissertation's main research objectives consist of:

- Conduct an extensive literature review on the harmful pollutants emitted by seagoing ships and the technological and operational measures available to reduce them.
- Set up a mathematical model to calculate the ship's efficiency, fuel oil consumption and emissions in a reverse-calculation procedure starting from the propeller thrust and vessel speed.
- Estimate the ship's efficiency, fuel oil consumption and emissions of a case study performed on a bulk carrier in a shallow and confined waterway and compare them with a similar situation in deep and unrestricted water.
- Evaluate the impact on the reduction of fuel oil consumption and harmful emissions when using different fuels in a shallow and confined waterway.

The scope of this research is focused on the case study of a bulk carrier sailing along the channel Ghent-Terneuzen, and comparing the emissions with a similar bulk carrier in deep and unrestricted water. This comparison will be performed under the assumption that the ship is sailing at similar conditions (engine speed, engine load) in both situations, in order to distinguish the main differences and the possible increased air pollutant emissions along these waters. If this is the case, this dissertation might serve as a starting point for further research to be conducted towards this important topic.

## 2 Methodology

The present approach to assess air pollution emission caused by shipping traffic will be based on the propeller-engine interaction in shallow and confined water. This reversed-calculation neglects the accelerations of the shaft in order to obtain a more simplified method, assuming a constant rotational speed of both engine and propeller.

The first part of the dissertation concerns an extensive literature review on ship air pollution and the different technologies available nowadays for their mitigation. Starting from the regulations already applied worldwide by different institutions, some technological and operational measures are considered as well as their impact on the emissions and fuel consumption of ships. These measures are divided in 4 main categories: Power and Propulsion, Alternative Fuels and Energy Sources, Hull Design and Operational Measures.

The second part and main focus of this dissertation is the impact of air pollution caused by shipping traffic, taking into account the effect of shallow and confined waterways. The propeller-engine interaction is used as a main factor in this study, starting from vessel speed and thrust values obtained from simulations made available by the Maritime Technology Division of Ghent University in co-operation with Flanders Hydraulic Research (FHR). Due to the limited time frame, additional constraints such as tidal currents and

control devices will not be accounted for. The main focus lies on the drivetrain and the reverse calculations of the pollutants from that drivetrain. To correctly quantify these emissions of harmful pollutants near densely populated areas along the shallow and confined waterways, a comparison is made between this case and the case of the same vessel sailing in deep and unrestricted water. These 2 cases are compared thoroughly. Besides this, some additional cases are compared based on the difference in emissions of harmful pollutants when different fuels are used. At the end some brief suggestions are made based on the literature review in order to reduce these emissions.

## 3 Thesis Outline

This thesis is further organised in five remaining chapters:

- Chapter II: Literature Review;
- Chapter III: Propeller-Engine Interaction;
- Chapter IV: Case Study: Bulk Carrier on channel Ghent-Terneuzen;
- Chapter V: Results and Discussion;
- Chapter VI: Conclusion and Future Research.

Chapter II poses as a literature review which discusses the regulations currently in place to counter the emissions of harmful pollutants by ships worldwide. Besides this, an extensive research is performed towards the technological and operational measures in existence or in development to reduce the emissions and fuel consumption of all types of ships.

Chapter III is a more theoretical chapter, explaining the mathematical background of the different components of the ship's drivetrain: the propeller, the shaft line and the engine. Besides this, the influence of resistance and sailing in shallow and confined water is also thoroughly discussed in order to give the reader some important information on the possible effects of these phenomena. With all this information, a mathematical model is constructed in *Matlab* which is made as generic as possible. This mathematical model serves as a central key structure of the thesis.

In Chapter IV, a case study is introduced concerning a bulk carrier sailing along the channel Ghent-Terneuzen. This bulk carrier will be subjected to the model of Chapter III.

Chapter V discusses the results obtained from the calculations performed in *Matlab* for the case study of the bulk carrier along the channel, compared with the same bulk carrier sailing in deep and unrestricted water. Besides this, a comparison between two different fuels is made as well.

The conclusions flow together with some fundamental statements about future research. These include subjects that were very interesting but were not possible in the current time frame, and others which were too advanced or too extensive with the limited data available.

# Chapter II

# Literature Review

## 1 Regulations

Due to the increasing concerns about the impact of the air pollution caused by ships on the environment and human health, global action was necessary, mandated by the International Maritime Organization (IMO). The IMO mainly orders regulations for global maritime shipping and emission limits for marine diesel engines and their fuels through MARPOL Annex VI. As a specialized agency of the United Nations, IMO is the global standard-setting authority for the safety, security and environmental performance of international shipping. Its main role is to create a regulatory framework for the shipping industry that is fair and effective, universally adopted and universally implemented [4]. The IMO oversees several technical committees, including the Marine Environment Protection Committee (MEPC). The aforementioned committee handles all pollution related matters. In 1997, Annex VI was adopted to the International Convention for the Prevention of Pollution from Ships (MARPOL), issued by the MEPC. Annex VI: *Regulations for the Prevention of Air Pollution from Ships* limits the main air pollutants contained in ships exhaust gases, including $CO_2$, sulphur oxides and nitrous oxides, and prohibits deliberate emissions of ozone depleting substances [4]. This regulation applies to all fuel oil, combustion equipment and devices onboard, and therefore includes both main and auxiliary engines as well as other combustion machines. Since 1997, several amendments were made to Annex VI, including the creation of Emission Control Areas (ECAs), the Energy Efficiency Design Index and the Ship Energy Efficiency Management Plan (SEEMP). With the help of Annex VI, the IMO hopes to achieve its ambitious goal, i.e. reduction of greenhouse gas emissions from international shipping by 50% by 2050 (compared to 2008).

### 1.1 Global Sulphur Cap 2020

Sulphur oxides ($SO_x$) are created during a chemical reaction with sulphur. The main type of fuel used in marine engines is Heavy Fuel Oil (HFO), which contains fairly large amounts of sulphur. $SO_x$ are known to be harmful to human health, these emissions have been linked to lung diseases and respiratory issues. Besides this, $SO_x$ can also lead to acid rain.
IMO regulations to reduce $SO_x$ emissions from ships first came into force in 2005, under Annex VI. Over the past few years, these regulations have become more strict by reducing the sulphur content allowed in marine fuels. According to the general requirements of MARPOL Annex VI in 1997, the sulphur content of the fuel oil consumed on board of seagoing vessels should not exceed 4.50%. In October 2008, during the

MEPC's 58th session, the sulphur content was tightened until 3.50%. During that same session, the global sulphur cap was discussed. Starting from January 2020, the limit for sulphur in fuel oil used on board ships operating outside ECAs must be reduced to 0.50% [5]. This regulation applies to all sizes of ships and will greatly reduce air pollution. This does not only result in a cleaner environment, but $SO_x$ reduction also reduces particulate matter (PM).
To comply with this regulation, ships need to use marine fuels with a drastically lower sulphur content. This can be accomplished by using marine gas oil (MGO) or ultra-low sulphur fuel oil (ULSFO). Some ships use LNG or biofuels, i.e. fuels that do not contain any sulphur. Another way of meeting the requirement of 0.50% sulphur content is by installing an exhaust gas cleaning system, also known as a "scrubber". These scrubbers can be used on HFO and are accepted by the IMO as long as they achieve the same level of emissions reduction.

## 1.2 Emission Control Areas

The global sulphur cap limits the sulphur concentration in fuel to 0.50% from January 2020. In 1997, Annex VI also included several areas with more stringent regulations. These Emission Control Areas (ECAs) are areas where the adoption of special mandatory measures for the emissions of ships is required to prevent, reduce and control air pollution from $NO_x$ or $SO_x$ and particulate matter or all three types of emissions and their attendant adverse impacts on human health and the environment [6]. These regulations came into effect in May 2005 and included the Baltic Sea and the North Sea as ECAs for $SO_x$.
Just as with the global sulphur cap, these regulations included several stages in order to give ship owners the time to comply. Until July 2010, the sulphur limit in ECAs was 1.50%. Between July 2010 and January 2015, only marine fuels with a sulphur content lower than 1.00% were allowed. From January 2015 the final stage went into effect. Every ship entering an Emission Control Area must sail with a fuel with a sulphur content limit of 0.1%. In addition to this, an amendment was made to Annex VI which reinforces the EU Marine Fuel Directive. This Directive states that all marine fuels of ships at berth within the whole of the EU must have a sulphur cap of 0.10%. Over the years, 2 other areas were added which limit the $NO_x$, $SO_x$ and particulate matter emissions: the North American ECA, including most of US and Canadian coast and the US Caribbean ECA, including Puerto Rico and the US Virgin Islands. From January 2019, the original ECAs in the North Sea and Baltic Sea also cover $NO_x$ regulations. Potential areas for future ECAs include the Mediterranean Sea, the Gulf of Mexico and the coasts of Japan. In 2015, the Chinese government also announced the creation of several ECAs in China. These ECAs however are not officially recognized by the IMO. A summary of all the (future) ECAs listed by the IMO is given in Figure 2.

To comply with these regulations, a ship owner has 3 options:

- HFO combined with selective catalytic reduction (SCR) and an open loop seawater scrubber.
- MGO combined with SCR.
- The use of alternative fuels or energy sources such as LNG and biofuels.

Although MGO is more expensive than HFO, the combination of MGO with SCR is still the least expensive option. These solutions are very successful in reducing emissions, but there are side effects which still require extra regulatory measures, such as the ammonia slip from the use of SCR and methane slip from


**Figure 2.** *Map of the (future) emission control areas.[7]*

LNG engines. Since these very strict regulations only apply inside the ECAs, most ships also use different fuel oils inside and outside the control areas.

The introduction of emission control areas has been remarkably successful in controlling marine pollution but it has had certain impacts on the shipping industry. Zhen et al. [8] researched their influence on cruise shipping and stated several side effects. The fuel costs affect the total operational costs for shipping. Since low-sulphur fuel is more expensive than bunker fuel, total operational costs will increase. This affects speed and routeing decisions, which are critical fuel cost determinants. Furthermore, cruise ships may choose longer routes to reduce the distance travelled within ECAs and increase speeds outside to satisfy the time windows required at all ports of call. This option is cheaper for cruise shipping but very counterproductive for emissions, since engines working at higher speeds emit more harmful substances.
Chen et al. [9] formulated a model to incorporate the route-choosing behaviour of liner shipping after the creation of an ECA in the Mediterranean Sea. Their investigation revealed that, if an ECA is established, a considerable portion of ships will re-route around the ECA. This would mean a much longer route around Africa via the Cape of Good Hope instead of through the Suez Canal, which would result in higher (regional) emissions. This is especially true for small ships, since larger ships are already quite environmentally friendly and re-routeing cannot further reduce the regional ship emissions.
Although ECAs have had a clear positive effect on emission mitigation, further international coordination and more research is still necessary to address certain loopholes such as the re-routeing of ships.

### 1.3 $NO_x$-regulation: Tiered System

Nitrous oxides or $NO_x$ is a generic term for nitric oxide (NO), nitrogen dioxide ($NO_2$) and other gases containing nitrogen. These oxides are formed as a reaction of nitrogen and oxygen during fuel combustion. Their formation is enhanced in high temperatures, which frequently occur in internal combustion engines. $NO_x$ are harmful for humans and for the environment, as they can react with ammonia to form nitric acid which worsens respiratory diseases and heart diseases. Smog and acid rain, which harm humans and nature alike, also originate from $NO_x$-gases.
Because of these harmful effects, the IMO implemented a policy in the MARPOL ANNEX VI regulations of 1997 to reduce $NO_x$ emissions from ships. The $NO_x$ Technical Code was constructed, covering engine testing, certification and onboard verification procedures to demonstrate the compliance of the ships with the applicable $NO_x$ emissions limits [10]. Amendments to this code were made in 2008. The code divides the $NO_x$ standards into 3 categories, or tiers. These tiers and their regulations are summarized in Table 1 and represented graphically in Figure 3.

| Tier | Ship construction date on or after | Total weighted cycle emission limit (g/kWh) n = engine's rated speed (rpm) | | |
|---|---|---|---|---|
| | | $n < 130$ | n = 130 - 1,999 | $n \geq 2{,}000$ |
| I | 1 January 2000 | 17.0 | $45 \cdot n^{-0.2}$ e.g., 720 rpm – 12.1 | 9.8 |
| II | 1 January 2011 | 14.4 | $44 \cdot n^{-0.23}$ e.g., 720 rpm – 9.7 | 7.7 |
| III | 1 January 2016 | 3.4 | $9 \cdot n^{-0.2}$ e.g., 720 rpm – 2.4 | 2.0 |

**Table 1.** *$NO_x$ Technical code: Tier System [11].*

The $NO_x$ limits are set for diesel engines depending on the rated engine speed. Tier I was the first attempt to control $NO_x$ emissions by ships, quickly followed by Tier II and III after the Annex VI amendments of 2008. Tier I and II are applied globally. Nowadays, these can quite easily be attained by optimisation of the combustion process, i.e. optimising fuel injection timing, exhaust valve timing, pressure, temperature, etc. Tier III is only applicable in the $NO_x$ ECAs and causes a drastic reduction compared to Tier II. Currently, these Tier III standards are in effect in the North American and US Caribbean ECAs. From 2021, the regulations will apply to the Baltic Sea and the North Sea as well.
To be able to comply to these strict regulations, manufacturers and/or operators will need to do more than just tune the combustion process. Some innovative technologies were developed, which will be discussed in some detail in the following sections. These include, but are not limited to: Selective Catalytic Reduction (SCR), Exhaust Gas Recirculation (EGR) and the use of alternative fuels such as LNG. Scrubbers however are not a solution to the $NO_x$ limits, as they only filter out sulphur.

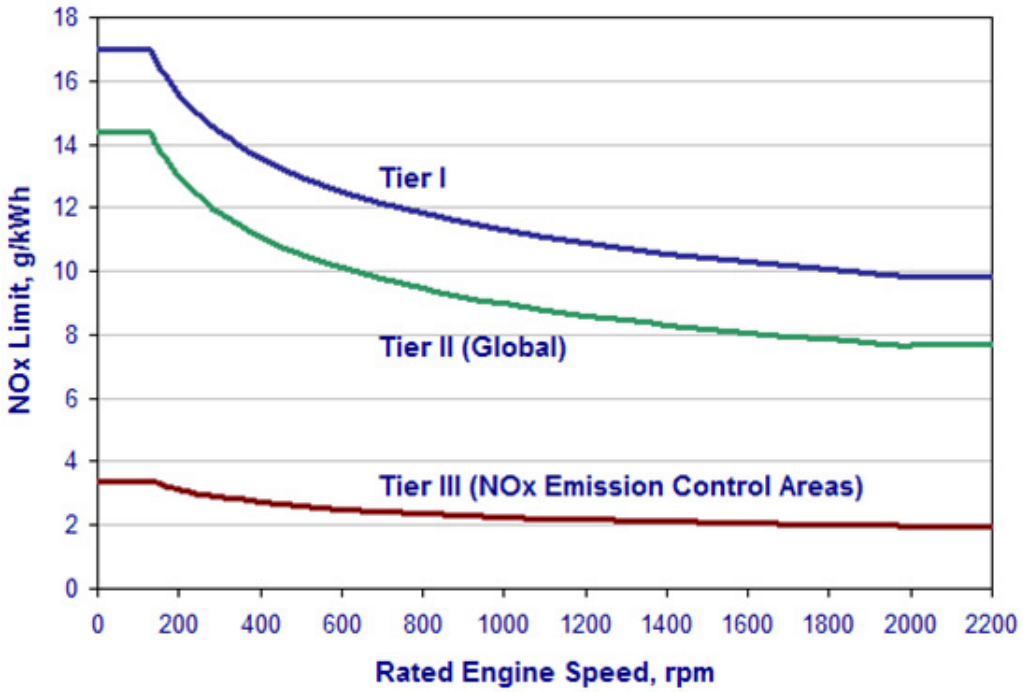


**Figure 3.** *MARPOL Annex VI $NO_x$ emission limits [12].*

## 1.4 Energy Efficiency Design Index

The Energy Efficiency Design Index (EEDI) is an index which estimates the grams of $CO_2$ per transport work (g of $CO_2$ per tonne-mile). It is the most important technical measure for new ships and it aims at the use of more energy efficient equipment and engines [13]. It was made mandatory by the IMO for new ships from 1 January 2013, following an initial two year phase zero. The principle of the EEDI is simple:

$$AttainedEEDI \leq RequiredEEDI = (1 - X/100) \cdot ReferenceLineValue \tag{1}$$

In this formula, X is a reduction factor specified by the IMO for different ship types and different phases. These phases represent the amount of $CO_2$ reduction, which is tightened incrementally every 5 years, starting with a 10% reduction. This way, the EEDI ensures that new ships are more energy efficient than an average ship is today. The Attained EEDI can be calculated by a very long formula, imposed by the IMO. This formula is far from perfect and is still being optimised as this thesis is written. The latest formula issued by the IMO (2018) is [14]:

$$\frac{\left(\prod_{j=1}^{n} f_j\right)\left(\sum_{i=1}^{nME} P_{ME(i)} \cdot C_{FME(i)} \cdot SFC_{ME(i)}\right) + \left(P_{AE} \cdot C_{FAE} \cdot SFC_{AE}*\right) + \left(\left(\prod_{j=1}^{n} f_j \cdot \sum_{i=1}^{nPTI} P_{PTI(i)} - \sum_{i=1}^{neff} f_{eff(i)} \cdot P_{AEeff(i)}\right) C_{FAE} \cdot SFC_{AE}\right) - \left(\sum_{i=1}^{neff} f_{eff(i)} \cdot P_{eff(i)} \cdot C_{FME} \cdot SFC_{ME}**\right)}{f_i \cdot f_c \cdot f_l \cdot Capacity \cdot f_w \cdot V_{ref}}$$

This formula is rich with correction and tailoring factors to suit different types of vessels, which makes it even more complex than at first sight. However, omitting all this, the Attained EEDI is essentially the

ratio of "environmental cost" divided by "benefit for society" or in other words, the ratio of $CO_2$ emission divided by transport work. This ratio can be written as:

$$EEDI = \frac{P \cdot SFC \cdot f_{CO_2}}{DWT \cdot V_{ref}} \tag{2}$$

| | | |
|---|---|---|
| Where: | P | 75% of the rated installed shaft power; |
| | SFC | The specific fuel consumption of the engines; |
| | $f_{CO_2}$ | $CO_2$ emission rate based on fuel type; |
| | DWT | The deadweight tonnage of the vessel; |
| | $V_{ref}$ | The reference vessel speed at design load. |

From this formula it is clear that the EEDI is a function of the installed power, the speed of the vessel and the capacity of the vessel. Every new ship needs to comply with the EEDI standards. The IMO does not differentiate between the different measures on how to get below the required EEDI. Bouman et al. [3] describes several different methods, both technical and operational, to reduce emissions and achieve the required EEDI. These measures are summarized in Figure 4. Bouman eventually categorizes these measures in 5 different groups, each divided in several subjects: Power and Propulsion, Alternative Fuels and Alternative Energy Sources, Hull Design and Operations. Each of these categories will be discussed in more detail in Section 2.

## 1.5 Energy Efficiency Operational Indicator & Ship Energy Efficiency Management Plan

The Energy Efficiency Operational Indicator (EEOI) is a monitoring tool for measuring the $CO_2$ gas emissions to the environment per transport work. While the EEDI is an important factor in the design and construction of new vessels in order to improve the performance, the EEOI is mainly used as a performance improvement tool during operation of existing ships. It represents the actual transport efficiency of a ship in operation over a consistent period. The EEOI allows the captain and the operators of the ship to measure the efficiency of the ship when in operation and see the effect of any operational changes. When it is used as a performance indicator, it might provide a basis for consideration of both current performance and trends over time. This indicator is calculated by the following formula, in which a smaller EEOI means a more energy efficient ship [15]:

$$EEOI = \frac{\sum_i \sum_j (FC_{ij} \cdot C_{Fj)}}{\sum_i (m_{cargo,i} \cdot D_i)} \tag{3}$$

| | | |
|---|---|---|
| Where: | $j$ | The fuel type; |
| | $i$ | The voyage number; |
| | $FC_{ij}$ | The mass of consumed fuel j at voyage i; |
| | $C_{Fj}$ | The fuel mass to $CO_2$ mass conversion factor for fuel j; |
| | $m_{cargo}$ | The cargo carried (tonnes) or work done (number of TEU or passengers) or gross tonnes for passenger ships; |
| | D | The distance in nautical miles corresponding to the cargo carried or work done. |

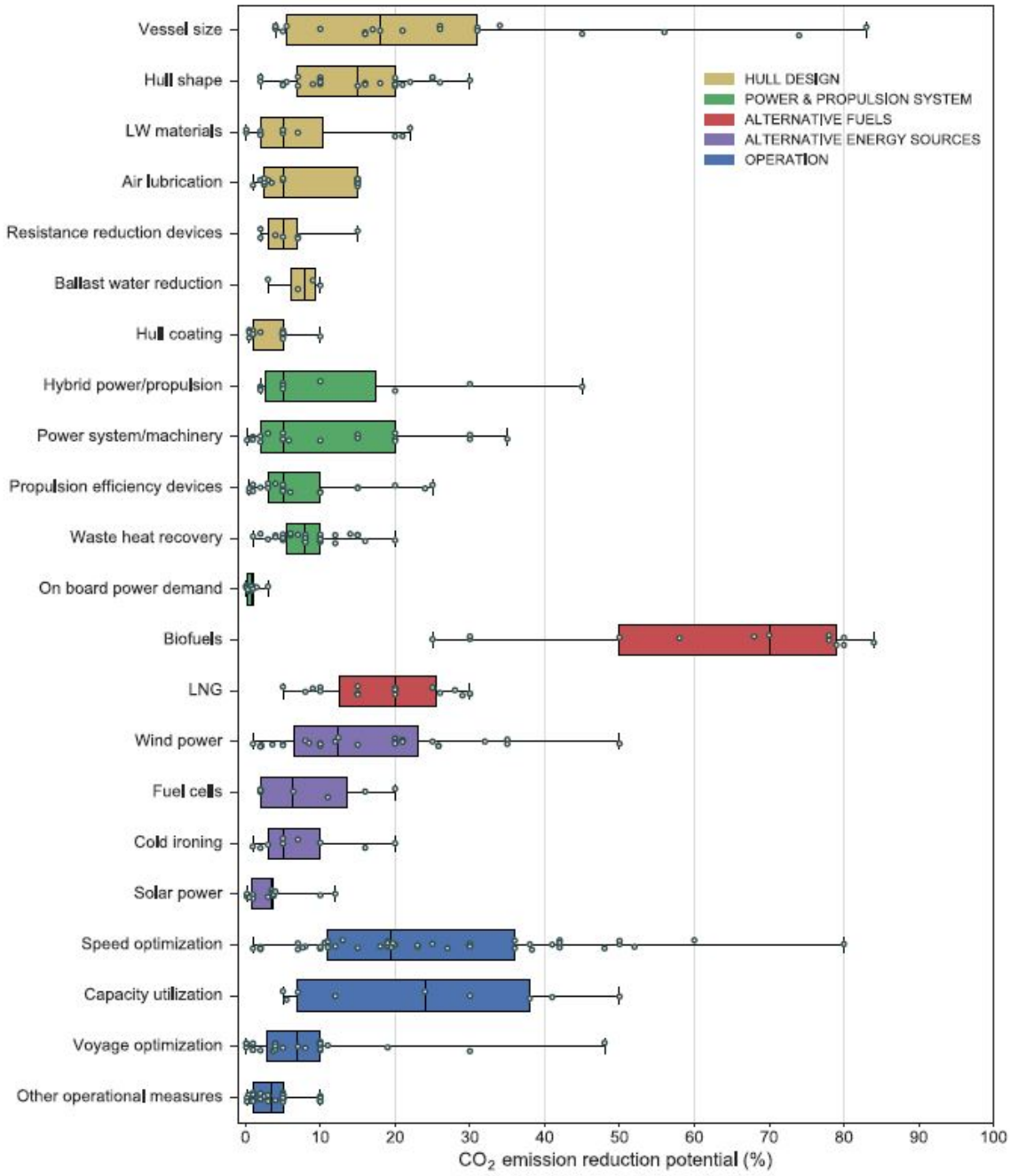


**Figure 4.** *$CO_2$ emission reduction potential from individual measures [3].*

In order to correctly establish the EEOI, the following main steps will generally be needed [15]:

- Define the period for which the EEOI is calculated;
- Define data sources for data collection;
- Collect data;

- Convert data to appropriate format;
- Calculate the EEOI.

As an example, the EEOI data could be used to set internal performance criteria and targets. However, contrary to the EEDI, the EEOI is not yet mandatory and thus its calculation is not necessary.

A last tool implemented by MARPOL Annex VI in order to monitor and reduce the emissions by ships is the ship energy efficiency management plan (SEEMP). This set of operational and technical measures that together provide an efficient framework for energy use is mandatory since January, 1 2013, applicable to all vessels larger than 400 GT. The SEEMP document details these type of measures that are being or will be implemented on-board to improve efficiency and therefore reduce fuel consumption [16]. The purpose of this plan is to establish a mechanism for a company and/or a ship to improve the energy efficiency of a ship's operation. This is preferably linked to a broader corporate energy management policy for the company that owns, operates or controls the ship. The SEEMP works according to four steps: planning, implementation, monitoring and review in a continuous improvement management cycle. This continuous improvement cycle is shown in Figure 5. In the monitoring step, IMO recommends the use of the EEOI as a benchmark indicator to monitor the energy efficiency of vessels.

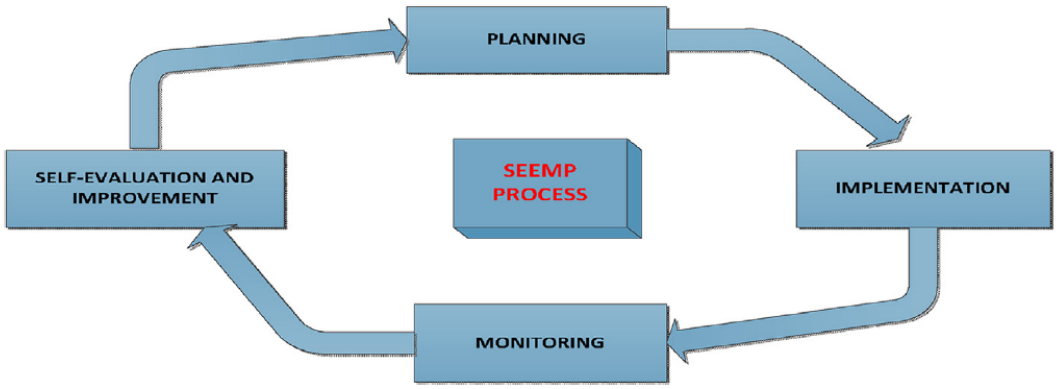


**Figure 5.** *Ship energy efficiency management plan process. [16].*

## 2 Technical & Operational Measures

When talking about emissions reduction and efficiency improvement, dozens of different strategies can be implemented, and each year new technologies and new ways of improving arise. Since it is impossible to describe them all, this literature review will focus on a few technologies and principles gaining the most attention in recent studies. A selection was made among the 4 pillars of the fundamental paper of Bouman et al. [3] as given in Figure 4: Power and Propulsion, Alternative Fuels and Energy Sources, Hull Design and Operational Measures. Some measures focus directly at reducing the emissions at the exhaust of the engine, while others decrease the emissions by increasing the efficiency of the ship and thus decreasing the fuel consumption for the same voyage. The operational measures aim at improving the energy efficiency of the ship by strategic planning at operational or fleet level. Note that although these measures are all

discussed separately, a lot of them may be combined and lead to significant reductions in fuel consumption and increases in overall efficiency.

## 2.1 Power and Propulsion

This part mainly focuses on the power plant of the ship, i.e. the main engine. Many procedures exist to improve the fuel efficiency and reduce the emissions at the exhaust. Only the most important are mentioned here, meaning the technologies that are necessary to comply to certain regulations from Section 1. Other methods such as pilot injection, injection of hydrogen, increased peak pressures, etc. will not be discussed since this differs to much from the actual thesis topic, i.e. pollution of ships in densely populated areas, and the literature review on how to reduce this pollution.

### 2.1.1 Exhaust Gas Recirculation

The combustion in an internal combustion engine (ICE) occurs at relatively high temperatures ($> 1,500°C$). These high temperatures enhance the formation of thermal nitrous oxide emissions which can cause severe health problems and acid rain. The reduction of these emissions is a heavily researched topic worldwide. One of the capital technologies that can achieve a substantial reduction in $NO_x$ emissions is exhaust gas recirculation (EGR). This technique consists of recirculating part of the exhaust gases back into the engine cylinders. This inert gas replaces part of the oxygen in the cylinder and, due to its higher heat capacity, acts as an absorbent for the high-peak temperatures. This causes the overall temperature in the engine to drop and thus reduces the formation of $NO_x$. With 40% EGR on a two-stroke marine diesel engine, the $NO_x$-emissions can be reduced down to Tier III levels [17]. Diesel EGR increases the fuel consumption slightly, as well as the formation of $CO$. Besides this, an increased soot or $PM$ formation is also noticeable, although this can be solved easily by installing diesel particulate filters (DPF). The typical EGR installation from *MAN B&W* is shown in Figure 6.

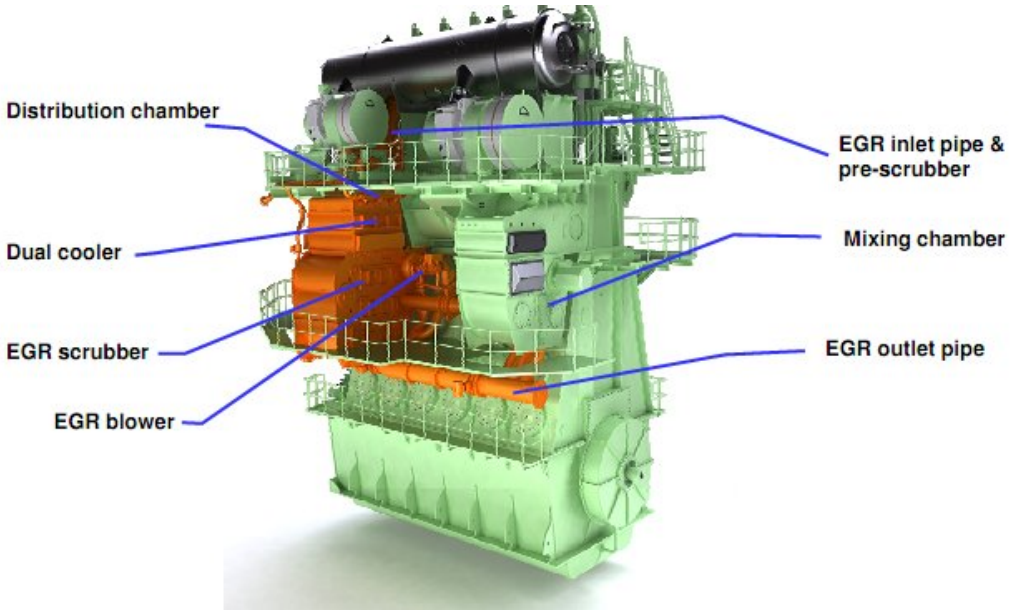


**Figure 6.** *EGR integrated engine design into a MAN B&W two-stroke marine diesel engine [18].*

In order to reduce emissions even further, or eliminating the negative side effects of EGR, several studies are still being conducted to improve this mature technology or to combine it with other engine features. Zhang et al. [19] proved that the combination of EGR with pilot- and post-injections can improve the trade-off between $NO_x$ and soot significantly. Pan et al. [20] also found a way to reduce both $NO_x$ and $PM$ values in the exhaust gases by combining EGR with blends of diesel and n-octanol, with the best reduction at a small EGR rate. This also caused a significant reduction of the $CO$-emissions. A last interesting study by Sai Kumar et al. [21] introduces a new term called reformed exhaust gas recirculation (REGR). This type of EGR is a combination of the traditional technique with a hydrogen addition into the fuel to reduce emissions. Soot and $NO_x$ were reduced at a higher percentage when compared to the same rates performed with normal EGR. The peak cylinder pressures with REGR may also increase compared to their EGR counterparts.

### 2.1.2 Selective Catalytic Reduction

Another way of reducing the thermal $NO_x$ emissions is with the help of selective catalytic reduction. This technique, widely known from the Dieselgate affaire [22], is fairly new regarding the implementation into ships and has the potential of converting $NO_x$ into nitrogen and water with the help of a catalyst, reducing $NO_x$ emissions by 80-90% to below 2 g/kWh [17]. A reducing agent is added to the exhaust gases which reacts with the catalyst to ease the process, mostly a water mix of 40% urea or AdBlue [23]. The urea solution reacts to form ammonia, which can react with the nitrogen oxides to consequently dissociate this into nitrogen and water. The catalyst material mainly consists out of metals or metal oxides. A system developed by *Wärtsilä*, called the $NO_x$ Reducer (NOR), is shown in Figure 7. This compact SCR system complies to IMO Tier III regulations, is compatible with the standard residual fuel oils and can be combined with a scrubber system as well.
The offset of this technology is again the initial cost, as well as the maintenance cost. Fouling and plugging may occur, which means the SCR system needs to be cleaned once in a while. Poisoning of the catalyst may also occur due to certain metals, which may cause malfunctioning of the SCR. Research around SCR mainly involves on the design of the reactor to be as compact as possible. Besides this, the influence of additives in the exhaust gases is also tested. For example, Magnusson et al. [25] researched the influence of sulphur dioxide and water on the performance of the SCR catalyst. While the addition of $SO_2$ clearly enhanced the $NO_x$ reduction, the addition of $H_2O$, in the absence of sulphur, resulted in a decreased $NO_x$ reduction and an inhibition of the $N_2O$ formation.

### 2.1.3 Scrubbers

One of the main bulletin points of the IMO is the reduction of $SO_x$-emissions by ships with the help of the recently implemented Global Sulphur Cap 2020 (Section 1.1). Besides the usage of ultra-low sulphur fuel oil, containing less than 0.1% sulphur, the best way of complying is the installation of a scrubber. A scrubber removes the harmful $SO_x$-emissions from the exhaust gases with the help of an alkaline material which neutralizes these substances. Besides this, particulate matter (PM) can be removed from the exhaust gases and collected as well. Some scrubbers even implement a $NO_x$ removal system.
The scrubber technology is already state of the art and widely implemented right now. The marine scrubbers can be split up into wet and dry scrubbers, dependent on the type of operation. The wet scrubbers are by far the most used type, removing sulphur oxides by spraying alkaline water over the exhaust gas.

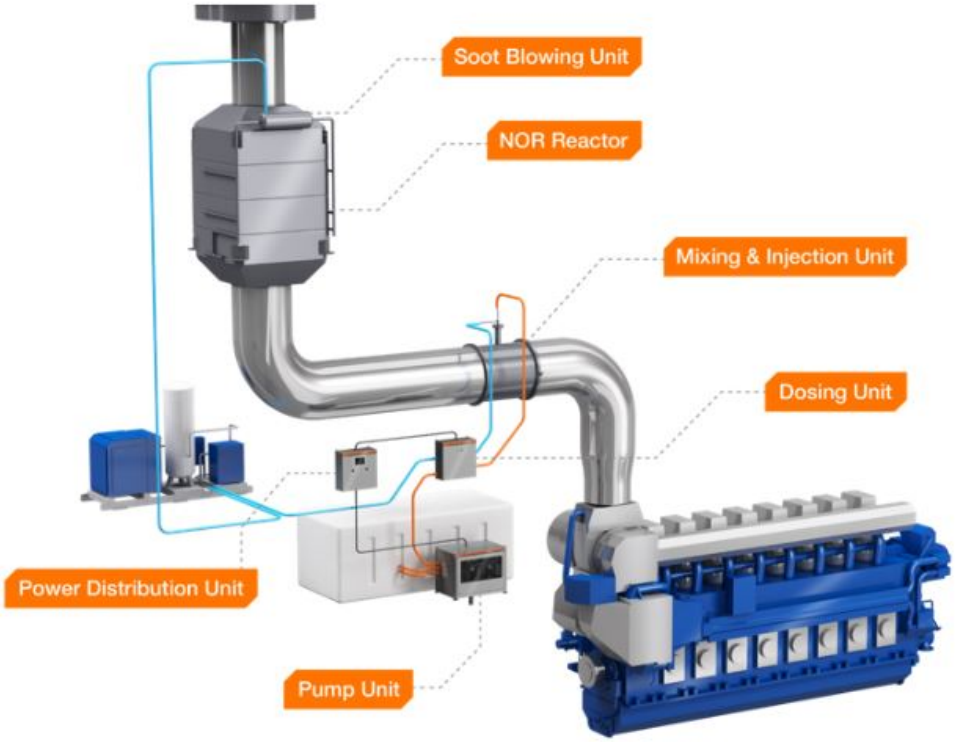


**Figure 7.** *Technical diagram of the Wärtsilä NOx Reducer [24].*

Wet scrubbers can be split up into open-loop and closed-loop scrubbers, both shown in Figure 8.
The open-loop scrubber uses seawater to neutralize the acidic content in the exhaust gases, without the use of other additives if the alkaline content is high enough. The seawater is then washed to remove the pollutants into a sludge tank, after which this washed water is pumped back into the sea. This simple design is easy to install and maintain on board, but large pumps are necessary in order to maintain the constant flow of a large volume of seawater to clean the exhaust gases.
The closed-loop scrubber system can use seawater or fresh water treated with sodium hydroxide or caustic soda as a scrubbing medium. Although it works on a similar principle, there is a fundamental difference. On a closed-loop, this waste treatment cleanses the washed water from pollutants after which it is partially recirculated through the system. The other (contaminated) part goes through an additional water treatment after which it is immediately discharged into the sea or kept in a holding tank. The holding tank is necessary when bleed off is prohibited. This may be the case when sailing in an ECA or near ports and harbours. The accumulated sludge can then be disposed in a suitable port facility. These systems are easy to maintain but more expensive due to the extra treatment required. Extra storage space is required as well due to the necessity of a holding tank and an additional process tank for recirculating the wash water. If SCR systems are installed as well, they should be operated before the wet scrubbers [27].
Nowadays, hybrid scrubbers exist as well, which can be switched with a simple press of a button to comply to more stringent areas such as ECAs. An example are the marine scrubbers developed by *Yara Marine Technologies* [28].

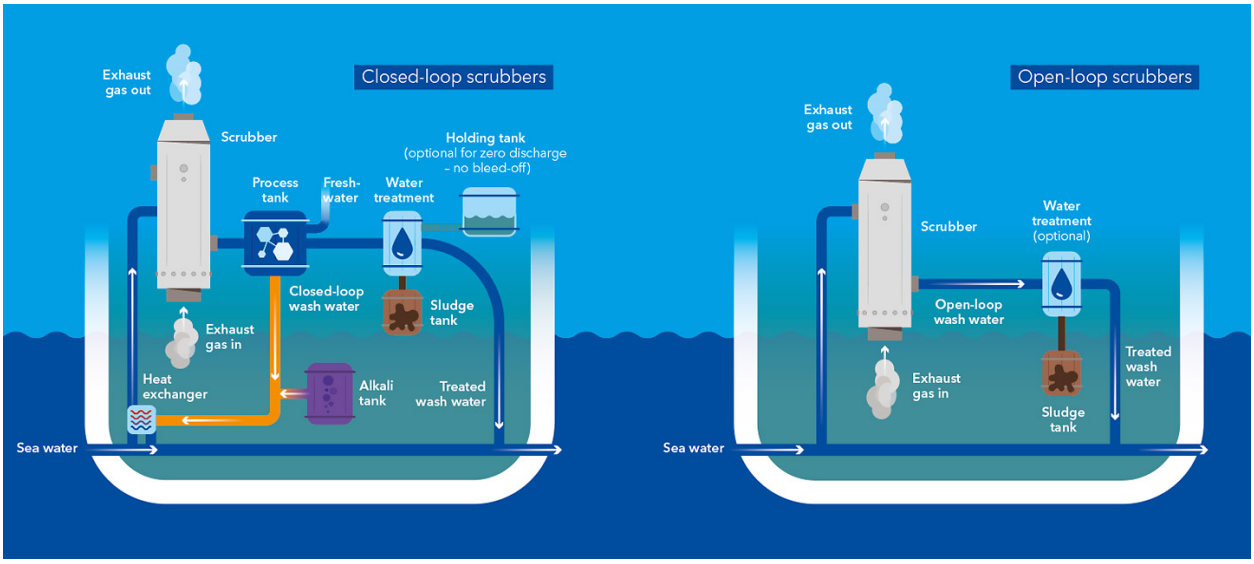


**Figure 8.** *The working process of closed-loop and open-loop marine scrubbers while sailing [26].*

Abadie et al. [29] researched the switch to ULSFO versus the installment of a scrubber in order to comply to the Sulphur Cap 2020, by implementing a stochastic cost model. While the best results were obtained with a combination of the 2 technologies, both are able to comply separately as well. Open loop scrubbers are the cheapest option. The choice should also depend on the remaining lifetime of the ship. The longer the ship has left and the longer it sails inside ECAs, the more attractive an investment in scrubbers will become. This was also confirmed by Jiang et al. [30] when comparing scrubbers with marine gas oil, where they concluded that a ship with a remaining lifespan of less than 4 years is not suitable for a scrubber installation. Lastly, Abadie et al. [29] also found that the installment of scrubbers caused both the fuel consumption and the carbon dioxide emissions to increase slightly.

### 2.1.4 Waste Heat Recovery

Slow speed marine diesel engines can attain efficiencies of 50% and higher, which is already not bad. However, with the current challenges regarding climate change and $CO_2$-reduction, every tool should be applied to increase this efficiency, which consequently reduces the fuel consumption and emissions of the vessel. One of the primary sources of waste heat is the dissipation of exhaust gas from the main engine. This can account up to 25% of the fuel energy [31]. A waste heat recovery system (WHRS) can be implemented to recover some of the energy inside these exhaust gases. This system consisting of steam and power turbines can be used to generate electrical energy with the help of a generator, based on the heat, flow and pressure from the exhaust gases. An example of a system is presented in Figure 9, where part of the exhaust gases is diverted to a power turbine generator, which supplies electrical energy to the main grid. This solution from *ABB* can recover up to 4% of the main propulsion shaft's power output as electricity [32]. The general reduction potential is estimated at 4-11% of the main engine fuel consumption [31]. These systems are implemented into ships at a relatively high rate. However, the cost of buying and installing such a system remains fairly high, which may offset some potential customers. Besides this, the

maintenance costs rise as well, and the system will take extra place which can not be used for transporting goods. These disadvantages may outweigh the benefit of fuel savings and efficiency improvement.

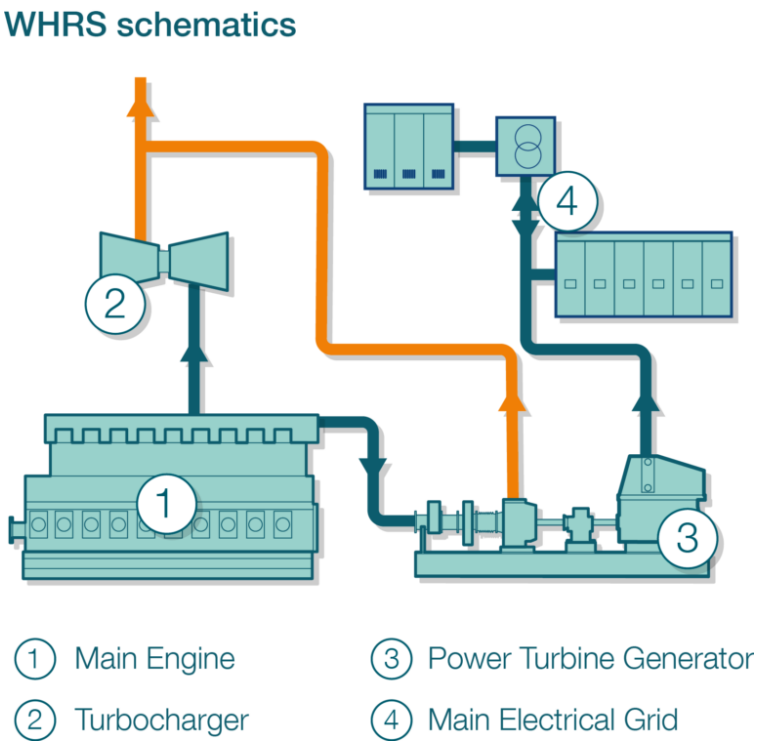


**Figure 9.** *An example of a waste heat recovery system developed by ABB [32].*

The installment of a WHRS can reduce the EEDI of a ship as well, helping to meet the increasingly stringent IMO requirements of the future. Senary et al. [33] researched the implementation of a WHRS on a LNG carrier. This LNG carrier, running on dual fuel engines with LNG as the main fuel, is equipped with a simple Rankine cycle consisting of a boiler, condenser, pump and power turbine. By implementing this, the EEDI of the vessel was reduced by almost 17% of its initial value. Besides this, the $NO_x$-emissions were reduced enough to comply to the Tier III requirements.
The fuel savings and economic viability of a standard water Rankine cycle were compared with organic Rankine cycles by Santiago Suarez de la Fuente et al. [34]. Tested on an Aframax tanker, the reduction in both fuel consumption and $CO_2$ emissions increased up to 5.0%. Several organic fluids were tested, such as benzene, toluene and R245fa. These increases for organic WHRS come at a cost of higher initial investment and larger space required inside the vessel. This work also shows that the initial investment of installing a WHRS is recovered in less than 3 years, regardless of the working fluid. The water Rankine cycle does remain the lowest earner due to its lower fuel savings compared to the organic cycles.

### 2.1.5 Propulsion Efficiency

One of the most important parts of the ship's drivetrain is the propeller. This large rotating part causes the ship to sail forward by moving water and delivering thrust. The propulsion efficiency is an important part of the total efficiency of the ship. A higher propulsion efficiency means that less power is neces-

sary to overcome the same resistance force, i.e. that the fuel consumption for the same resistance will be less. Therefore, improvements in propulsion efficiency are researched widely. This may be done by implementing special propellers which slightly increase the efficiency or the application of appendages to the propulsion system to improve the water flow and reduce the total ship resistance. These appendages may range from nozzles and ducts to fins, as well as pre-swirl stators.

One example of an appendage causing improved efficiency is the Kort nozzle, hydrodynamically designed to improve the overall efficiency of the propeller at low speeds. Above a certain speed, the drag overcomes the efficiency gain made by the lift of the shrouds. Therefore, the Kort nozzle is used mostly for low speed, high thrust vessels such as tugboats. A schematic is shown in Figure 10.

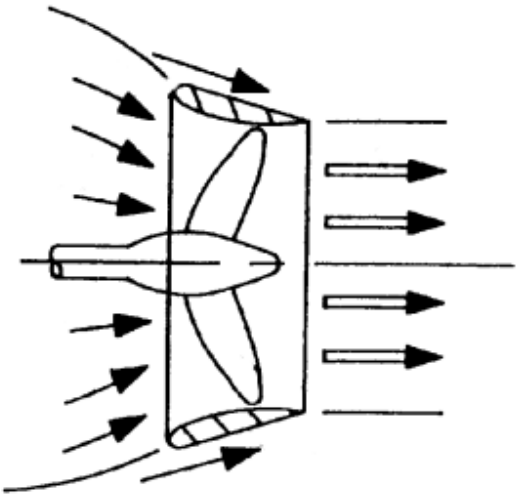

**Figure 10.** *Working principle of a Kort nozzle [35].*

An increased propeller efficiency of 5-8% over an equivalent conventional propeller is possible with a Contracted and Loaded Tip (CLT) propeller. This efficiency gain is achieved together with lower vibration and noise levels, better manoeuvrability and less chance of cavitation by providing an end plate at the blade tip with an increasing pitch from root to tip [36]. The end plates are unloaded and act as barriers between pressure and suction side of the blades. An example is shown in Figure 11.

**Figure 11.** *A contracted and loaded tip propeller [36].*

## 2.2 Alternative Fuels and Energy Sources

In this part, several alternative fuels are researched and compared in order to obtain the highest reduction of emissions while bearing in mind the retrofitting cost and technological advancements of this time. Besides this, alternative energy sources are discussed as well, ranging from ships which can sail completely independent of any kind of fuel, to supplementary technological aids which can significantly reduce the fuel consumption of entire fleets.

### 2.2.1 Biofuels

The first viable alternative presented here to be used as an alternative fuel in the shipping sector is biofuel. These fuels, with the most common types being bioethanol and biodiesel, are gaining increasing attention in a world that is trying to reduce the greenhouse gas (GHG) emissions substantially in a short time frame. Biofuels can be produced from various sources, including crops, lignocellulosic biomass and algae, and even a small amount from animal fat waste. They can be considered as a form of renewable energy if the biomass in the fuel can regrow quickly. Some of the most researched marine biofuels nowadays are represented in Figure 12. Based on existing biofuel technologies, marine biofuels can be designed and produced to be directly integrated into the existing marine engines as “drop-in” fuels. This way, the implementation costs can already be cut substantially. However, biofuel is still more expensive than the standardized marine fuels. The density of biofuel, and thus the energy content per unit of volume, is less than that of marine diesel oil or heavy fuel oil, meaning that extra capacity might be necessary for the fuel storage tank, which can’t be used for storage of transportation goods [37].

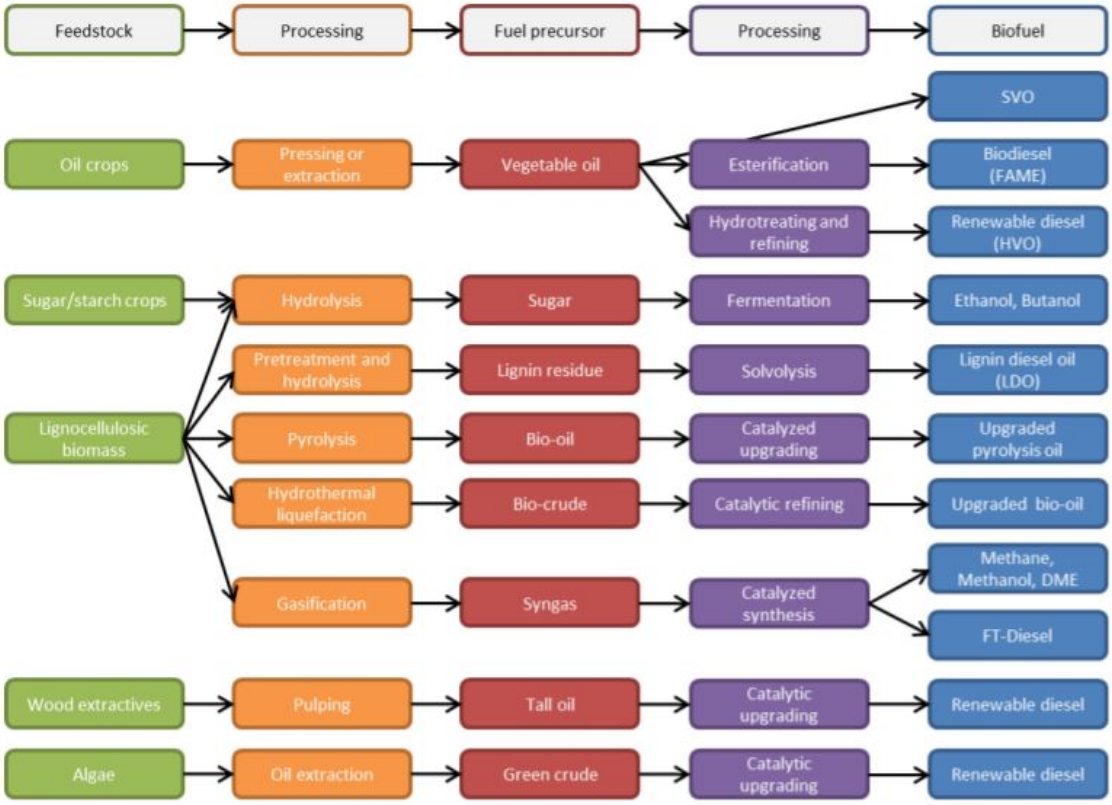


**Figure 12.** *Overview of different feedstock conversion routes to marine biofuels including both conventional and advanced biofuels [37].*

Although the usage of marine biofuels could mean a large reduction in sulphur and particle matter emissions, as well as a $CO_2$-reduction from the shipping sector, large concerns remain. Gilbert et al. [38] performed a full life-cycle assessment for various alternative shipping fuels, including bio-diesel, bio-LNG and straight vegetable oil (SVO). They found that the reduction of emissions when using biofuel is misleading, as the upstream emissions need to be accounted for. The main hotspots for biodiesel and SVO include the impact of land use change and the emissions from fertilisers. Bio-LNG suffers from the extent of flaring and methane yield and slip. The land use is one of the main issues in using biofuel massively as an alternative fuel. Hectares of forest would have to be cut in order to make new land, choices need to be made between using crops for fuel or for food, the fertilizers will produce pollutants which may be more damaging than the usage of standard marine fuels. Until a viable solution is available to this, the worldwide implementation of biofuels remains small. Besides this, the $NO_x$-emissions in operations remain fairly high for SVO and biodiesel, ranking even higher than marine diesel oil used nowadays [38]. This is presented in Figure 13, together with $SO_x$- and $PM$-emissions.

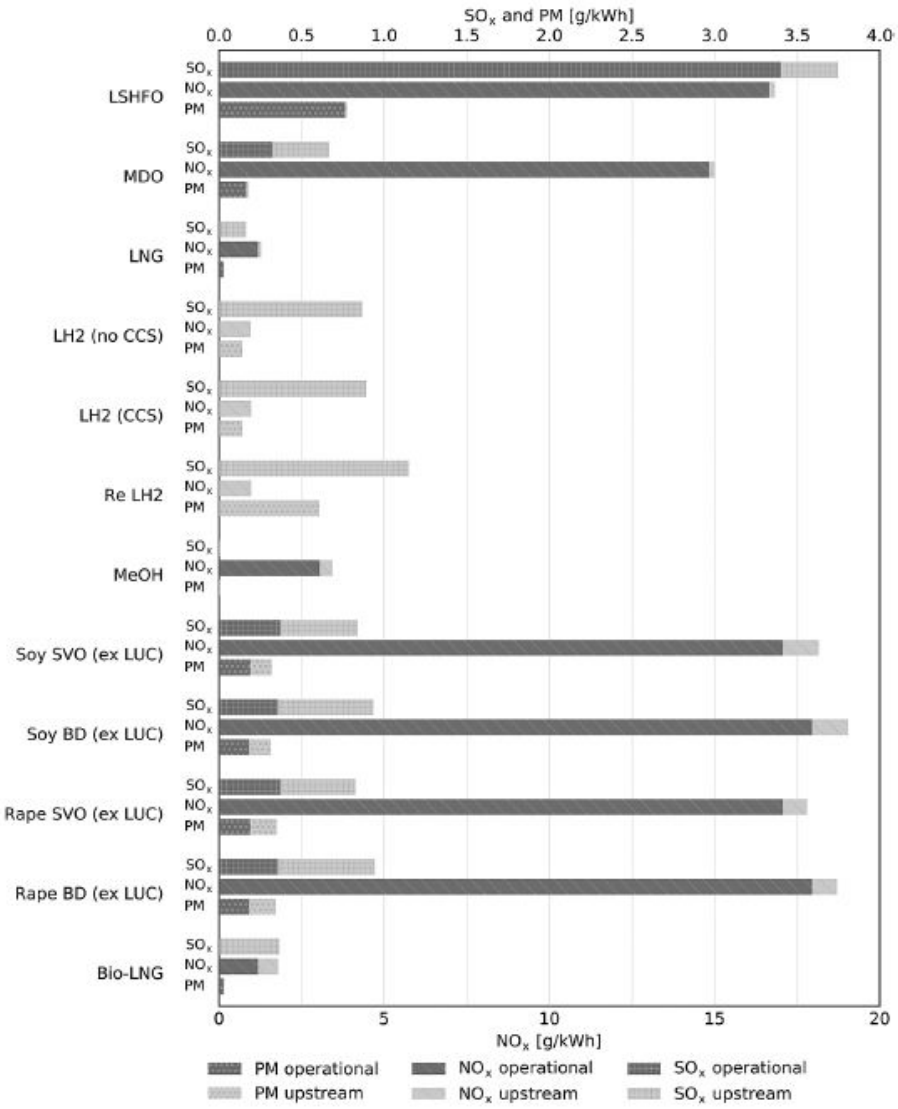


**Figure 13.** *Non-greenhouse gas emissions per kWh shaft output on ships for operational and upstream situations [38].*

The most promising biofuel at the moment is based on algae. These require much less land and grow much faster than traditional crops. The algae contain up to 30 times more fuel than equivalent amounts of other biofuel. Hossain et al. [39] confirmed the technical feasibility of microalgae biocrude in diesel engines and indicate that this could be used in the high speed diesel engines currently available without significant changes in engine performance. The high cultivation and harvest cost of algae biomass is currently the biggest obstacle for wide implementation as biofuel.

### 2.2.2 LNG

Liquefied natural gas (LNG) is one of the most discussed topics regarding cleaner marine fuels in the current maritime technological society. Consisting of mainly methane ($CH_4$), LNG has been used for several

decades for transporting natural gas in a liquefied form using LNG carriers without needing high-pressure tanks. These LNG carriers already implement LNG as a fuel with the help of a dual fuel engine together with diesel oil. LNG is transported in cooled tanks which try to keep the fuel in a liquefied state (hence the name). Insulation is not perfect, thus this means that some of the fuel will evaporate when heating affects the cooling tank, causing an increase in volume and thus and increase in pressure. This "boil-off gas" needs to be released to relieve the pressure inside the cooling tank. There are several ways to do this. In emergency situations, it may be released into the air in its gaseous state. As $CH_4$ is a very unfavourable greenhouse gas (GHG) emission, this should be prevented unless absolutely necessary. A second option is burning the fuel which is again unwanted. Reliquefaction is also a possibility but this requires new infrastructure which could increase the cost significantly while also taking up a lot of space. The final and most preferred option is the burning of LNG as a fuel in a dual fuel engine. This can be done with a few structural changes and can be beneficial to both the environment and the owner, especially when the price of LNG itself is low. At this point, it might be more beneficial for the owner to use the cheap LNG instead of the more expensive fuel oil.

The use of this fuel could reduce both emissions and fuel consumption, while (almost) completely eliminating $SO_2$-emissions due to the lack of sulphur in the fuel. The complete possibilities of emissions reductions when replacing HFO with LNG is given in Table 2. Note that the $SO_2$-emissions may be reduced completely when pure gas engines are used. Because of this, it is an excellent fuel to meet today's ever-increasing stringent regulations regarding pollution. It is an excellent solution regarding the ECAs and the Sulphur Cap 2020. However, LNG is not a clean fuel as it remains a "fossil" fuel which still produces a significant amount of $CO_2$. Therefore, it is useful as a temporary solution during the transition towards cleaner solutions. Beside this, a negative side-effect of using LNG as a fuel is the "methane slip", defined as a leak through the engine of unburned methane because of pre-mixing [40]. Another disadvantage is the increased capital cost for LNG-fueled ships, due to the more expensive propulsion plant and associated technology. The biggest cost is the LNG-tank, ranging from 5-20 million USD [41].

**Table 2.** *Reduction potential of LNG compared to HFO [42].*

| **LNG emissions** | **$SO_x$** | **$NO_x$ diesel cycle** | **$NO_x$ Otto cycle** | **PM** | **$CO_2$** |
|---|---|---|---|---|---|
| **Reduction compared to HFO** | $> 85\%$ | up to 35% | up to 85% | up to 85% | up to 29% |

### 2.2.3 Hydrogen

An alternative gaseous fuel which is gaining increasing popularity is hydrogen fuel cells. These electrochemical cells convert the chemical energy of hydrogen and oxygen into electrical energy, heat and water with the help of redox reactions [43] with a relatively high efficiency of 40-60%. Many types of fuel cells exist, with the one thing in common is that they are all a zero-emission option consisting of an anode, a cathode and an electrolyte. A schematic of this is shown in Figure 14. These fuel cells will keep producing electricity as long as the fuel is available. This fuel, i.e. hydrogen, can be formed from various renewable sources as well, including solar, wind, hydroelectric and geothermal energy. Besides this type of "green

hydrogen", "blue hydrogen" can also be formed via fossil fuels. This negates the clean fuel advantage, unless the $CO_2$ emissions can be captured and stored. This is one of the main disadvantages of implementing hydrogen fuel cells nowadays, since not enough green hydrogen can be produced with the current technologies available. Besides this, fuel cells and hydrogen aren't cheap and are difficult to transport and store as high-pressure cryogenic tanks are necessary. A solution to this transport problem is the binding of hydrogen and nitrogen to form ammonia, which can be stored at much higher temperatures. After the transport, this chemical can be split once more into its base products. Due to the high auto-ignition temperature of hdyrogen, it is also one of the safer alternative fuels to be used in shipping, ranking higher than LNG, methanol and ethanol, according to an assessment of alternative marine fuels made by Deniz et al. [44]. This assessment also concludes that hydrogen fuel cells score quite high regarding bunker capability, durability and adaptability of existing ships, as long as a pure water reserve or a fresh water generator is available. Previously, a lot of research was performed towards the use of hydrogen as a fuel inside an internal combustion engine (ICE). This concept was however mostly abandoned due to the lack of storage in automotive applications and the increasing emissions of nitrous oxides when burning oxygen together with hydrogen in the combustion chamber.

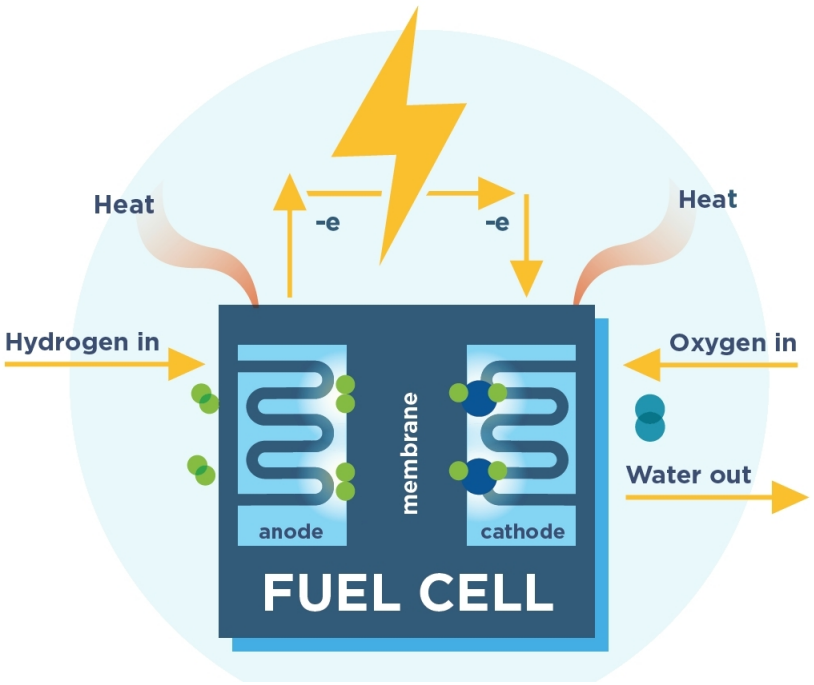


**Figure 14.** *Schematic of the fuel cell process [45].*

As with LNG, hydrogen carriers create an inevitable amount of boil-off gas. This also creates possibilities of using the hydrogen in a dual fuel system as a first step towards zero-emission shipping. A pioneering example of this was already created in 2017 by *CMB* [46]. The *Hydroville* is the first officially recognized passenger ship worldwide sailing on a dual fuel hydrogen diesel co-combustion engine with pressurized hydrogen. Together with the marine engine manufacturer *ABC Engines*, *CMB* is developing hydrogen engines applicable to use in large ships [47].

### 2.2.4 Nuclear Energy

Nuclear marine propulsion is one of the few solutions readily available for creating a shipping industry which is emission-free, yet capable of handling the expanding market for cargo transfer overseas. This type of propulsion offers very long intervals of operation before refuelling, and has a high grade of operational reliability. Nuclear naval reactors also allow better flexibility in ship design due to the smaller volume necessary. Nuclear ships are also much faster, due to the fact that nuclear reactors provide more miles per unit of raw fuel compared to combustion engines. This is one of the main reasons why nuclear propulsion is used for military ships.

Although nuclear propulsion is readily available and offers some clear advantages compared to conventional means, it was never really adapted into the shipping industry, except for certain niche markets such as military ships, submarines and icebreakers. The main reason for this is the large initial expense of building a nuclear vessel, which is mostly not compensated by the very low fuel cost. This offsets a large percentage of the commercial shipping industry. Another large cost is regarding the safety of the crew and the environment. A lot of protection measures are required. The reactor should be small, light and stable regardless of the ship motion. There should be sufficient shielding against radioactivity and the ship design should take into account the impact load due to collision, stranding or sinking. Anti-meltdown measures need to be implemented to avoid the risk of nuclear disasters.

Despite all of this, some experimental commercial ships were built. Besides icebreakers, in which nuclear propulsion is basically essential to provide the power needed for breaking thick ice, an example of a nuclear merchant ship is the NS Savannah. This was the world's first nuclear-powered merchant ship, ordered by President Eisenhower and delivered in 1959 [48]. She operated until 1970, after which she was defueled and made inoperable. However, most of the power plant is intact and still onboard of the ship. It has been ordered to have the ship fully decommissioned by 2031.


**Figure 15.** *NS Savannah [49].*

Over the last few years, there has been a peak interest in reintroducing nuclear propulsion to the shipping industry, due to global warming and the fact that it is a clean fuel. In 2019, Russia launched the world's first floating nuclear power plant, the Akademik Lomonosov [50]. This power plant can operate for several years without refuelling, and is the first of 7 Russian power plants planned. It is operated by a twin pressurized reactor system.
Another innovation for nuclear propulsion is the small modular reactor (SMR) [51]. This reactor's operational flexibility, small capacity, ease of installation on site and lower cost price is releasing new opportunities for nuclear-powered vessels. Research is still ongoing, with the main issue being the safety when the ship is sailing in waves. The coolant fluid used in the SMR can have centrifugal or vertical forces acting on it. Once this passive safety system is optimised, there is a possibility of nuclear vessels re-entering the commercial market.

### 2.2.5 Wind Energy

Wind-assisted marine propulsion is not a recent concept. It has existed for thousands of years and, before the invention of engines, sails were a necessary concept to travel across the seas and oceans. It wasn't until the development of steam engines in the late 18th/early 19th century that sail ships started phasing out and being replaced by steam ships. Over the last decades however, under the threat of global warming, a lot of research has been done on using wind energy for ship propulsion. There are currently 3 different technologies by which wind energy can be harnessed for propulsion purposes: towing kites, Flettner rotors and sails.

Towing kites are installations attached to the bow of the ship which provide a thrust force directly from the wind. These kind of kites are very easy to implement, have a low retrofitting cost and have a minimal interference with the existing structure. This makes a towing kite one of the most attractive forms of wind-assisted propulsion on commercial ships. The largest difference with sails is that a kite is usually at higher altitudes, and is thus able of grasping higher wind speeds. The most famous example of towing kites are *SkySails* [52]. These consist of 4 components: a towing kite with a rope, a launch and recovery system, a wind-optimised routeing system and a control system for automated operation. This control system determines the ideal kite angle and position. The kite has a nominal power of up to 5,000 kW and may reduce fuel consumption rates by 10-50%, depending on wind conditions. Besides emission reductions, the SkySails system also improves the ship's safety and performance on water as it damps the waves such that the ship suffers from less slamming and torsion forces. This auxiliary propulsion system is shown in Figure 16.

Flettner rotors are spinning vertical rotors that convert wind power into propulsive energy. These rotors operate according to the Magnus effect. The Magnus effect is the generation of a sidewise force on a spinning cylindrical or spherical solid immersed in a fluid when there is relative motion between the spinning body and the fluid [53]. Talluri et al. [54] applied a techno-economic and environmental assessment methodology in order to assess the performance and economic benefits that may be gained when using Flettner rotors. Their results show that the economic viability of the towers was still significantly dependent on the wind conditions and tower dimensions. Besides this, it was found that the wind direction has a larger impact on the performance than the wind speed, and that larger diameter towers provided a higher propulsive contribution. Nonetheless, the implementation of Flettner rotors on commercial vessels could result in up to 20% savings in term of fuel consumption, and similar values in term of emissions reduction.

In 2008, the German wind turbine manufacturer Enercon launched one of their ships with Flettner rotors. The *E-Ship 1* has 4 towers that are 27 meters tall and 4 meters in diameter, and the ship is shown in Figure 17a.

A recent example of a modern implementation of sails on ships is the DynaRig. The DynaRig is a modern square-rigger with free-standing and rotating masts. It was designed in the 1960s in Germany but was never built until 2001, when an American investor implemented these sails on his luxury yacht, the *Maltese Falcon*, using carbon fiber technology. The DynaRig masts are freestanding, meaning that the entire mast rotates in place to engage the wind angles. When fully deployed, the sails on each mast have no gaps between them. This sail is estimated to have twice the efficiency of a traditional square rig [55]. A more recent yacht that implemented these DynaRigs is Oceanco's Black Pearl, shown in Figure 17b.

Besides these 3, several other prototypes are being developed while this thesis is being written. One of these ideas which looks quite promising, is a concept designed by Eco Marine Power. This company designed Energy-Sails as renewable energy collectors, which incorporate both solar energy and wind energy into their innovative system [56]. This way, it can be used even when a ship is at anchor or in port. The flexible design of the EnergySail will also allow for it to be upgraded during the life-cycle of the ship so that newer technologies can be incorporated if required.


**Figure 16.** *Towing kite SkySails [52].*


**(a)** *The E-Ship 1, manufactured by Enercon and equipped with 4 Flettner rotors [57].*

**(b)** *Oceanco's Black Pearl, incorporating modern square rigs [58].*

### 2.2.6 Solar Energy

Photovoltaic (PV) systems such as solar panels absorb and convert sunlight into electricity, by means of using semiconducting materials which exhibit photovoltaic properties. This technology is quite mature and already largely developed for land use. However, it has an extremely low applicability on ships because of its low conversion factor and high investment cost. Due to its low conversion factor, quite a large amount of solar panels are needed to make this system economically viable. The inclination of the solar panel surface is highly associated with the geographical latitude. However, such an approach has no practical application on marine vessels. In order to maximize the solar plant efficiency, all solar panels should be placed above the deck of the vessel at zero angle. However, most ships do not have these large surfaces on board to place solar panels.

Whenever solar panels are used for the propulsion of ships, they are used in a hybrid system together with engines. The PV system is then often used as an auxiliary power source to drive electricity or auxiliary machinery equipment. Yu et al. [59] developed a coordinated control strategy of a hybrid ship which works with solar panels, lithium-ion batteries and a Diesel engine. From their case ship study it is found that, compared with conventional power systems, the emission of $CO_2$ is significantly decreased, as is the energy cost. This type of ship should be used mainly in areas with a high level of solar radiation, such as the Mediterranean Sea. Here, it has the highest reduction of operation cost, and the payback time for the initial investment (solar panels and battery packs) is 19 years. However, the result of only using batteries is also a profitable strategy, which may be used in less sunny areas.

Glykas et al. [60] examined the feasibility of installing solar panels onto vessels and also calculated the payback period from the adopted investment with respect to fuel oil savings. They concluded that the investment of PV systems is more profitable around the equator. The installed solar panels will produce the most energy here, which may be directly consumed for vessel needs. In some cases however, the solar energy production may exceed the momentary need of energy. In that case, a storage medium could be introduced. Batteries are the most common example of such a medium, yet they are also expensive and harmful for the environment. An alternative way is to store energy by electrolysis of water, through which hydrogen is produced. All the stored hydrogen can be either used in fuel cells or burned in an internal

combustion engine (ICE) , where the ICE is financially more beneficial. The cost-benefit analysis of Glykas et al. revealed that installation of PV systems on merchant marine vessels highly depends on the annual average increase of fuel oil. The higher this increase, the smaller the payback period of the investment, with a convergence period at a minimum value of about 10 years.

### 2.2.7 Cold Ironing

One of the main polluting issues in ports and harbours originates from ships which are berthed but still need their auxiliary engines for basic power functions such as heating, lighting and refrigeration. These densely populated areas suffer from the emissions of harmful pollutants coming from ships while loading or unloading their cargo. Cold ironing or alternative maritime power (AMP) is the process of providing shoreside electrical power to ships at berth in ports or harbours in order to reduce the harmful emissions by turning off the main and auxiliary engines. The extent of the reduction of harmful pollutants depends not only on the type of fuel used by the ship, but also the origin of the electricity generation onshore. Still, large reductions may be noticed since the power supplied from the national electricity grid is subject to stricter emissions control than power supplied from auxiliary engines [61]. The main disadvantage is once again the cost. Shoreside electricity is usually more expensive than electricity from burning fuel in auxiliary engines. Besides this, the infrastructure required to connect the ships to port is expensive as well. Due to ships being built in yards all over the world, no uniform voltage and frequency requirements exist. Cables and connectors depend on the ship's origin, and the cold ironing infrastructure has to be able to supply electricity to very different vessels, ranging from car carriers to reefers and cruise ships. A standard schematic of cold ironing is given in Figure 18.

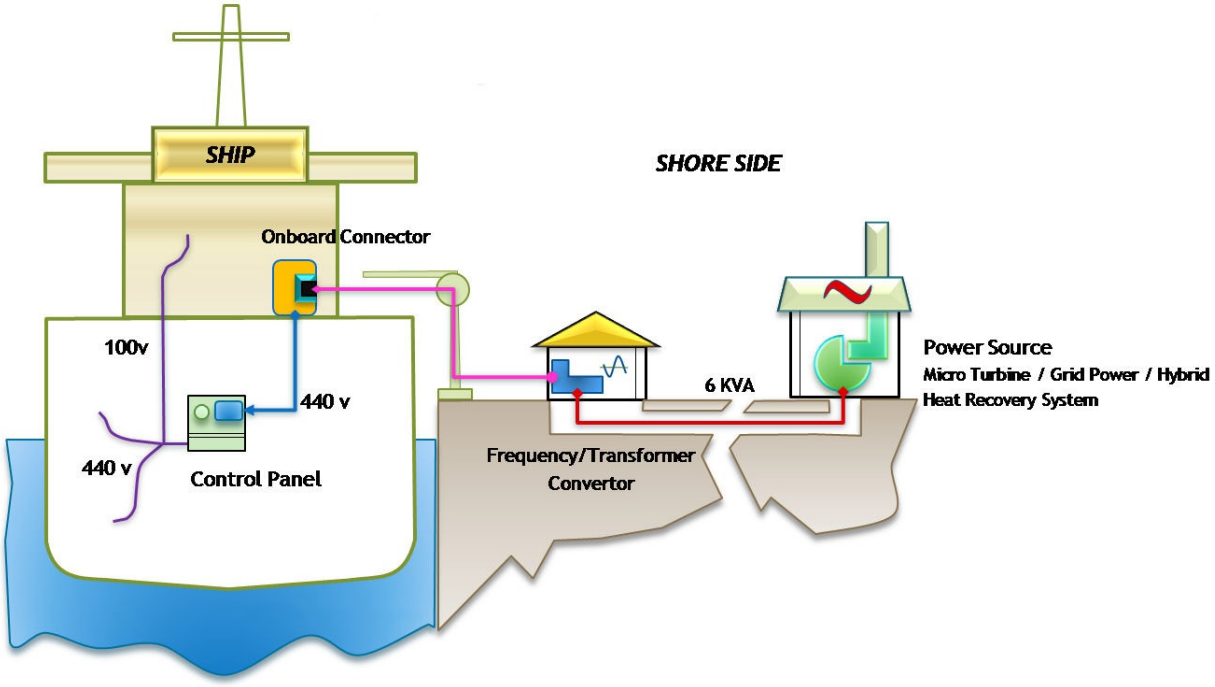


**Figure 18.** *Cold ironing schematic [62].*

In Californian ports the local regulation stipulates that terminal operators are required to be able to provide shorepower; in the EU this is not the case [63]. According to EU Directive 2014/94 [64], all European ports are required to have cold ironing provision by 2025. Ballini et al. [65] researched the socio-economic benefit of cold ironing and found that the implementation of this technology for cruise ships in Copenhagen could result in a 60% health cost benefit with a capital cost return balance of 12-13 years with respect to the infrastructure cost. Various other studies are being performed to change this and look at the socio-economic and technological benefits of cold ironing in Europe. Right now, it is one of the most promising technologies in substantially reducing emissions and fuel consumption during hotelling near densely populated areas.

## 2.3 Hull Design

The focus of hull design lies on the aspects which contribute to improving the hydrodynamic performance and minimizing the resistance. Besides this, the concept "economies of scale" is also discussed as increasing the vessel size reduces the emissions per unit transport work. By focusing on hull design measures, the drag can be reduced and thus the power necessary to sail the ship at the same speed is reduced as well. Additional smaller measures such as hull coating and air lubrication are briefly touched.

### 2.3.1 Vessel Size

Over the past decades, various ship types have continuously increased in size to meet the rising market demands. This replacement of smaller vessels by larger vessels can be termed "Economies of Scale". Although the maritime industry has done this from a cost-abatement perspective, the increasing vessel size has a potential benefit for emission reduction as well. Larger vessels which have an increased capacity will use more fuel than smaller vessels. The fuel consumption per tonne-km, and thus the emissions per tonne-km will decrease however, indicating that the total emissions will be less for a fleet of larger vessels compared to the same fleet of smaller vessels. Obviously when larger vessels are operating, less vessels will be required to transport the same amount of cargo. An example is shown in Figure 19, showing the evolution of $CO_2$ emissions per tonne-km for increasing bulk carrier types. The strongly decreasing trend of the yellow line can easily be noticed, with the emissions per tonne-km being more beneficial for increasing capacity.

Lindstad et al. [66] researched the importance of economies of scale and found that the emissions can be reduced by as much as 30% by replacing the existing fleet with larger vessels. Note that this replacement is done in a gradual way and thus it might take 25 years before the entire fleet is renewed. One of the main issues here is that most ports, harbours, locks and inland waterways/channels are not adapted to these large vessels. The infrastructure should change drastically, bringing with it large investment costs. Another fundamental problem is that these values are calculated for ships optimally using their capacity, i.e. always sailing at full load. Due to the increasing size of fleets all around the world, a situation of undercapacity ensues, meaning that the industry can not produce enough to fill every vessel optimally. Therefore, lots of ships will sail their routes filled below their capacity, meaning that more ships than necessary are used, thus increasing the emissions.

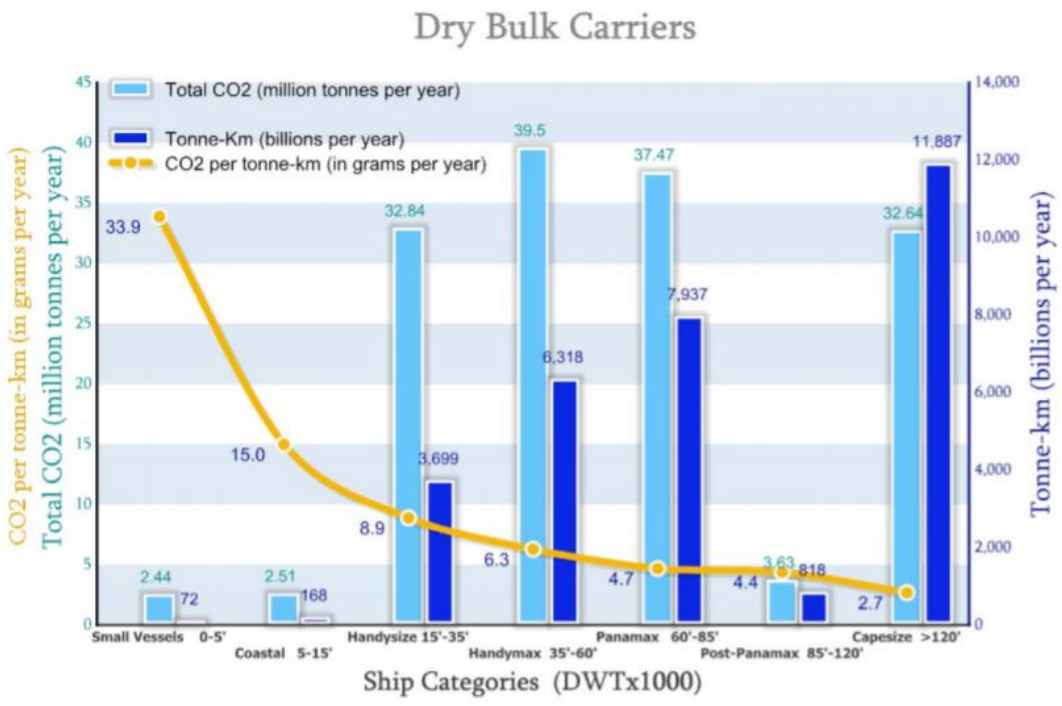


**Figure 19.** *Evolution of $CO_2$ emissions with an increasing ship size of bulk carriers [67].*

### 2.3.2 Hull Shape

In order to reduce the resistance of a ship sailing in waves, the shape of the ship can be optimised to minimise the drag encountered. An example which is already widely implemented is the use of a bulbous bow. The bulbous bow causes a significant reduction of the total resistance of a vessel, especially at high speeds, by cancelling out the pressure wave induced by the ship.

By designing ships with new dimensions, significant reductions may be noticed. Optimizing the length and block coefficient of the ship can lead to significant resistance reductions, which translates into a reduced fuel consumption. Lindstad et al. [68] investigated the effect of changing the ship's dimensions as a consequence to the expansion of the Panama Canal in 2013. For bulk vessels, a reduction of the block coefficient would lead to a more slender hull which is more energy-efficient. The decrease in emissions ranges from 15-25% for a Panamax 80,000 dwt bulk carrier capacity, with the highest reduction achieved by using the longest and widest of the alternative designs. A last example is the use of aft waterline extension, reducing the flow turbulence and thus reducing the fuel consumption possibly by 2-7% [69]. This mature technique is already widely available.

### 2.3.3 Lightweight Materials

A simple yet effective measure would be to replace the standard building material heavy steel with more lightweight materials to construct the hull. Examples such as high tensile steel and composite materials will drastically reduce the weight of the hull while maintaining the overall strength. This reduction in

weight will improve the fuel consumption and power necessary to propel the ship at the same speed as a ship incorporating a steel hull. Not only the hull, but also the superstructure can be constructed from these lightweight materials, thus reducing the weight even more. At present, lightweight materials are mainly used on high-speed vessels [70], although high-tensile steel is seeing an increase in use. The potential reduction in fuel consumption ranges from 2-7%. The implementation of these materials still encounter some structural problems, including fatigue and welding issues. Until these problems are resolved, the use of these lightweight materials will remain limited.

### 2.3.4 Air Lubrication

The concept of air lubrication consists of pumping air beneath the hull through very small outlets, creating small air bubbles and thus reducing the wetted area of the hull and creating an air boundary layer around the hull. This reduces the frictional resistance with an increasing effect as the air-layer thickness increases. The bubbles should remain small, generally less than 0.1 mm, to gain a more efficient effect and prevent the influence of turbulence on the bubble flow [71]. Fuel consumption savings of 5-15% are possible, however, a lot depends on the smoothness of the hull. Good and regular hull cleaning and maintenance is thus required to actually realize these savings in fuel consumption. This may increase the operational cost of this technology. An example is shown in Figure 20, showing the Mitsubishi Air Lubrication System.

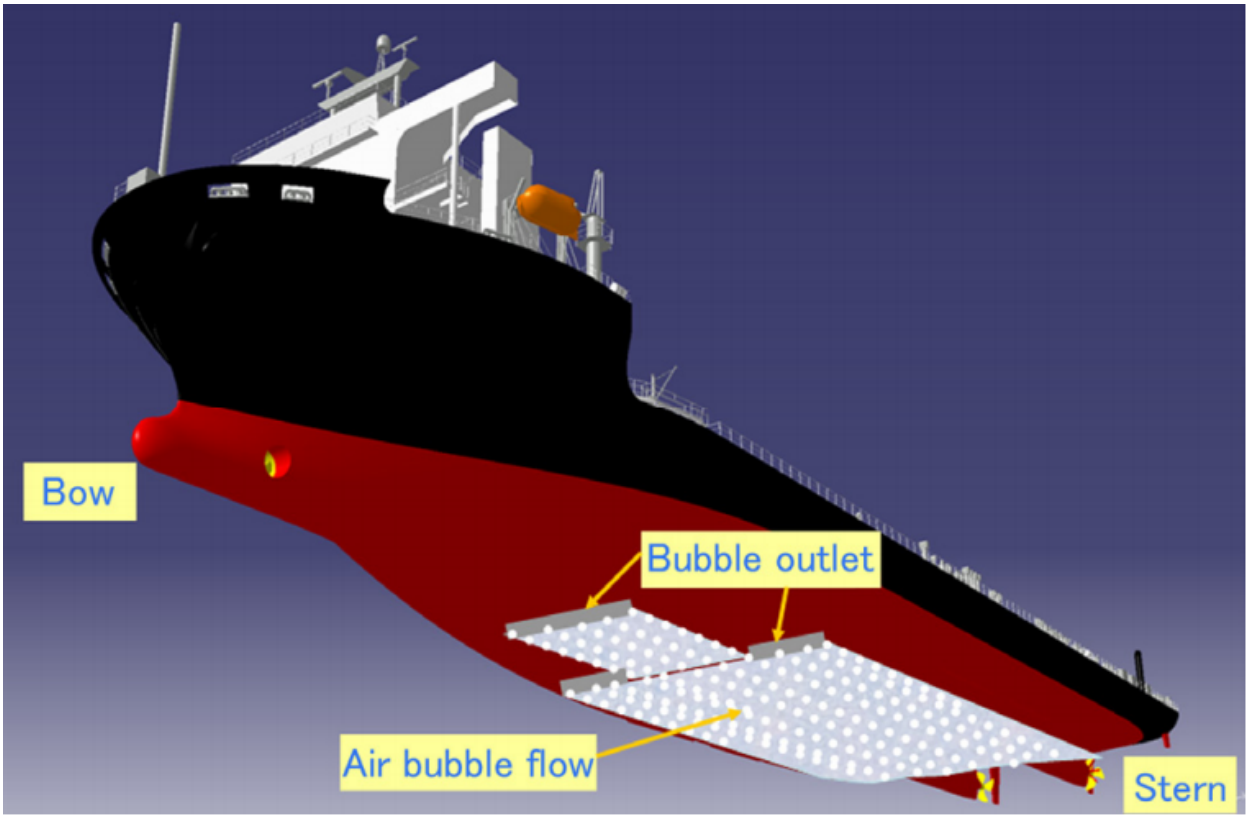


**Figure 20.** *Illustration of the Mitsubishi Air Lubrication System [72].*

### 2.3.5 Hull Cleaning and Propeller Polishing

During the sailing, hotelling and berthing of ships, marine plants and animals may settle and grow on the hull and propeller of the ship. This may be classified as "fouling". Besides the macrofouling of weeds and animals, microfouling of algae and bacteria also occurs. These growths on the hull structure increase the resistance of the ship significantly, causing the fuel consumption of the ship to increase as well. An example is shown in Figure 21, showing how the resistance may increase over time. To decrease the frictional resistance, cleaning of the hull is very important. Especially macro-fouling should be cleaned regularly to prevent significant increases in fuel consumption. Once in a while, drydocking will be necessary to give the hull an extensive cleaning and perhaps a new coating. Besides this, regular cleaning is also beneficial to prevent damage to the coating. The accurate time to clean can be based on performance monitoring or on regular under-water inspections [73].

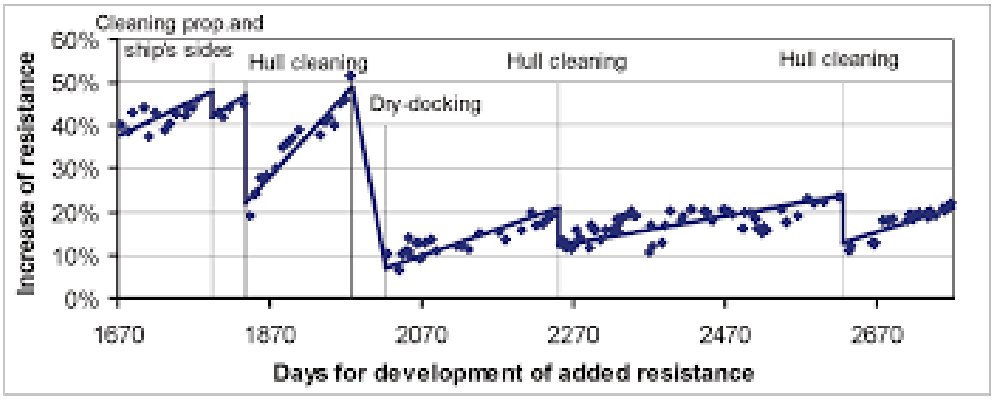


**Figure 21.** *Resistance development over time due to fouling and regular cleaning of the hull [74].*

Similar to the hull, propellers also suffer from the accumulation of organic materials and thus a decrease in performance. Corrosion and cavitation may also cause an increased roughness of the propeller, which may be treated by polishing. Polishing a roughened propeller surface may result in a decrease in fuel consumption of up to 3% [73]. This may be done at the same time as cleaning of the hull, but propeller monitoring should still be implemented to check if the propeller needs to be polished at intermediate times as well.

### 2.3.6 Hull Coatings

For large vessels sailing at low speeds, most of the resistance will come from skin frictional resistance on the hull. This may go from 40-90% depending on the type of vessel. This main contributor should be reduced as much as possible in order to save some fuel and thus repress the emissions and fuel costs. One way of reducing this frictional resistance is by applying a coating on the hull to increase the smoothness. These coatings prevent the fouling of the hull with the help of non-toxic chemicals which repel organic material. These coatings range from cheap, short-term coatings towards more advanced and expensive ones. A good coating should be re-applied once every 5 years during drydocking, since they disappear over time. The high end coatings are able to reduce the overall ship resistance up to 8%, with possible fuel savings of 1-5% [69]. The cost of applying such a coating may be quite high, but might quickly be equalized

by the savings in fuel costs due to the decreased resistance.

## 2.4 Operational Measures

The last part of this literature review concerns the implementation of measures for a ship or fleet during operation of the vessels. These measures impact the overall parameters of the vessel and its voyage such as the speed and the trajectory and thus do not directly require any fundamental technological changes. Many more exist but again only the most important ones were touched briefly in this section.

### 2.4.1 Slow Steaming

An effective yet easy countermeasure against the emissions of pollutants is slow steaming. Slow steaming involves the process of reducing the vessel's speed in order to save fuel and consequently also reduce emissions. This happens because the drag force imparted by a fluid increases quadratically with an increase in speed. A ship travelling twice as fast will need four times as much energy (fuel) for a given distance. This practice was first introduced by Maersk Line for its container ships. Besides the obvious primary reason of saving fuel, another reason for slow steaming is to match the arrival time to a slot opening at the port. Ships spent quite some time at ports, waiting at anchor due to several port delays. This results in congested ports and raises the risk of accidents while also emitting harmful substances.
Several studies have been performed concerning slow steaming and its environmental, social and economical effects. Chang et al. [75] investigated the fuel consumption and corresponding $CO_2$ emissions for international dry bulk carriers. Their results show that speed reductions of 10%, 20% and 30% reduce fuel consumption by 27.1%, 48.8% and 60.3% and $CO_2$ emissions by 19.0%, 36.0% and 51.0% respectively.

Although there are some serious environmental benefits, most ship owners remain opposed to (mandatory) slow steaming. The primary reason is the reduced market flexibility. A restriction on speed also increases the operational costs. This causes the speed reduction to not be cost-effective for all ship types or on all routes. Areas with mandatory speed reduction, such as inside ECAs, may also be counterproductive in the long end. Given the weekly service requirements shippers will, as mentioned earlier in Section 1.2, increase their speed outside of these areas, with increased fuel consumption as a consequence. Because of the dependency on bunker fuel price, slow steaming is only a short-term measure.
Besides these economic disadvantages, there is also the danger of possibly emitting more emissions than before. Ship engines are designed for optimal combustion at specific loads near the high end of their rated power. Reducing this load will lead to less optimal combustion and an increase in specific fuel consumption (SFC), which means an increase in the amount of fuel consumed per unit of power produced. Also, at lower rated power, a lower temperature is needed, which may lead to an increase in $NO_x$ and PM emissions, which are linked to human health concerns. A final disadvantage was researched by Tezdogan et al. [76] concerning slow steaming in the presence of waves and bad weather. There is a possibility of stability problems due to parametric rolling at lower speeds. In these adverse conditions, a ship needs to have sufficient power to easily sail away from this situation. This may not be the case while slow steaming. Therefore, more research needs to be conducted into these disadvantages and whether or not slow steaming is more than a temporary solution.

### 2.4.2 Ship and Weather Routeing

Due to the ever-increasing motivations and regulations to reduce carbon emissions, new ways need to be found to optimize the voyage of the vessel. Until recently, the economic objective of ship routeing was to minimize the total distance travelled, in order to reduce fuel costs and decrease the travel time. Weather routeing consists of planning an optimal trajectory where the fuel consumption is minimized, by predicting the weather (wind and waves) together with ocean currents in various parts of the planned sailing route. These weather factors may cause an increased resistance which influences the power needed to propel the ship. Besides this, weather routeing is also an important application regarding the safety of the crew and cargo, avoiding any unnecessary heavy weather conditions [77]. Therefore, an optimum will be necessary between the most fuel efficient route, the safest route and the quickest route. Depending on the ship size and type, the reduction potential for fuel consumption has been assessed between 0% to 5% for different segments of a voyage [78].

Weather routeing is only a subdivision of the grand scheme of ship routeing. As mentioned, an optimum between the most fuel efficient, the safest and the quickest route is wanted. Another element used here is a traffic separation scheme, aimed at the separation of opposing streams of ships by appropriate means and by the establishment of traffic lanes [77]. These schemes have already been adopted in most of the major congested shipping areas of the world. Because of this, numerous accidents and collisions may have been avoided. An example of a congested area and traffic optimisation is shown in Figure 22.

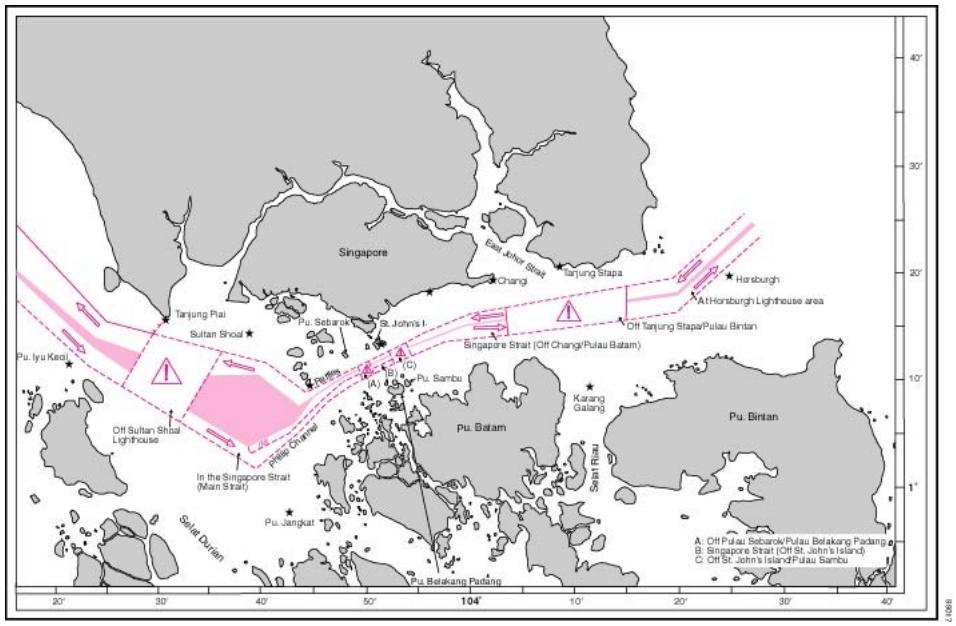


**Figure 22.** *Traffic separation scheme in the higly-congested shipping route near Singapore [77].*

### 2.4.3 Trim Optimisation

Trim optimisation is a quite recent development recommended by the IMO, which requires no modifications and can be achieved simply by management of the ballast water and load distribution. The captain

of the ship receives a guidance table for trim. Trim optimisation has a quite large influence on the performance, and hence the emissions of a ship. These dependencies can be explained because a change in trim causes [73]:

- Changes to wave resistance;
- Changes to frictional resistance;
- Changes to form resistance;
- Changes to propulsion coefficients such as resistance coefficients, thrust deduction and wake fraction;
- Changes to propulsive efficiencies including the relative rotative efficiency and the propeller efficiency.

Trim optimisation is applicable for all vessel types, although some may have more flexibility in applying this than others. Cruise ships for example are designed for passenger comfort and trim optimisation may have an adverse effect. Also, full-body ships will generally benefit less from trim optimisation due to the fact that the resistance is rather viscous-dependent than wave-dependent with these kind of ships. Since the significance of trim changes is a function of resistance, it is also a function of speed and draft. Every ship has an optimal trim range, which may be determined through extensive model testing or CFD analytical methods. This may then be implemented through the on-board computer with trim assistant software tools. With the help of these tools, fuel savings of up to 4-6% can be achieved [79]. However, these percentages are limited to calm water conditions. Du et al.[80] performed a study which overcomes this drawback and proves, with the help of numerical experiments, that the additional application of dynamic trim optimization at sea would always be beneficial and bring considerable fuel savings. In this study, optimization happens in two phases. In the first phase, the onshore officers plan the ship's sailing speeds during the voyage, while the captain at sea decides the changes in trim during the second phase based on the weather and sea conditions. 3 different solutions are proposed:

- Dynamic trim optimisation at sea, instead of using static trim tables and charts.
- Real-time trim optimisation at sea, as prescribed in the first option, while also allowing onshore officers to conduct speed optimisation with zero trim.
- Similar to option two, but sailing speeds and trim settings are optimized simultaneously during the onshore speed planning phase.

With the last option, bunker fuel savings of more than 8% are possible. Du et al. thus provide a tangible solution to fulfill fuel savings and mitigation of $CO_2$ emissions without any large modifications or operational costs.

# Chapter III

# Propeller-Engine Interaction

## 1 Overview

This chapter will describe the propeller-engine interaction of a standard commercial seagoing vessel equipped with a diesel engine. The engine delivers work by releasing the energy in the fuel with the help of combustion. This energy is partially converted to work at the crankshaft, which can be transferred to the propeller with the help of a shaft connecting these two parts. With the help of the work developed by the engine, the propeller delivers a force to the water. A reaction force, named thrust, is exerted onto the propeller, pushing the entire ship forward. The drivetrain is illustrated in Figure 23.

The resistance is described in this section as well. The resistance of a ship mainly consists of three components: viscous resistance, wave-making resistance and air resistance. Due to the fact that the propeller thrust is already assumed to be given in the following calculations, the resistant is not explicitly used in the calculations to determine the emissions. Nonetheless, it is still important background material on how a ship operates and it is directly related to the propeller thrust. In Section 4 this subject is investigated deeper with respect to shallow and confined water.

To have a better idea of the problem, i.e. the emissions of ships in shallow and confined water, some more information is given regarding ship operation in shallow and confined water. The latter has an effect on the resistance and propulsion of a ship.

The final part of this chapter consists of creating a mathematical model on how to calculate the emissions of the engine. While a ship is designed by choosing its engine, calculating the engine output and obtaining the thrust at the chosen propeller, the mathematical model will work backwards. The emissions are obtained from the vessel speed and propeller thrust by working back from the propeller along the shaft line towards the engine.

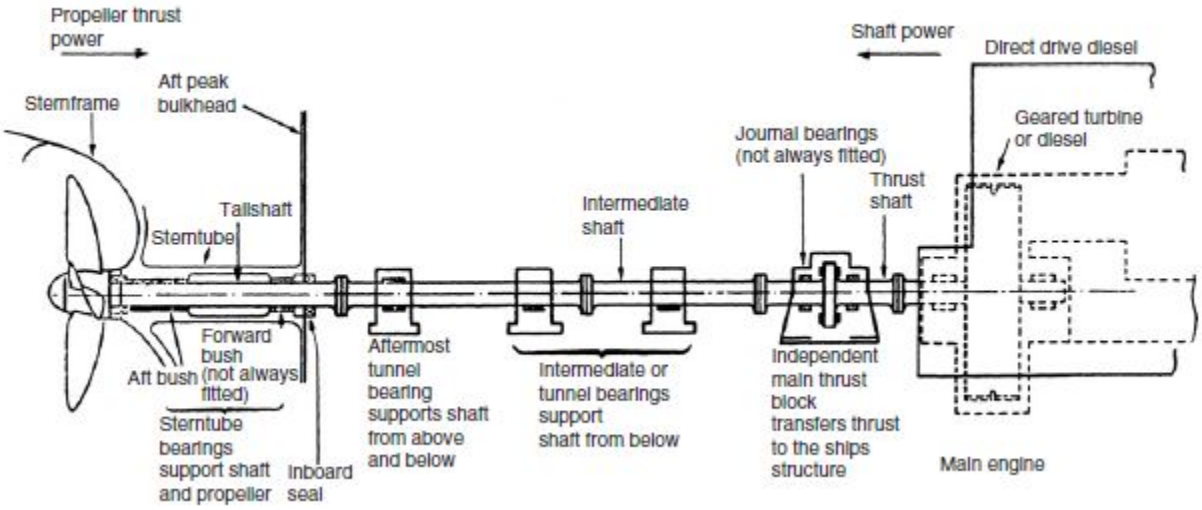


**Figure 23.** *The drivetrain of a ship [81].*

# 2 Drivetrain

## 2.1 Propeller and Propeller Curve

The propeller is the connection in the drivetrain between the shaft and the water. It converts the rotational power into linear thrust which propels the ship forward. Most of the propellers are designed according to a certain standard series such as Wageningen or Gawn series [82]. For commercial seagoing vessels, a Wageningen B-series propeller will be the most common. Slow vessels like bulk carriers and container ships are mostly implemented with a fixed-pitch propeller. This means that the pitch of the propeller is given and cannot be changed in operation. A controlled-pitch propeller may be useful when a high degree of manoeuvrability is necessary. However, this is much more expensive and not really necessary for these types of ships since they sail for a long time at sea with nominal load service.

When designing a ship and its propulsion system, the propeller and the engine characteristics need to match. This means that two criteria should be fulfilled: the engine should be able to develop its maximum power near the design condition, and the engine should be able to develop the required power in all operation states. On top of this, fuel consumption should be optimised.
The effective power $P_e$ of the engine is equal to:

$$P_e = c \cdot p_e \cdot n \tag{4}$$

where $c$ is a constant, $p_e$ the mean effective pressure and $n$ the engine speed.

For a constant mean effective pressure, the power is thus proportional to the speed:

$$P_e = c_p \cdot n \tag{5}$$

The power required to drive the propeller is a function of the resistance encountered by the ship. This resistance force varies quadratically with the ship's speed for lower speeds:

$$P_e = R \cdot V = c_V \cdot V^2 \cdot V = c_V \cdot V^3 \tag{6}$$

When running with a fixed pitch propeller and neglecting slip, the ship's speed is a function of the engine speed. The required power may be expressed according to the propeller law [82] as:

$$P_e = c_n \cdot n^3 \tag{7}$$

The exponent three is valid for frictional resistance. For vessels having sufficient engine power to sail fast enough to experience significant wave-making resistance, the exponent may be higher in the high-load range. For low-speed ships like tankers and bulk carriers, a more reasonable relationship is given by in [83]:

$$P_e = c_n \cdot n^{3.2} \tag{8}$$

These power functions will be linear functions when using logarithmic scales. The propeller curves will be parallel to lines having an inclination $i = 3$. Therefore, in the layout and load diagrams of diesel engines, logarithmic scales are often used, giving simple diagrams with straight lines. An example of a layout diagram with propeller curves is given in Figure 26 in Section 2.3.

In general, the necessary propeller power and speed are estimated based on calculations assuming optimal operating conditions such as a clean hull and nice weather. The propeller curve that responds with an optimal combination of speed and power is the light running curve. This necessary power depends on several factors such as weather conditions, hull fouling, operating conditions, etc. Generally, the more severe these factors become, the larger the ship resistance is. A larger power will thus be necessary to propel the ship. This is translated in the heavy running propeller curve. The engine must allow this and thus has to make sure that all possible propeller curves are within the allowable range on the engine load diagram. A light running margin of 4-7% is usually advised for propeller design [84]. This means that the propeller can be up to 7% heavier running than in calm weather, i.e. at the same propeller power, the rate of revolution may be 7% lower. An example is shown in Figure 24, where a ship is sailing in heavy seas and head wind with a fouled hull. The increase in resistance for this condition is much greater, corresponding to an extra power demand of maybe even over 100%.

When sailing in shallow waters, the residual resistance will increase due to the increased difficulty of the water under the ship moving aftwards. This will also cause the propeller to be heavy running, since the increased residual resistance will cause the propeller to be subjected to a larger load than during free sailing [83].

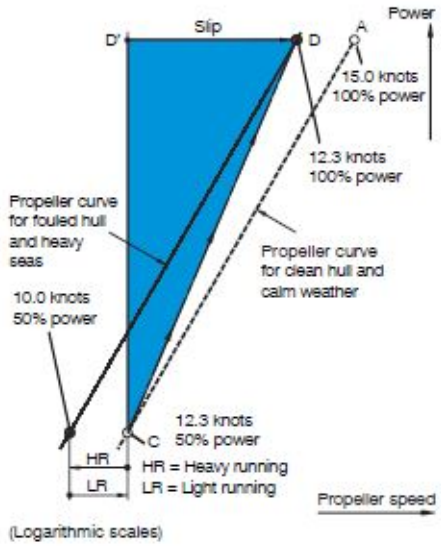


**Figure 24.** *The propeller speed performance at a large extra ship resistance [83].*

## 2.2 Shaft Line

The shaft line, also known as the transmission system, transmits the torque produced by the engine to the propeller, where thrust can be developed. This shaft line must be supported at points along its length and the whole arrangement must be designed to absorb and compensate for the forces that will be acting upon it. This is done with the help of several bearings and a thrust box. The purpose of this thrust box is to transmit the propeller torque into the ship's structure and to reduce the axial movement of the shaft line. This way, damage is prevented. The bearings support the shaft and aid in transferring these forces to the structure as well. Besides this, they also form a measure against misalignment of the shaft. The thrust block and bearings can be seen in Figure 23.

In general, in any shaft line there are three power definitions:

- Brake power $P_B$: power delivered at engine coupling/flywheel;
- Shaft power $P_S$: power available at output coupling of the gearbox;
- Delivered power $P_D$: power available at the propeller after deducting bearing losses.

Typically, the delivered power $P_D$ is 1-2% lower than the shaft power, depending on the length of the shaft and the number of bearings [82].

## 2.3 Engine

The engine is probably the most important part regarding the propulsion of a ship. Most commercial vessels nowadays are equipped with diesel engines. They burn fuel to create thermal energy which is then transformed into mechanical energy. A two-stroke engine, which will be used in this dissertation's case study, finishes the complete sequence in two cycles:

1. Suction and compression stroke. While the air intake ports are uncovered, pressurized air fills the cylinder. An upward movement of the engine piston compresses the air-fuel mixture.

2. Power and exhaust stroke. The highly compressed air ignites inside the chamber. The force of this combustion causes a downward movement of the piston followed by the removal of the exhaust gas. This transverse motion is then transformed into a rotary motion at the crankshaft.

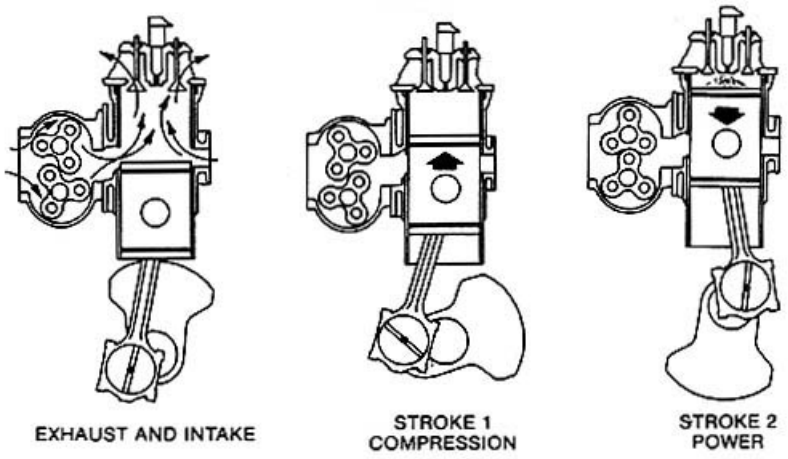


**Figure 25.** *The working principle of a 2-stroke engine [85].*

**Engine layout diagram**

A standard engine layout diagram is shown in Figure 26. It is characterised by two constant mean effective pressure (MEP) lines $L_1$-$L_3$ and $L_2$-$L_4$, and by two constant engine speed lines $L_1$-$L_2$ and $L_3$-$L_4$. The $L_1$ point refers to the engine's nominal maximum continuous rating (NMCR). The area confined by these lines delimit the freedom to select a combination of engine power and speed to indicate an optimal operating point for the ship. The axes are shown in logarithmic percentage scales. The advantage of this is that exponential curves like the propeller curves are displayed as straight lines.
In this diagram, several engine running points can be defined. For example, the maximum continuous rating (MCR) is defined as the required rating to enable continuous operating of the engine. Overload (e.g. 110% of MCR) is only permissible for about one hour every twelve hours. The specified MCR point for propulsion (MP) must be inside or on the edge of the diagram. If this is not the case, another engine or propeller speed must be chosen. The continuous service rating for propulsion (SP) is the power at which the engine is normally assumed to operate.

The lines numbered with 2 and 6 in Figure 26 are a heavy running and a light running propeller curve, respectively. At the light running curve, the combination of speed and power which is then obtained is called the ship's propeller design point (PD). In order to translate the propeller design point to the specified MCR for propulsion, two margins are needed.
The sea margin represents the extra power necessary due to the increase in resistance when sailing in bad weather with headwind. This margin helps to maintain the design speed in average conditions at sea. It is usually about 15% of the power required to achieve design speed in normal conditions [83].

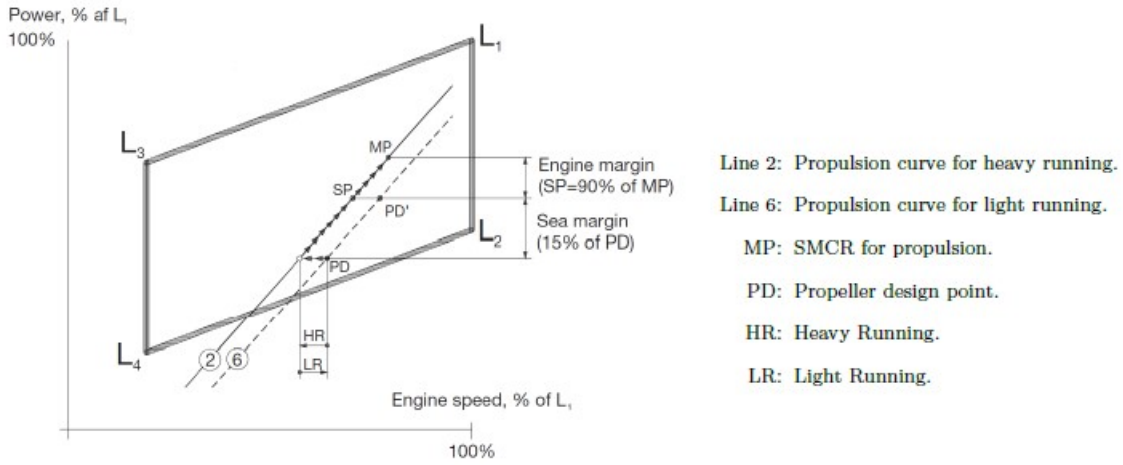


**Figure 26.** *Engine layout diagram in logarithmic scales [84].*

When sailing at design speed, it is undesirable to have a power utilisation of 100%. In order to lower the fuel and maintenance costs and to have some reserve power for increased speed, an engine margin of 10% of the MCR is added [83]. Adding this on top of the sea margin results in the specific MCR for propulsion. Unless a generator is installed on the main engine shaft, the propulsion SMCR is equal to the MCR.

**Engine load diagram**

The engine load diagram defines the power and speed limits for continuous as well as overload operation of an installed engine having a specified MCR point that corresponds to the ship. In the example of Figure 27, this point is represented as M.
Lines 1, 2 and 6 are various versions of the propeller curve. The propeller curve described by line 1 goes through the specified MCR and can thus also be described as the engine layout curve. Lines 2 and 6 are respectively the propeller curves for heavy and light running. The service range of this engine is limited by four lines: 4, 5, 7 and 3 (9). Line 4 is the torque/speed limit, which exists due to the lack of oxygen during combustion. Line 5 represents the maximum MEP level which can be accepted for continuous operation, while line 7 is actually the maximum power limit for continuous operation. Line 3 and 9 are both maximum speed limits. However, line 9 is only used for sea trials. Lastly, line 8 represents the overload limitations. The engine also has a low load running limit, equal to 15-20% of the nominal MCR speed.

During operation, these limits are used in various circumstances. The area enclosed by lines 1, 3 and 7 is used for continuous operation without limitation. On the other hand, the area between lines 4, 5, 7 and 8 is the overload operation area, which may be used for 1 hour every 12 hours. The area between 1, 4 and 5 is available for non-steady operation without any strict time limitation. This includes heavy weather, acceleration and sailing in shallow waters.

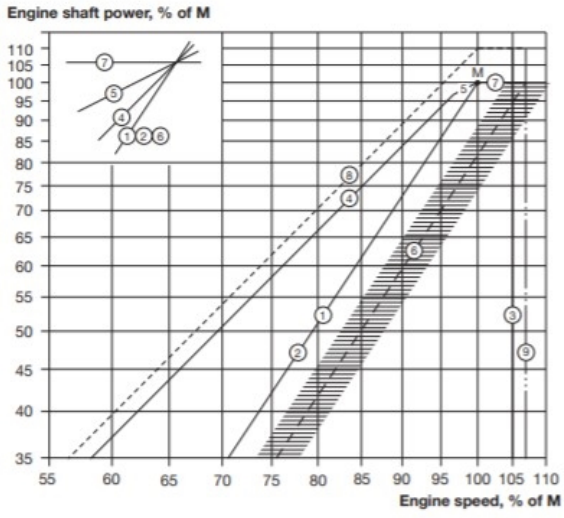


*Regarding 'i' in the power function $P = c \times n^i$, see Section 2.01.*

*M Specified MCR point*

*Line 1 Propeller curve through point M (i = 3) (engine layout curve)*
*Line 2 Propeller curve, fouled hull and heavy weather – heavy running (i = 3)*
*Line 3 Speed limit*
*Line 4 Torque/speed limit (i = 2)*
*Line 5 Mean effective pressure limit (i = 1)*
*Line 6 Propeller curve, clean hull and calm weather – light running (i = 3), for propeller layout. The hatched area indicates the full recommended range for LRM (4.0-10.0%)*
*Line 7 Power limit for continuous running (i = 0)*
*Line 8 Overload limit*
*Line 9 Speed limit at sea trial*

**Figure 27.** *Engine load diagram for an engine specified with MCR on the $L_1/L_2$ line of the layout diagram (maximum MCR speed) [84].*

## 3 Ship Resistance

When a ship is moving through water, it experiences a force acting opposite to its direction of motion. This "resistance force" must be overcome by the propeller thrust in order to propel the ship forward. The total resistance $R_T$ is particularly influenced by the speed, displacement and hull form of the vessel in deep water. It consists of several factors which affect the ship resistance separately and can be split in:

$$R_T = R_V + R_W + R_A \tag{9}$$

where: $R_V$ [N] is the viscous (friction) resistance;
$R_W$ [N] is the wave-making resistance;
$R_A$ [N] is the air resistance when moving through calm air.

The calculation or measurement of resistances is often done by means of dimensionless resistance coefficients $C$. In practice, the resistance of a ship can be measured by sailing a model ship in a towing tank or obtained numerically by CFD. These dimensionless coefficients then allow to compare model test data to full-scale ship data. For example, the coefficient of total hull resistance is found as:

$$C_T = \frac{R_T}{\frac{1}{2}\rho \cdot S \cdot V^2} \tag{10}$$

Where: $\rho$ [kg/m$^3$] The fluid density;
$S$ [m$^2$] The wetted surface area of the hull;
$V$ [m/s] The speed of the ship.

Besides this, the use of the Froude number of Equation 11 as a dimensionless coefficient is quite common as well.

$$F_n = \frac{V}{\sqrt{gL}} \tag{11}$$

with $L$ the length of the ship in meter.

Figure 28 shows how the magnitude of each component of resistance varies with ship speed for a bulk carrier. At low speeds the viscous resistance is the main factor, while at higher speeds the wave-making resistance dominates completely. The air resistance is a relatively small component for ships as bulk carriers and tankers, while it can become quite large with container ships. Each of these resistances will be treated in more detail in the following sections.

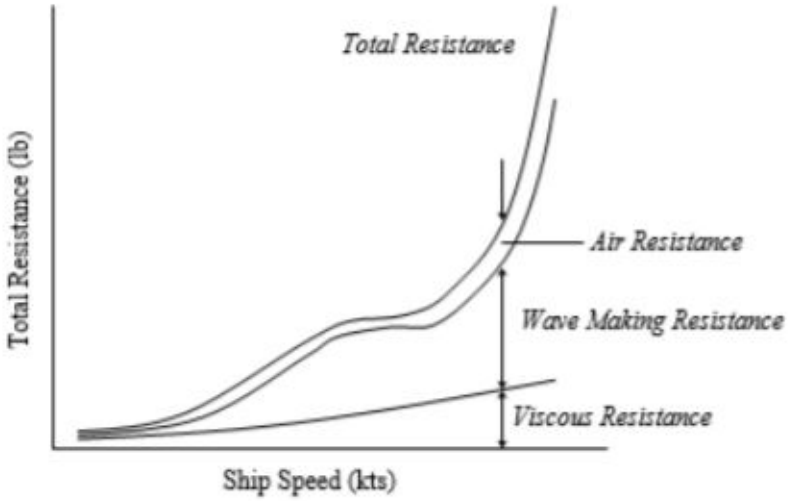


**Figure 28.** *Visualization of the fluctuation of the resistance components with speed [86].*

## 3.1 Viscous Resistance

When a ship is moving through water, a boundary layer is created over the surface of the underwater body. The presence of this boundary layer and its growth towards the aft of the ship modifies the pressure distribution acting on the body. Two forms of resistance as a result of viscosity exist, being the friction resistance and the viscous pressure resistance.

The friction resistance works on the bare hull and on its appendages, and arises from the shear stresses in the non-ideal fluid. This resistance force acts tangential to the body and causes a net force opposite of the ship's motion, acting over the entire submerged hull. When the ship is moving, this frictional resistance increases at a rate quadratically dependent on the speed.

The viscous pressure resistance acts normal to the submerged body. In an inviscid fluid, this normal pressure would result into a zero net force over the complete body [86]. However, due to the boundary layer which exists in a viscous fluid such as water, the forward acting component of pressure acting in the aft part of the ship is reduced significantly. This results in a net resistance force known as form drag. As the name suggests, this form drag is also strongly dependent on the form of the underwater body.

The friction along the hull due to the viscous resistance increases with fouling and with an increased dis-

placement of the vessel. For ships which sail at lower speeds such as bulk carriers, this friction represents the dominant part of the forces, with values up to $70 - 90\%$ of the ship's total resistance.

## 3.2 Wave-making Resistance

A ship can be modelled as a system of pressure points moving through the water. These pressure points cause a very specific wave pattern when moving through a free surface. This *Kelvin* wave pattern consists of a set of transversal waves and a set of diverging waves. These are visualized in Figure 29. The system is located within two lines through the pressure point which make an angle of 19°28' with the direction of motion [73]. The interference between these two sets of waves creates the characteristic shape of the waves.
Since the making of waves requires energy, the height of these waves decreases strongly with increasing distance from the pressure point. As the ship speed increases, the height increases and therefore the energy required to make these wave systems increases as well.

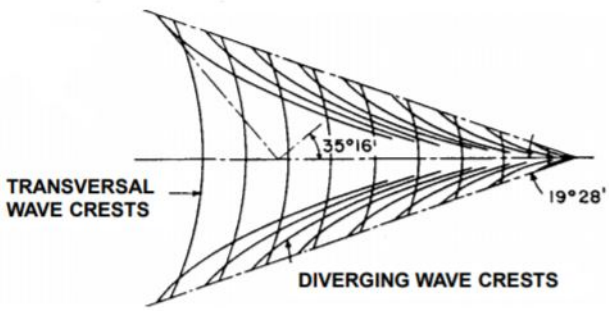


**Figure 29.** *Kelvin wave pattern: transversal and divergent waves originating from a pressure point [73].*

For a ship, the most important pressure point systems are the bow, the fore shoulder, the aft shoulder and the stern. These result in an over- or underpressure near the hull. They can have both a cancelling or an enhancing effect on each other, called interference between the different wave systems. The result of these systems is given in Figure 30. This interference depends on the combination of wave length and the length of the ship. This explains the existence of humps in the resistance curve of Figure 28. At low speeds, the wave resistance is proportional to the square of the speed, while it can reach a much higher dependency at higher speeds. It can be reduced by increasing the ship length or incorporating a bulbous bow into the ship design [86].

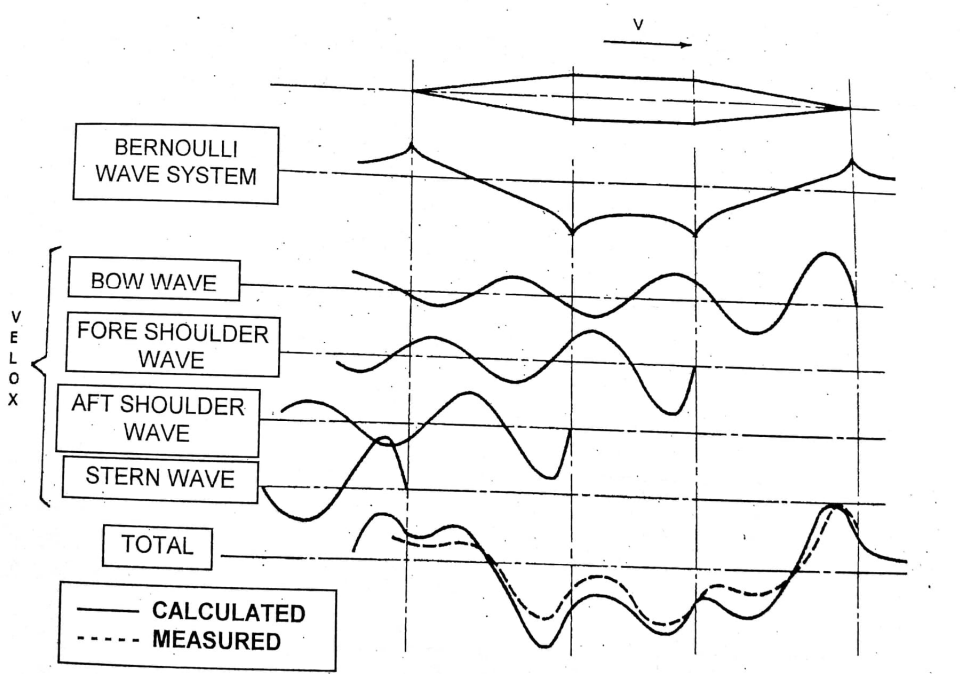


**Figure 30.** *A wave system composed of several waves in specific pressure points for a simplified, angular ship shape with infinite draft [73].*

### 3.3 Air Resistance

The air resistance depends on the weather (i.e. wind and waves) and on the windage area. It also has a quadratic dependence on the speed of the vessel in calm weather. The prediction of this resistance can be done in several ways, ranging from a simple calculation to a series of model tests in a wind tunnel. At its simplest, the still air resistance can be estimated as proposed by *Holtrop* [87]:

$$R_A = \frac{1}{2}\rho_a \cdot V \cdot A_a \cdot C_a \tag{12}$$

in which $\rho_a$ is the air density, $A_a$ is the transverse area of the ship subjected to wind and $C_a$ is the air resistance coefficient. For low-speed ships such as bulk carriers and tankers, air resistance normally represents about 2% of the total resistance.

## 4 Shallow and Confined Water

Before a mathematical model of the emissions in shallow and confined water can be constructed, it is important to understand what shallow and confined water is. The drivetrain and its most important theoretical aspects have been covered in Section 2. In this section, shallow and confined water and its influence on the resistance and propulsion of the ship are discussed.

## 4.1 Definition

Inland waterways, together with ports and their approach channels, are often less suitable for seagoing vessels. Due to their constant increase in size, these vessels encounter an important problem when attempting to sail through inland waterways, due to their limited width and depth.

To distinguish between deep and shallow water, the Permanent International Association of Navigation Congresses (PIANC) defines shallow water based on the water depth $h$ to draft $T$ ratio [88]. Another way of classifying this is with the term under keel clearance (UKC). The UKC is the vertical distance between the bottom of the hull and the bottom of the sailing water. This clearance should be sufficient to ensure the ship's safety in unfavourable conditions (e.g. storms and low tide). Regarding the hydrodynamics and manoeuvrability of a vessel, the water depth is assumed to be deep or of "infinite depth" when a $\frac{h}{T}$-ratio of 3 is reached, or in other words, with a UKC of 200% of the ship's draft. Shallow water occurs with a water depth to draft ratio smaller than 1.5, while in extreme cases, very shallow water may occur as well. These water depths, as a function of the $\frac{h}{T}$-ratio, are defined in Table 3.

**Table 3.** *Deep to shallow water as $h/T$-ratio and in terms of UKC [88].*

| $\mathbf{3.0 \leq h/T}$ | deep | $\mathbf{300\ \% \leq UKC}$ |
|---|---|---|
| $\mathbf{1.5 \leq h/T \leq 3.0}$ | medium deep | $\mathbf{150\ \% \leq UKC \leq 300\ \%}$ |
| $\mathbf{1.2 \leq h/T \leq 1.5}$ | shallow | $\mathbf{120\ \% \leq UKC \leq 150\ \%}$ |
| $\mathbf{1.0 \leq h/T \leq 1.2}$ | very shallow | $\mathbf{100\ \% \leq UKC \leq 120\ \%}$ |

Restricted water is when a waterway is limited by boundaries in the horizontal sense. These banks or horizontal edges of the waterway introduce additional hydrodynamic forces which have to be taken into account. This bank effect is limited until a certain horizontal reach. Beyond this reach, no significant influence of the bank on the ship is to be expected. A systematic series of tests was conducted at the Towing Tank for Manoeuvres in Confined Water at Flanders Hydraulic Research (FHR) in Antwerp, Belgium (in cooperation with Ghent University) to define a (speed dependent) expression of the horizontal reach [89]. A ship model of a tanker was towed in an "empty" towing tank (only water) at different speeds, water depths and lateral positions. For each combination of speed and water depth, the measured variables were plotted as a function of the distance between the ship's centreline and the closest wall. These tests eventually determined 3 ranges, going from a negligible to a significant influence of the bank on the ship. These results showed the dependency of the influence of bank effects on the depth based Froude number $Fr_h = \frac{V}{\sqrt{gh}}$.

$$y_{infl} = 5 \cdot B \cdot (Fr_h + 1) \tag{13}$$

This may be considered as the width of the influence zone for bank effects.

The combination of shallow water and restricted water is defined as confined water. This definition is applicable to inland waterways most of the time, especially in Belgium.

## 4.2 Influence on Resistance

In order to navigate a ship, it has to overcome the total resistance, mainly caused by the hydrodynamic pressure distribution around the hull. This hydrodynamic part may be subdivided in the viscous resistance, caused by the viscosity of the fluid, and a wave-making resistance, which is the result of the presence of a free surface. These components are quite sensitive to the effects of shallow water.

### Viscous Resistance

The viscous resistance is a net force acting opposite to the relative motion of the ship with respect to the surrounding water volume. The flow around the submerged part of the hull attains a three-dimensional character for deep water. In the case of confined water, the bottom proximity causes an increase in potential flow due to the restricted area around the hull. This represents itself into a more two-dimensional flow character [89]. As a consequence, the flow will reach larger velocities along the ship than in a more 3-dimensional case which yields an associated decrease in pressure. This higher relative velocity of the ship's hull will result in an increased frictional resistance, absolute trim and sinkage. If the waterway is restricted in the lateral sense as well, these effects are amplified. Because these effects are strongly related to the velocity, the speed will be limited in shallow water to reduce the risk of grounding.

A simplified manner to formulate the increase of viscous resistance due to shallow water is defined with the help of the form factor $k$. This form factor, first used by *Hughes* [90], is defined such that $1 + k$ equals the ratio of the hull viscous resistance to the flat plate frictional resistance. This term is very useful for resistance calculations, since the factor $(1 + k)$ is assumed constant for both ship and model. In other words, it generally is independent of speed and scale in the calculation of the resistance. The viscous resistance may be written as:

$$R_V = (1 + k)R_F \tag{14}$$

with $R_F$ the frictional resistance. *Millward* developed an empirical formula for the form factor in shallow water [89]:

$$k_h = k_\infty + 0.644\left(\frac{T}{h}\right)^{1.72} \tag{15}$$

Where $k_h$ and $k_\infty$ are form factors for resistance in finite and infinite water depth.

### Wave-making Resistance

The second effect that shallow water has on the resistance is caused by the changes in wave pattern which occur in passing from deep to shallow water. The length $\lambda$ and period $T$ of a regular wave are linked through the dispersion relation:

$$k \cdot tanh(kh) = \frac{\omega^2}{g} \tag{16}$$

With $k = \frac{2\pi}{\lambda}$ the wave number and $\omega = \frac{2\pi}{T}$ the angular frequency. This implies that the phase velocity $c_w$ of a regular wave with wave length $\lambda$ will depend on the local water depth $h$:

$$c_w(h) = \sqrt{g\frac{\lambda}{2\pi}tanh(\frac{2\pi}{\lambda}h)} \tag{17}$$

For a given wave length, the phase velocity will decrease with decreasing water depth. For small values of $h/\lambda$, the phase velocity approaches $\sqrt{gh}$, while for larger values $c_w(h) = c_w(\infty)$ at infinite water depth. It may be concluded that the wave has a limiting value in shallow water, coherent with the critical velocity $\sqrt{gh}$. If the ship velocity equals this critical velocity, the transverse waves in the wave system disappear, leaving only diverging waves.

Havelock [91] investigated the effect of shallow water on the wave-making resistance and the wave pattern for a pressure disturbance of linear dimension $l$ travelling over water of depth $h$. The resistance curves are shown in Figure 31 for different $h/l$ values.

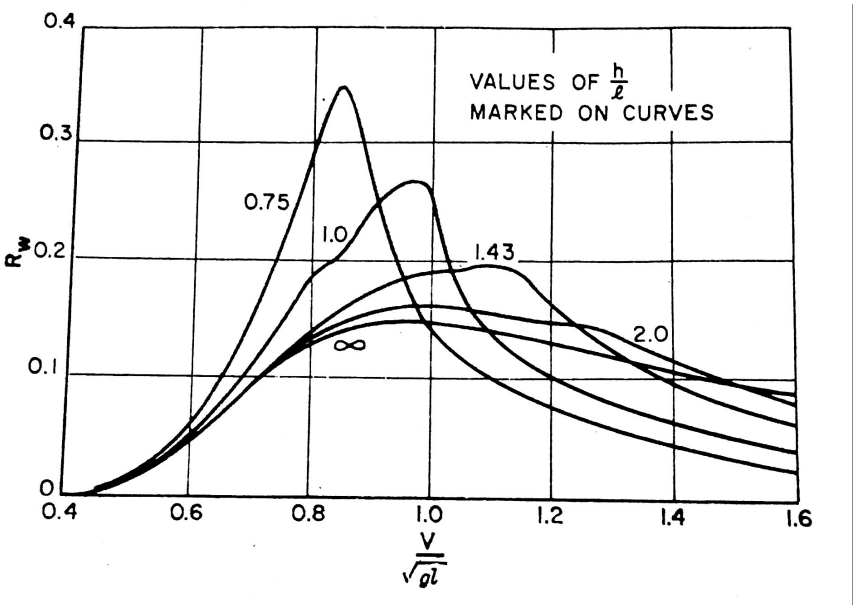


**Figure 31.** *Effect of shallow water on wave resistance ($R_W$: wave resistance ; $l$: characteristic length) [91].*

From Figure 31, it is clear that a peak resistance is reached for a $Fr_h$ value of approximately 1 [89], which is much larger than the resistance value in deep water. However, at sufficiently high speed the resistance in shallow water becomes less than in deep water. These supercritical speeds are not achievable with a normal screw propeller.

## 4.3 Influence on Propulsion

### Open water effects

In order to investigate the effects of shallow water on the open water characteristics of a propeller, *Harvald* (1976) developed several model tests for different water depth - propeller diameter ratios. For normal propeller loadings at constant propeller rotational speed, the effects are quite small and result into an

improved propeller efficiency in shallow water. This is shown in Figure 32 for a propeller going ahead. However, this improvement is only apparent. The propeller loading will increase as well, while the velocity of the ship decreases, due to the increased resistance and increased values for the wake and thrust factors [89].

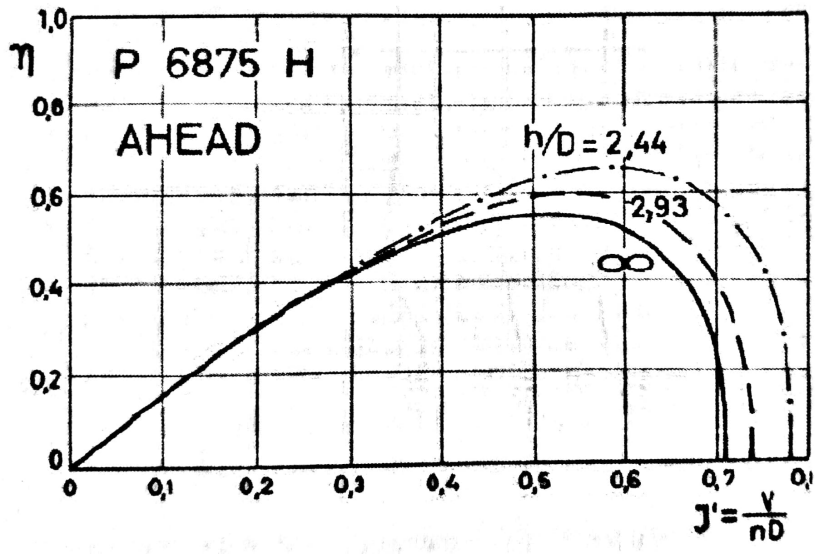


**Figure 32.** *Propeller efficiency curves for propeller going ahead for different water depth to propeller diameter ratios [89].*

### Wake fraction, thrust factor and hydrodynamic propeller efficiency

When a ship is moving, the friction of the hull will create a boundary layer of water around the hull. The thickness of this friction belt increases with its distance from the fore part of the ship, with a maximum at the aft part. This causes the propeller to be working in a wake field, mainly originating from this friction wake. The wake fraction is defined as the difference in speed between the speed $V$ of the vessel and the speed of advance $V_A$ of the propeller relative to the water:

$$w = \frac{V - V_A}{V} \tag{18}$$

For ships sailing with one propeller in normal conditions, the wake fraction $w$ will attain values between 0.20-0.45, corresponding to a flow velocity to the propeller $V_A$ of 0.80 to 0.55 of the ship's speed $V$. *Taylor* derived an expression as a first estimate depending on the block coefficient [92]:

$$w = 0.50C_B - 0.05 \tag{19}$$

The wake fraction depends largely on the shape of the hull, as well as the size and position of the propeller. It affects the efficiency of the propeller quite significantly. When sailing in shallow water, the presence of the bottom and walls will affect the flow around the ship, resulting in changes of the flow at the stern of the ship. Because of this, the local wake fraction will increase with a decreasing water depth.

When a self-propelling ship is sailing with a speed $V$, the pressure field around the hull changes due to the action of the propeller. The water in front of the propeller tends to be "sucked" back towards it. The velocities of the flow over the hull surface increase and thus the local pressure field decreases. The thrust $T_P$ required to propel this ship will be greater than the total resistance $R_T$ when it is towed at the same speed. This resistance increase can also be considered as a "loss of propeller thrust". This fraction of the thrust is called the thrust deduction factor $t$:

$$t = \frac{T_P - R_T}{T_P} \tag{20}$$

*Taylor* made an estimate of the thrust deduction factor $t$ by relating it to the wake fraction $w$ [92]:

$$t = 0.6 \cdot w \tag{21}$$

Thus the thrust deduction factor will also increase with a decreasing water depth.

The hydrodynamic propeller efficiency $\eta_P$ is defined as the ratio of thrust power $P_T$ and the power delivered to the propeller $P_D$:

$$\eta_P = \frac{P_T}{P_D} \tag{22}$$

With the thrust power given by

$$P_T = (1 - w) \cdot V \cdot T_P \tag{23}$$

With $T_P$ the thrust developed at the propeller. The propeller power $P_D$ is defined as:

$$P_D = 2 \cdot \pi \cdot n \cdot Q_P \tag{24}$$

With $Q_P$ the torque at the propeller.

When sailing in shallow water, assuming a solid ground absent of mud, the thrust $T_P$ increases slightly with decreasing under keel clearance. A stronger increase however is observed with the torque $Q_P$. The cause of this torque increase is mainly the increased resistance and slower speed at small under keel clearances. When this is reflected on the hydrodynamic efficiency, it is clear that the overall efficiency decreases significantly with a decreasing under keel clearance. This is also shown in Figure 33.

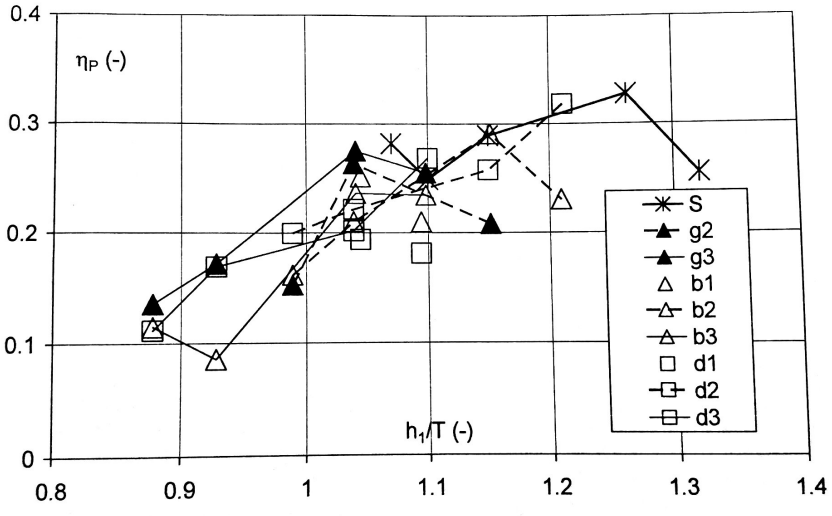


**Figure 33.** *Overall propeller efficiency: influence of bottom characteristics and under keel clearance. Only solid part S of interest here [89].*

# 5 Mathematical model

## 5.1 Propeller

Once a propeller is chosen, the torque can be calculated with the help of the $K_T - K_Q$ propeller diagram. An example of this diagram is shown in Figure 34. The coefficient $K_T$ is determined as:

$$K_T = \frac{T}{\rho n^2 D^4} \tag{25}$$

| | | |
|---|---|---|
| Where: | T [N] | The thrust delivered by the propeller; |
| | $\rho$ [kg/m$^3$] | The density of the water; |
| | n [rps] | The rotational speed of the propeller; |
| | D [m] | The propeller diameter. |

The advance number $J$, given on the horizontal axis of Figure 34, can be calculated as:

$$J = \frac{V_A}{nD} \tag{26}$$

with $V_A$ the advance speed, which can be written as $V_A = V(1 - w)$. The wake fraction $w$ is calculated with the help of Taylor's empirical formula:

$$w = 0.5C_B - 0.05 \tag{27}$$

with $C_B$ the block coefficient of the ship. The thrust deduction factor is also determined with Taylor's empirical formula:

$$t = 0.23C_B + 0.05 \tag{28}$$

The wake fraction, necessary to calculate the advance speed $V_A$, changes when sailing in shallow water. An empirical formula is proposed by *Yasukawa*, valid for $\frac{T}{h} > 0.5$ [93]:

$$\frac{w}{w_\infty} = 1 + a(\frac{T}{h} - 0.02)^b \tag{29}$$

Where:
- $T$ [m] The draft of the vessel;
- $h$ [m] The water depth along the trajectory;
- $w_\infty$ [-] The wake fraction in deep water, as calculated in Formula 27;
- $a$ [-] A parameter, equal to $6.6 - 7C_B$;
- $b$ [-] A parameter, equal to $5.4C_B - 2.2$.

The thrust deduction factor is defined with another formula developed by Taylor, relating the thrust deduction factor to the wake fraction. This was already given in Equation 21.

With a value for both $K_T$ and $J$, the diagram can be used to extrapolate a value for the torque coefficient $K_Q$.

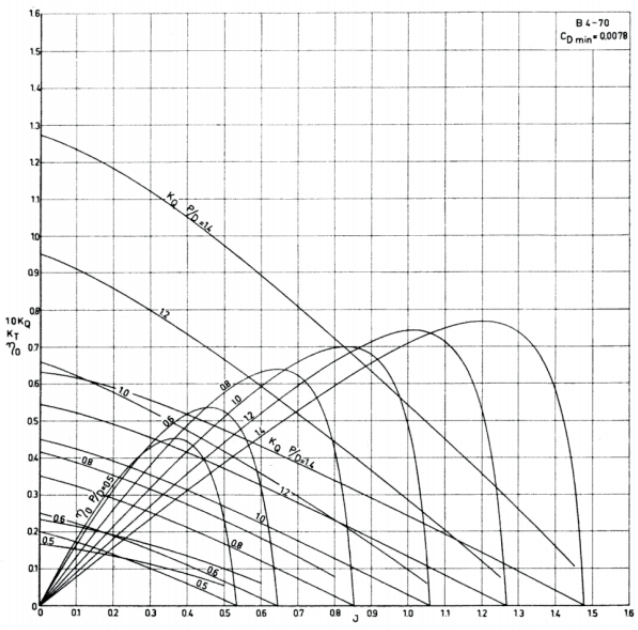


**Figure 11.4 Characteristics for Wageningen B-Screw Series B4-70 Propellers [9]**

**Figure 34.** *$K_T$-$K_Q$-diagram for a B4-70 Wageningen Series propeller [94].*

This torque coefficient can be used to calculate the torque $Q_P$:

$$Q_P = K_Q \cdot \rho \cdot n^2 \cdot D^5 \tag{30}$$

The propulsive efficiency, also called the quasi-propulsive coefficient, is calculated as:

$$\eta_D = \eta_{prop} \cdot \eta_{hull} \cdot \eta_{rot} \tag{31}$$

Where: $\eta_{prop}$ [-] The propeller efficiency, equal to $\frac{K_T}{K_Q}\frac{J}{2\pi}$;
$\eta_{hull}$ [-] The hull efficiency, equal to $\frac{1-t}{1-w}$;
$\eta_{rot}$ [-] The rotative efficiency.

Generally, the best propulsive efficiency is achieved when the propeller works in a homogenous wake field. Therefore, the efficiency may drop significantly when sailing in shallow water.

## 5.2 Shaft Line

The shaft delivers the power made by the engine at the crankshaft and converts this to the torque which may be used to rotate the propeller. Since the torque was calculated in the previous section, the delivered power $\mathrm{P}_D$ can be calculated:

$$P_D = Q_P \cdot 2 \cdot \pi \cdot n \tag{32}$$

This delivered power is the power available at the end of the shaft line, i.e. at the propeller. The brake power $\mathrm{P}_B$, available at the start of the shaft, is easily calculated:

$$P_B = \frac{P_D}{\eta_{shaft}} \tag{33}$$

$\eta_{shaft}$ is the shaft efficiency, consisting of three parts:

- $\eta_{gearbox}$, the gearbox efficiency;
- $\eta_{bearings}$, the efficiency left after loss due to bearings;
- $\eta_{length}$, an efficiency factor depending on the shaft length.

An important assumption is made here. One of the equations of motion states:

$$2 \cdot \pi \cdot I_{pp} \cdot \dot{n} = Q_E - Q_P \tag{34}$$

with $Q_E$ the engine torque. This equation basically explains how an acceleration of the rotational speed of the engine causes a net torque difference to exist between engine and propeller due to the moment of inertia of the shaft line $I_{pp}$. In this dissertation, this inertial effect is neglected and a constant rotational speed is assumed, in order to simplify the calculations. Because of this, the rotational acceleration $\dot{n} = 0$ and the engine torque equals the propeller torque.

## 5.3 Engine

The goal of this part is to calculate several efficiencies, such as the Carnot efficiency $\eta_C$ and the effective efficiency $\eta_{eff}$. The total efficiency $\eta_{tot}$ of the entire drivetrain will be calculated as well. Besides this, the rate of fuel consumption will be calculated, together with the total fuel mass used during the trajectory.

Before the calculations start, some constants are summarized:

- $\chi$ [-]: the number of crankshaft rotations for a complete engine cycle;
- $n_c$ [-]: the number of cylinders;
- $D_b$ [m]: the bore diameter of the engine;
- $s$ [m]: the stroke length of the engine;
- $\eta_{mech}$ [-]: the mechanical efficiency of the engine;
- $l$ [m]: the travel distance of the ship.

In this dissertation, 2 fuel oils will be used and the efficiency and emissions of both will be compared. These are heavy fuel oil (HFO) and marine diesel oil (MDO), with the lower heating values (LHV) given in Table 4

**Table 4.** *The lower heating values of the fuel oils.*

| | |
|---|---|
| HFO | 39.6 $\frac{MJ}{kg}$ |
| MDO | 42.7 $\frac{MJ}{kg}$ |

The effective power, also called the engine brake power or the power available at the crankshaft, is equal to the brake power calculated in Section 5.2. The effective work available at the crankshaft afer one cycle is calculated as:

$$W_{eff} = bmep \cdot V_s \cdot n_c \tag{35}$$

where: $bmep$ [Pa] The brake mean effective pressure at the crankshaft of the engine;
$V_s$ [m$^3$] The swept volume of 1 cylinder equal to $s \cdot {D_b}^2 \cdot \pi/4$.

The brake mean effective pressure of an internal combustion engine is just a performance parameter and does not refer to any actual pressure inside the engine. It can be calculated as a function of the torque developed at the crankshaft.

$$bmep = \frac{2 \cdot \pi \cdot Q_P}{\chi \cdot n_c \cdot V_s} \tag{36}$$

The torque $Q_P$ has been calculated in Section 5.1. With the effective work now known, some efficiencies can be calculated.

The simplest one is the Carnot efficiency. This efficiency describes the maximum thermal efficiency that a heat engine can possibly achieve. It is only dependent on the temperatures of the hot source $T_H$ and the cold source $T_C$:

$$\eta_C = 1 - \frac{T_C}{T_H} \tag{37}$$

The cold source is just the environmental temperature, while the hot source is the highest temperature reached during combustion.
The effective efficiency $\eta_{eff}$ of an engine is the efficiency of converting the energy available in the fuel into work at the output of the engine.

$$\eta_{eff} = \frac{W_{eff}}{m_{fuel} \cdot LHV} \tag{38}$$

This formula represents the efficiency over one cycle. The fuel mass $m_{fuel}$ represents the amount of fuel used in this one cycle. This can easily be calculated if a relationship is established between the rotational speed of the crankshaft and the engine rotational speed. In a two-stroke engine, these rotational speeds are equal, meaning that the time it takes to complete one full cycle is just equal to $\frac{1}{n}$. If a four-stroke engine would be used, two crankshaft revolutions are necessary for one complete cycle. Therefore, the time necessary to complete this would be equal to $\frac{2}{n}$. The fuel mass can then be calculated as the fuel mass rate $\dot{m}_{fuel}$ multiplied with this time necessary to complete a cycle, with $\dot{m}_{fuel}$ calculated as:

$$\dot{m}_{fuel} = BSFC \cdot P_B / 3,600 \tag{39}$$

in which BSFC is the brake specific fuel consumption.

Finally, the total ship efficiency can be calculated, by multiplying the separate efficiencies of the propeller, shaft line and engine.

$$\eta_{tot} = \eta_D \cdot \eta_{shaft} \cdot \eta_{eff} \tag{40}$$

## 5.4 Emissions

The last part of this mathematical model consists of calculating and comparing the emissions emitted by the ship when running on different fuels. Due to the increasingly stringent regulations, a ship may have to switch fuels when entering certain zones. Therefore, most ships may be equipped with engines which can run on multiple fuels. In this thesis, a comparison is made between the emissions while running on heavy fuel oil (HFO) and while running on marine diesel/gas oil (MDO/MGO).
Heavy fuel oil is actually comprised of all the residual fuel oils and may be identified as a worst-case substance. It is the most contaminating fuel, but since it has the lowest cost as well, it is predominantly used for the propulsion of ships. Due to its content it needs to be preheated before it can be used as fuel.
Marine diesel oil is a blend of gasoil and heavy fuel oil and is also widely used in the marine sector. As this fuel contains less sulfur and particulate matter than HFO, it is mainly used where HFO is prohibited, e.g.

near ports and channels, as well as in emission control areas. However, in order to make a correct comparison, this will be neglected for now and it will be assumed that the ship is only sailing on a single type of fuel.

All emissions analysed here result from fuel combustion and are therefore calculated by multiplying fuel consumption with an emissions factor. These factors are representative values that attempt to relate the quantity of a pollutant released to the atmosphere with an activity associated with the release of that pollutant [95]. They are dependent on the type of fuel, which is distinguished here between HFO and MDO/MGO. Emission factors may also be affected by certain modifications made to the propulsion plant, such as exhaust gas recirculation or the use of scrubbers. Some may reduce the emission factor, resulting in less emissions for the same type of fuel, while others may have a detrimental effect. In this dissertation, the influence of these types of technologies on the calculations of the efficiency and emissions will be neglected.
The emissions factors which are used in this section were determined in the IMO's $3^{rd}$ Greenhouse Gas Study [1]. They are expressed as grams emission per grams fuel (g/g fuel) and are summarized in Table 5. The used values are the 2012 values, which was the base year for the IMO's study. Several emissions will be investigated according to the data made available. The emissions and emission rates may be calculated as:

$$\dot{EM}_i = \dot{m}_{fuel} \cdot EF_i \tag{41}$$

$$EM_i = m_{fuel} \cdot EF_i \tag{42}$$

Where: $\dot{EM}_i$ [g/s] The rate of emissions for emission type i;
$EM_i$ [g] The complete amount of emissions over the entire trajectory for emission type i;
$EF_i$ [$\frac{g}{gfuel}$] The emission factor used for emission type i.

**Table 5.** *Emissions factors for different types of greenhouse gas emissions [1].*

| Emission factor [g/g fuel] | Fuel type | |
|---|---|---|
| | HFO | MDO/MGO |
| $CO_2$ | 3.114 | 3.206 |
| $CO$ | 0.00277 | 0.00277 |
| $CH_4$ | 0.00006 | 0.00006 |
| $NO_x$ | 0.0903 | 0.0961 |
| $PM$ | 0.00728 | 0.00097 |
| $SO_2$ | 0.025 | 0.010 |

# Chapter IV

# Case Study: Bulk Carrier on Channel Ghent-Terneuzen

## 1 Overview

To analyze the emissions in shallow and confined water in the vicinity of densely populated areas, a case study was performed. A bulk carrier was intensely studied coming from the Western Scheldt, sailing through the channel Ghent-Terneuzen and berthing near Zelzate. For this bulk carrier, an engine and a propeller will be selected and the drivetrain will be examined. The trajectory of the bulk carrier was simulated with the help of a fast-time track captive simulation developed by FHR. With the help of several measurement tools aboard the vessel, including tools to obtain the engine speed and GPS to obtain the vessel coordinates, the inputs of this model were obtained. Together with the acceleration, the simulation resulted in the forces and moments working upon the vessel. Although these forces and accelerations are not relevant for this thesis, the measurements aboard the vessel will be used to create a relationship between the propulsion power required to sail the vessel and the emissions emitted.

## 2 Channel Ghent-Terneuzen

Data has been collected of a bulk carrier coming from the Western Scheldt, and sailing south along the channel Ghent-Terneuzen following the route shown in Figure 35. This channel was originally dug in 1823 to connect Ghent with the North Sea via the river Scheldt. It stretches from the Tolhuis barrage in Ghent until the connection to the Western Scheldt at the locks in Terneuzen. The total length of the channel is 30.8 km with 17.1 km on Belgian territory. Nowadays, three locks are available, of which the largest may contain vessels with a length up to 265 m and a beam of 37 m, allowing a maximum fresh water draft of 12.5 m. A new lock, predicted to be ready in 2022, will have a length of 427 m and a width of 55 m, capable of handling ships with a length of 366 m, a beam of 47 m and a DWT up to 150,000 t [96]. The distance between the Port of Ghent and the locks in Terneuzen is about 10 nautical miles (18 km). The theoretical width and depth of the channel at several points is depicted in Figure 36, along with the corresponding maximum draft and beam of ships sailing along the channel.


**Figure 35.** *The trajectory of the bulk carrier along the channel Ghent-Terneuzen.*

The bulk carrier from this case study has a draft of 12.5 m along the channel. Since the minimal depth of the channel is near to 13.5 m, this gives a gross under keel clearance of 1 m. With the maximum allowable draft in this channel being 12.5 m, the bulk carrier is sailing on the limit. This ship is not only subjected to shallow waters. Due to the limited width of the waterway, the channel Ghent-Terneuzen may also be defined as a restricted, and thus a confined waterway, as shown in Section 4 of Chapter III. To achieve this low UKC in this channel, the speed of the ship must be reduced heavily to avoid bottom contact and decrease bank effects. Together with other obstacles such as several bends and some bridges which restrict the available width, these phenomena cause the ship to be vastly inefficient along these waters in terms of propulsion power. An example is the bridge at Sas van Gent, shown in Figure 37, where the ship will sail at low speeds and thus the engine is operating below its rated capacity and will also be more inefficient. This may cause an increase in the harmful emissions compared to the ship sailing at nominal conditions. Since several cities lie along the channel, including Ghent, Terneuzen, Zelzate and Sas van Gent, this possible emission increase is an important subject for further investigation.

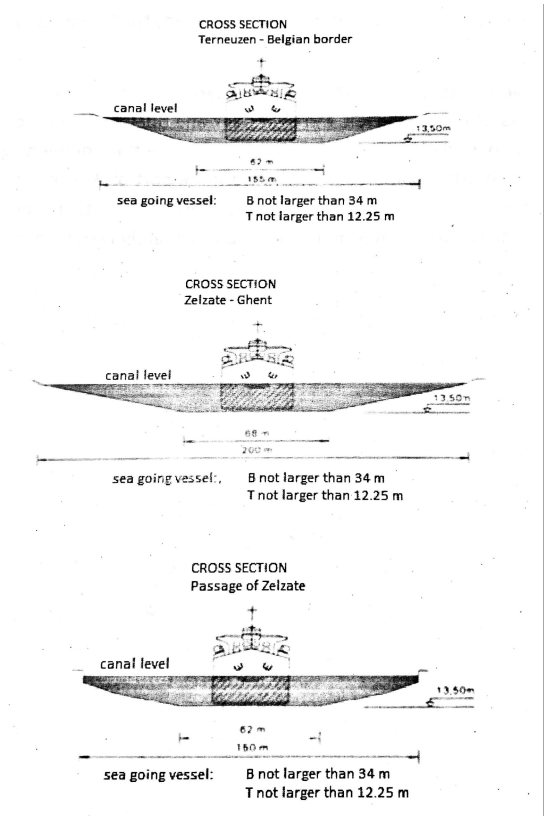


**Figure 36.** *Theoretical profile of the channel Ghent-Terneuzen [89].*

**Figure 37.** *Turning bridge on the channel Ghent-Terneuzen at Sas van Gent [97].*

## 3 Bulk Carrier

The ship subjected to measurements and calculations on behalf of this case study is a bulk carrier. This ship transports non-packaged goods in large quantities, such as grains, ores, coals and even cement. The International Convention for the Safety of Life at Sea (SOLAS) defines a bulk carrier as "a ship constructed with a single deck, top side tanks and hopper side tanks in cargo spaces and intended to primarily carry dry cargo in bulk" [98]. In 2018, this type of ship represented more than 33% of the world fleet in terms of gross tonnage [99]. Bulk carriers are divided into six major size categories depending on the deadweight tonnage (DWT) of the vessel: small, Handysize, Handymax, Panamax, Capesize and very large. The bulk carrier studied here, shown in Figure 38, is a Capesize type. This term is used for vessels which are too large to pass through the channels of Panama and Suez. The characteristics of this vessel are summarized in Table 6.

**Table 6.** *Basic ship parameters.*

| **Type** | Bulk carrier |
|---|---|
| **Service speed** | 14.5 kn |
| $\mathbf{L_{oa}}$ | 230 m |
| $\mathbf{L_{pp}}$ | 221.6 m |
| **B** | 37 m |
| **D** | 20.5 m |
| **T** | 12.5 m |
| **DWT** | 91,913 t |
| $\nabla$ | 108,021 t |


**Figure 38.** *A photograph of a Capesize bulk carrier with similar dimensions as the one used in the case study [100].*

## 3.1 Engine Selection

The engine is one of the most important parts regarding the emissions calculations. The info about this ship contained barely any engine performance data. A two-stroke low speed engine will be chosen as this is the common type of engine used for this type of ship. An extra advantage is that a gearbox need not be present between engine and propeller. Therefore, the engine type will be calculated with the help of a design procedure by *MAN B&W* [101]. This design procedure depicts in detail how to relate the size and tonnage of a vessel to its speed and propulsion power. Once this engine is known, a correct construction of the engine layout and engine load diagram can begin. The left part of Figure 39 shows that this vessel, as with most bulk carriers of average/large size, sails at a design service speed of 14.5 kn.

The right graph in Figure 39 illustrates the specified maximum continuous rating (SMCR) as a function of the size of the vessel. For a deadweight tonnage of 91,913 t, the SMCR power falls near a minimum of 10,000 kW.

*MAN B&W* constructed an overview for vessels with a typical design speed, and with typical sea and engine margins. All cases consider a four-bladed propeller. After comparing this table with the vessel particulars from Table 6 an engine is eventually selected. This engine, as indicated in Figure 7, is a G50ME-C9 type.

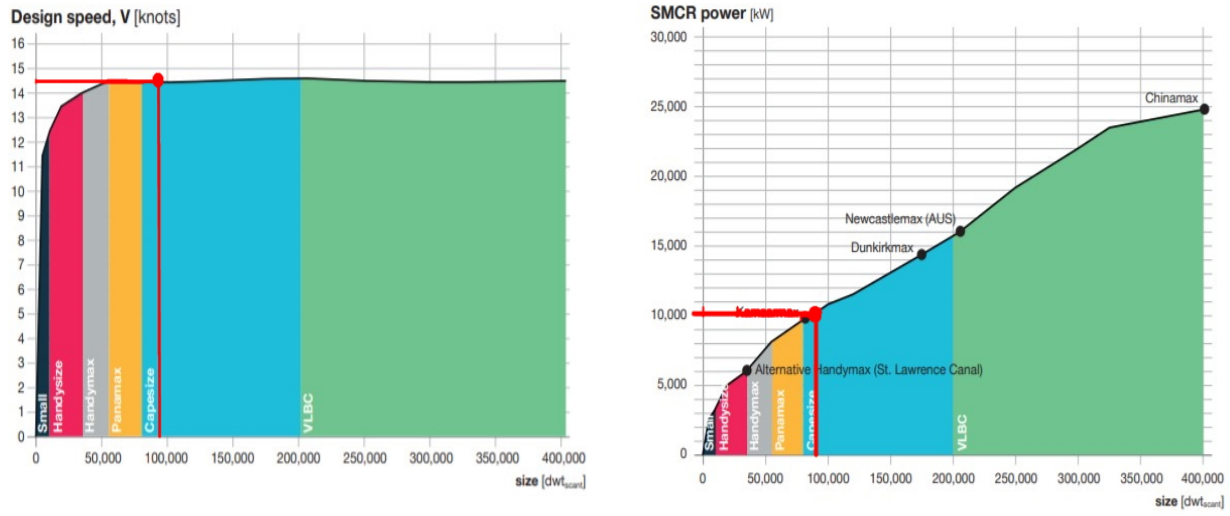


**Figure 39.** *Left: Average design ship speed of bulk carriers. Right: Propulsion SMCR power demand of Capesize, Large Capesize and VLBC bulk carriers [101].*

| size {$dwt_{scant}$} | 55,000 | 80,000 | 84,000 | 100,000 | 120,000 |
|---|---|---|---|---|---|
| $T_{scant}$ | 126 | 14.5 | 14.5 | 14.5 | 15 |
| $L_{os}$ | 189 | 225 | 229 | 245 | 250 |
| $L_{pp}$ | 182 | 211 | 225 | 236 | 240 |
| B | 32.2 | 32.2 | 32.2 | 38 | 43 |
| $T_{design}$ | 11.2 | 12.2 | 12.2 | 12.2 | 14 |
| Sea margin | 15 | 15 | 15 | 15 | 15 |
| Engine margin | 15 | 15 | 15 | 20 | 25 |
| **Average speed** | **14.5** | **14.5** | **14.5** | **14.5** | **14.5** |
| IMO minimum power level 1 | 7,571 | 9,478 | 9,784 | 11,004 | 12,530 |
| SMCR kW/rpm | 8,049 / 89 | 9,500 / 81 | 9,700 / 80 | 11,180 / 78 | 13,050 / 76 |
| Engine options | 5S60ME-C10 | 8G50ME-C9 | 8G50ME-C9 | 7G60ME-C10 | 8G60ME-C10 |
| | 6G50ME-C9 | 6S60ME-C10 | 6S60ME-C10 | 6S65ME-C8 | 7S65ME-C8 |
| | 7S50ME-C9 | 6G60ME-C10 | 6G60ME-C10 | 5S70ME-C10 | 6S70ME-C10 |
| | 8S50ME-C9 | 5S65ME-C8 | 5S65ME-C8 | | 5G70ME-C10 |
| **EEDI [% of reference line]** | | | | | |
| MDO | 84 | 81 | 81 | 83 | 86 |
| MDO + EcoEGR | 82 | 79 | 79 | 81 | 84 |
| MDO + PTO | 79 | 76 | 76 | 78 | 82 |
| MDO + EcoEGR + PTO | 77 | 74 | 74 | 76 | 79 |
| LPG | 74 | 71 | 71 | 73 | 76 |
| LNG | 65 | 62 | 62 | 64 | 66 |
| **Speed for phase 2 w. MDO** | **14.2** | **14.3** | **14.4** | **14.2** | **14** |
| SMCR kW/rpm | 7,388 / 87 | 9,250 / 80 | 9,450 / 79 | 10,400 / 76 | 11,480 / 73 |
| Engine options | 5S60ME-C10 | 8G50ME-C9 | 8G50ME-C9 | 7G60ME-C10 | 8G60ME-C10 |
| | 6G50ME-C9 | 6S60ME-C10 | 6S60ME-C10 | 6S65ME-C8 | 7S65ME-C8 |
| | 7S50ME-C9 | 6G60ME-C10 | 6G60ME-C10 | 5S70ME-C10 | 5S70ME-C10 |
| | 8S50ME-C9 | 5S65ME-C8 | 5S65ME-C8 | | 5G70ME-C10 |
| EEDI [% of reference line] | 79 | 79 | 79 | 79 | 79 |

**Table 7.** *Ship particulars and engine properties, depending on deadweight tonnage [101].*

The two-stroke slow speed engine of the G50ME-C9.5-TII type is designed by *MAN B&W* [84] and has electronically controlled hydraulic activation. This is contrary to what one would expect of an engine required for a bulk carrier. Since bulk carriers are made as cheaply as possible, with the ship and it's engine just complying with all the regulations, a camshaft controlled engine would be a more logical choice. However, these camshaft driven engines of the MC-C type have limited flexibility with regard to fuel injection and exhaust valve activation, which is probably the main reason why all the engines suggested in Table 7 are of the ME-type.

The engine is compact and complies with IMO Tier II level regarding the $NO_x$ emissions. The standard layout diagram of this engine is depicted in Figure 26. This diesel engine has a piston diameter of 50 cm and a stroke of 2,500 mm. With 9 cylinders, the $L_1$ power value equals 15,480 kW with a 100% engine speed of 100 rpm. These parameters together with a few others are summarized in Table 8. A visualization of the engine is shown in Figure 40. The layout diagram associated with this engine is plotted in Figure 41.

**Table 8.** *The properties of the engine used in the case study [84].*

| **Type** | G50ME-C9.5 |
|---|---|
| **Piston diameter D** | 0.5 m |
| **Stroke s** | 2.5 m |
| **Cylinders** | 9 |
| **NMCR ($P_{L_1}$)** | 15,480 kW |
| **100% engine speed ($n_{L_1}$)** | 100 rpm |
| **Mass (dry)** | 345 t |
| **$L_1$ MEP** | 21 bar |

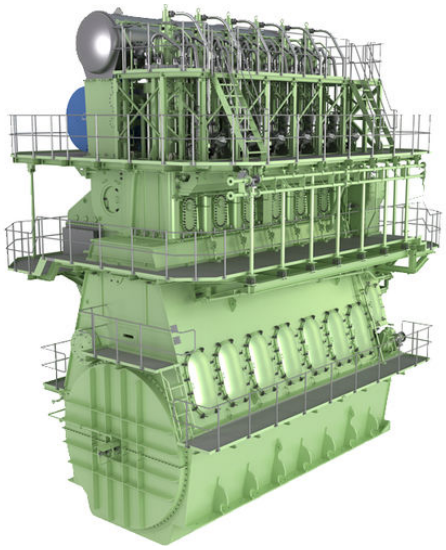

**Figure 40.** *The G50ME-C9.5 engine developed by MAN B&W which is used in this case study [84].*

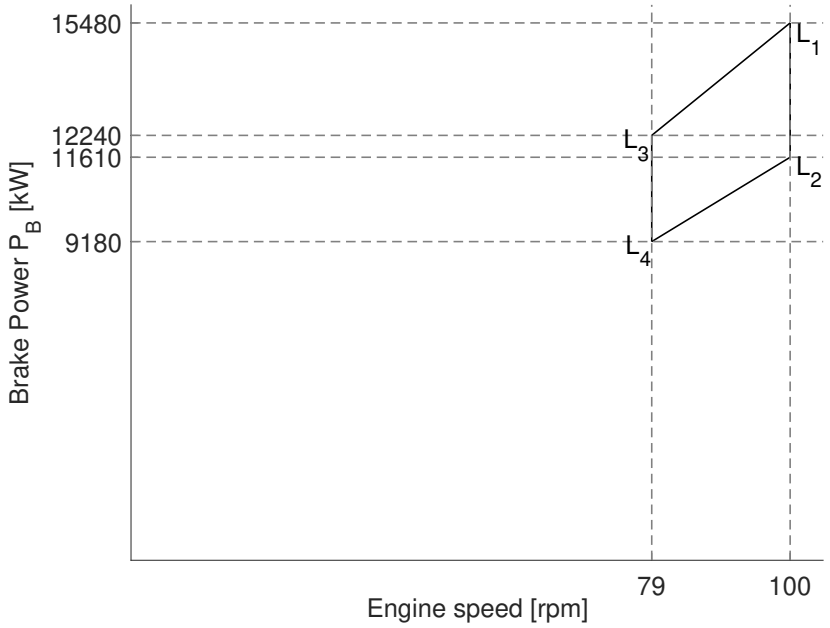


**Figure 41.** *MAN B&W 9 cylinders G50ME-C9.5 engine layout diagram.*

**Heavy Running Engine Load Diagram**

Now that an engine has been chosen, the load diagram can be constructed. The specified MCR (SMCR) necessary for this load diagram is chosen to be equal to the NMCR. Another assumption is that there is no generator installed on the main engine shaft, such that [101]:

$$SMCR_{propulsion} = SMCR_{engine} = NMCR = 15,480\ kW \tag{43}$$

With the SMCR point known, the propeller law can be used to construct the load diagram. The coefficient $c_n$ is determined from Formula 8 for the bulk carrier:

$$c_n = \frac{P_{SMCR}}{{n_{SMCR}}^{3.2}} = 6.16\frac{W}{{rpm}^{3.2}} \tag{44}$$

With this, the propeller curve for heavy running is constructed on Figure 42 together with the load diagram for this engine. Through the SMCR, denoted as $M$ in Figure 42, the constant power line and the MEP limit line are drawn. The engine has a lower speed limit of 33 rpm and an upper speed limit of $105\% n_{SMCR} = 105$ rpm. On the low-pressure side the diagram is limited at 25% of the MEP limit. The torque/speed limit is drawn between the low speed limit of 33 rpm and $96.5\% n_{SMCR}$.

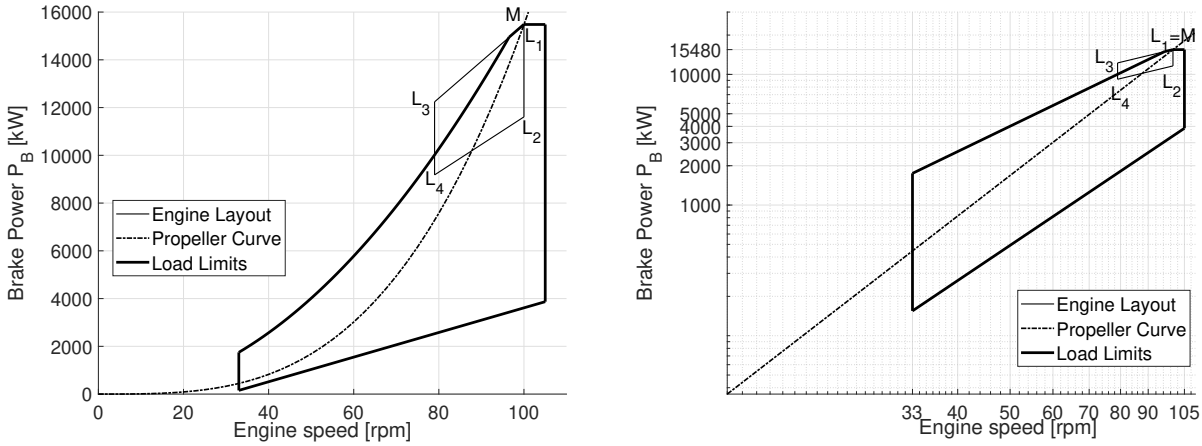


**Figure 42.** *Load diagram with heavy running propeller curve. Left: linear, right: loglog.*

## 3.2 Propeller Selection

The propeller converts the rotational power obtained from the shaft line into linear thrust which propels the ship forward. A standard design for a propeller is the Wageningen B-series, developed worldwide for different blades and pitch/diameter-ratios. An online tool [102] was used to obtain a propeller for this case study. The input parameters are given in Table 9. The propeller rate was chosen to be equal to the engine rate due to the lack of a gearbox. As was already explained with Formula 34 in Chapter III, the propeller and engine torque are assumed equal as well by neglecting the rotational shaft acceleration, in order to simplify the model. The online tool generates a propeller which complies with the required input. The propeller chosen here is a B4-70 propeller which is shown in Figure 43. The design efficiency and thrust which it may develop are given as output parameters in Table 10.

**Table 9.** *Propeller input parameters.*

| | |
|---|---|
| **Diameter [m]** | 8 |
| **# blades** | 4 |
| **Rotation** | Clockwise |
| **Expanded area ratio** | 0.7 |
| **Rake** | 9 |
| **Material** | Ni-Al Bronze |
| **Engine output / shaft [kW]** | 15,480 |
| **Engine rotational speed [rpm]** | 100 |
| **Gear ratio** | 1 |
| **Design speed $V_s$ [kn]** | 14.5 |
| **Wake number** | 0.2 |

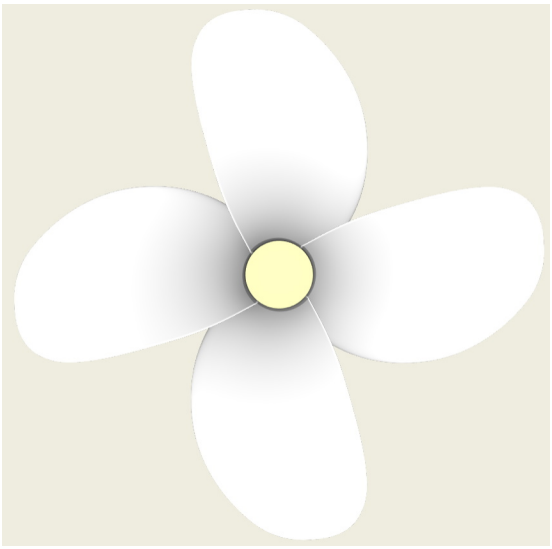

**Figure 43.** *Three-dimensional view of the propeller.*

**Table 10.** *Propeller output parameters.*

| | |
|---|---|
| **Propeller efficiency** | 0.591 |
| **Pitch-Diameter ratio P/D** | 0.619 |
| **Propeller Thrust [kN]** | 1,095.88 |
| **Weight [kg]** | 41,050.63 |

### 3.3 Data Acquisition

A simulated trajectory of the bulk carrier was obtained in the form of an *Excel*-file. This file gives a lot of input measurements and calculated data. The simulation was performed according to the fast-time track captive type [103]. During these simulations, the vessel performs a predefined trajectory as a function of time by imposing the values for the horizontal acceleration components. If the accelerations would be set to zero then the ship simply continues at the same speed in all directions. The output of this simulation concerns time series of the net forces and moments that are computed by the mathematical model. One of the applications of this type of fast-time simulation is the comparison with full-scale measurements. When a full-scale measurement is performed, this is done with extra equipment on board to measure the position of the ship with high accuracy and to register the use of propeller and rudder. With these measurements, the accelerations may be derived . The input of the simulation is then a matrix containing the accelerations $\dot{u}, \dot{v}, \dot{r}$, together with the propulsion and control settings. In this way, the full-scale measurement is replayed in the simulation, which is exactly what happened for this bulk carrier. The calculation scheme of this simulation type is given in Figure 44.

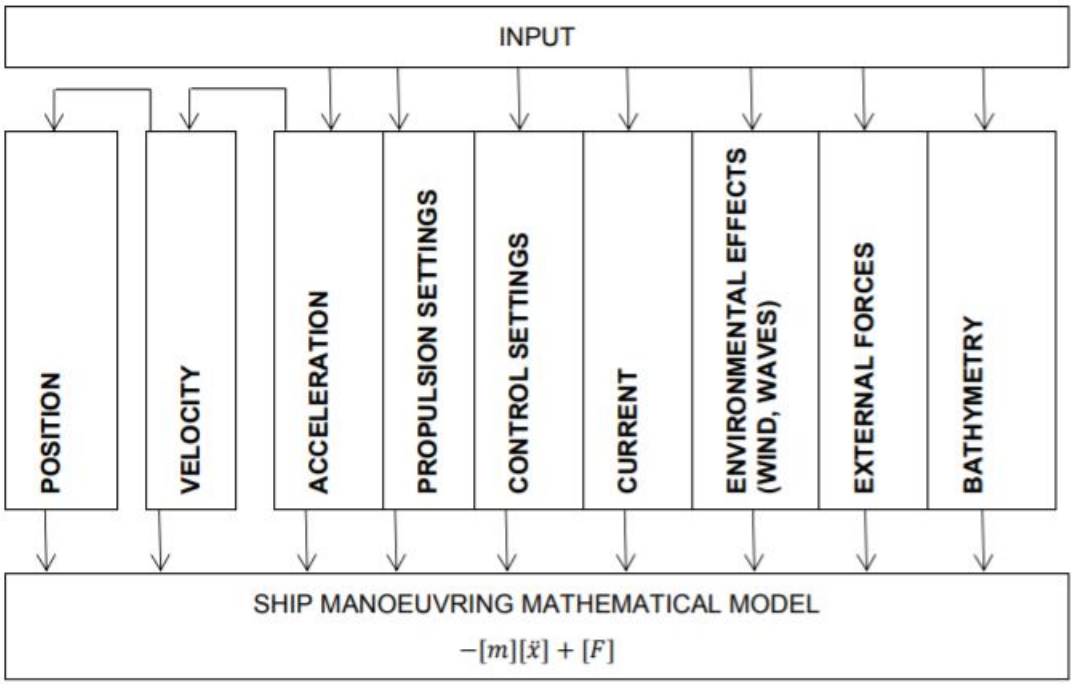


**Figure 44.** *Calculation scheme of the Fast-time Track Captive method [103].*

The input measurements start just past the lock in Terneuzen, and stop near berthing site 5350 1 hour and 55 minutes later, with a measurement taken each second. This amounts to a total of 6,900 moments that were recorded. No information is available on any possible tug boat interaction. The effect of wind is taken into account by the simulation of the bulk carrier along the trajectory. This and the effect of waves will be neglected in the model of the ship sailing in deep and unrestricted water. Figure 45 shows the most important measurements in function of the travel time.

The ship had already started its engine while still inside the lock. Once it had passed the lock, it started to gain speed until an average speed of $2.5\ m/s$ was maintained, visible in Figure 45b, which is the speed limit on the channel. This speed is kept until the end of the measurements, where the engine was probably shut down to berth near the quay with the help of tug boats. The rotational speed of the propeller (and thus the engine) maintains a nearly constant value of $51\ rpm$ once the ship has left the lock and started its trajectory. The only exception here is near the end of the measurements, where the engine speed is increased for a short period of time in order to increase the manoeuvrability while passing Zelzate bridge. This is shown in Figure 45c. Near the lock, the channel depth may exceed 19 m, with a steep decrease to about 14 m once the channel trip is resumed, with a minimum of 13.73 m. Since the bulk carrier remains at a constant draft of 12.5 m, neglecting squat, this corresponds to a minimum $h/T$-ratio of 1.098, which may be defined as very shallow water according to Table 3. More specifically, the depth-to-draft ratio remains between 1.1 and 1.2 along the entire trajectory (Figure 45g), which allows to conclude that very shallow water is maintained throughout the channel.

**(a) *Distance***

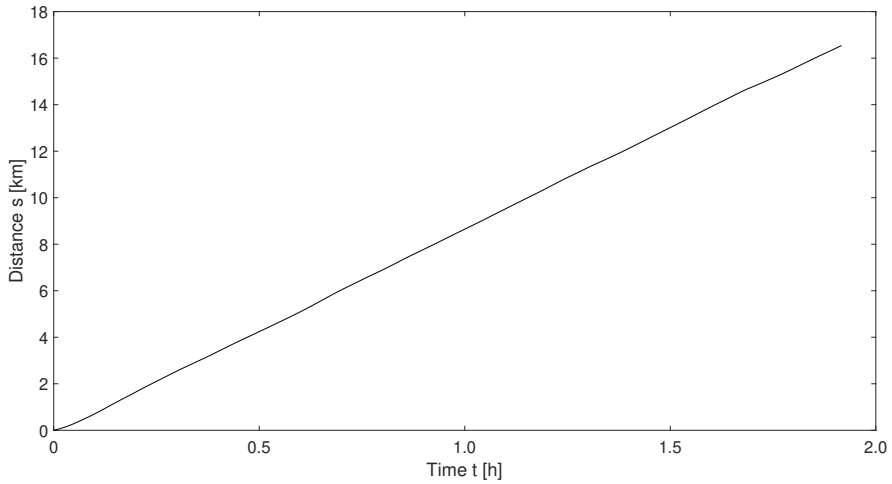


**(b) *Longitudinal velocity***

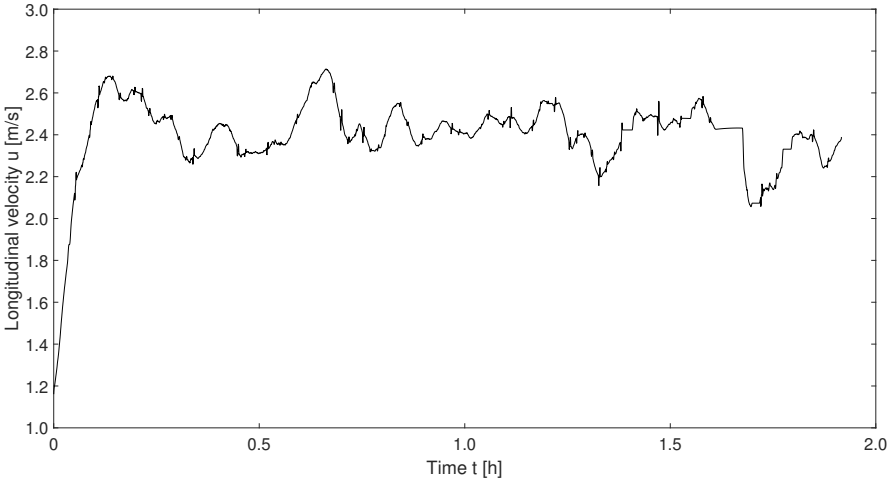


**(c) *Propeller speed***

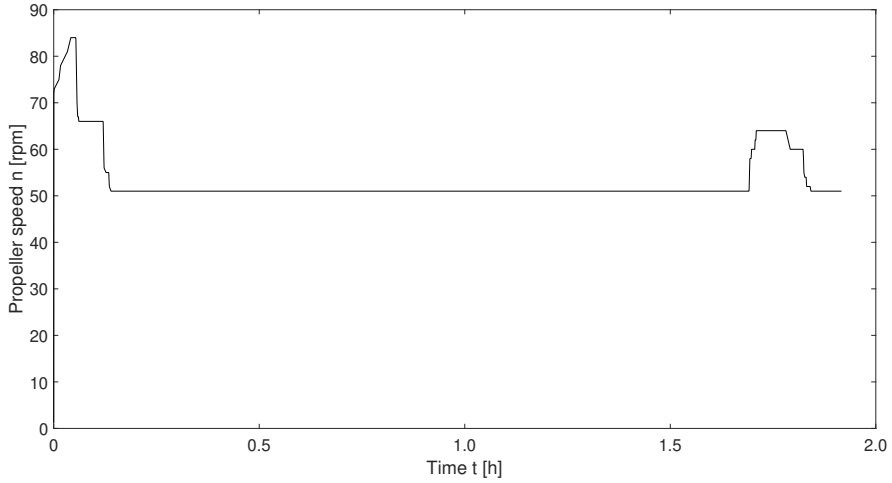

**(d) *Rudder deviation***

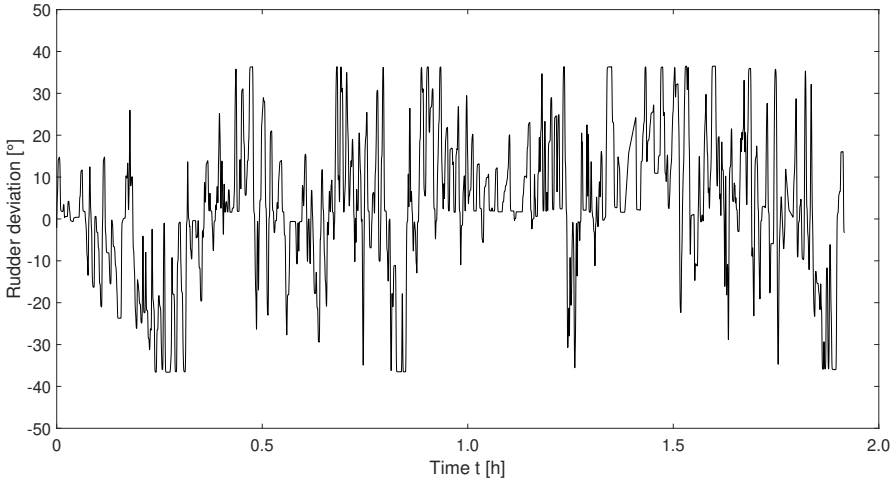


**(e) *channel depth***

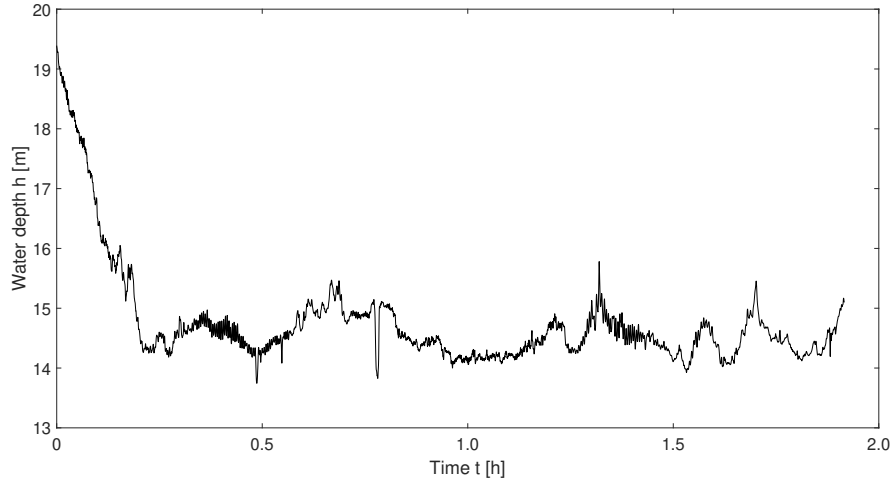


**(f) *Blockage***

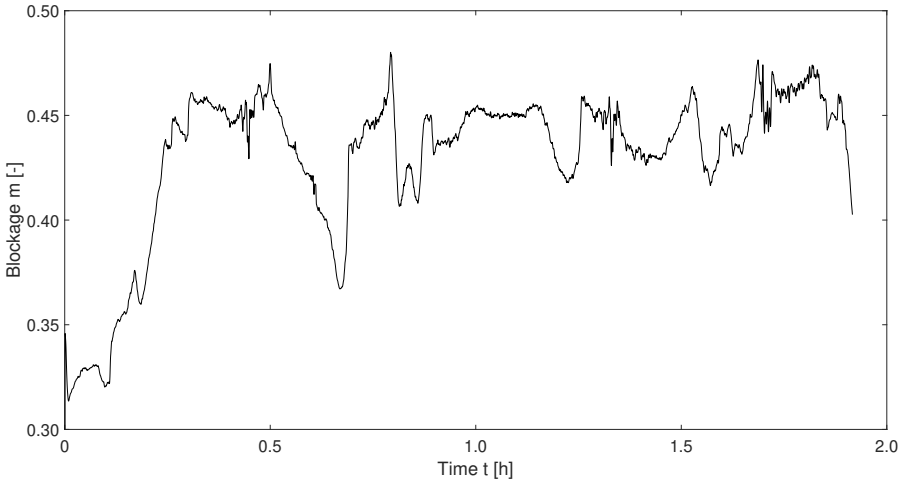

**(g) *h/T-ratio***

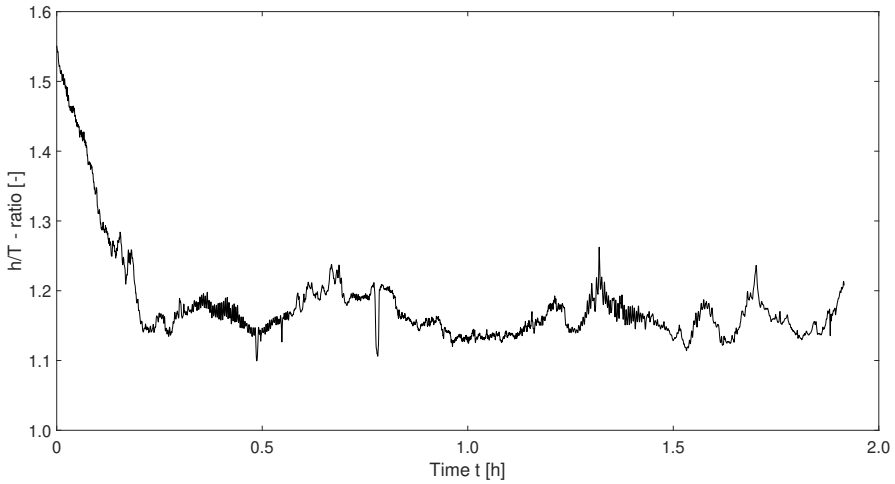


**Figure 45.** *Data measurements of the ship sailing along the channel Ghent-Terneuzen.*

# Chapter V

# Results and Discussion

## 1 Overview

The bulk carrier studied in Chapter IV was used in a simulation along the channel Ghent-Terneuzen. The calculated values from this simulation are subjected to the mathematical model from Chapter III in order to gain relevant results about the efficiency and emissions of the ship along its trajectory. These results will be compared with the same bulk carrier following the same trajectory in deep and unrestricted water, at the same engine speed. The efficiencies of the drivetrain components will be compared and discussed separately as well as the fuel consumption. Besides this, an additional comparison is made between 2 marine fuels: HFO and MDO. These fuels are used as an input in the mathematical model for both deep and unrestricted as well as shallow and confined water. Each of these cases is treated separately here.

## 2 Shallow Water

The calculations in shallow and confined water are done according to the mathematical model described in Section 5 of Chapter III. The bulk carrier sails along the channel Ghent-Terneuzen, with the measurements starting just past the locks at Terneuzen, and ending near berthing site 5350. The trip of the bulk carrier along this trajectory was simulated and data was made available, including the rotational speed $n$ of the propeller and the thrust $T_P$ developed by the propeller. The calculation will be done with the help of the $K_T - K_Q$ propeller diagram of the $B4 - 70$ Wageningen propeller with a $P/D$-ratio of 0.62, shown in Figure 46.

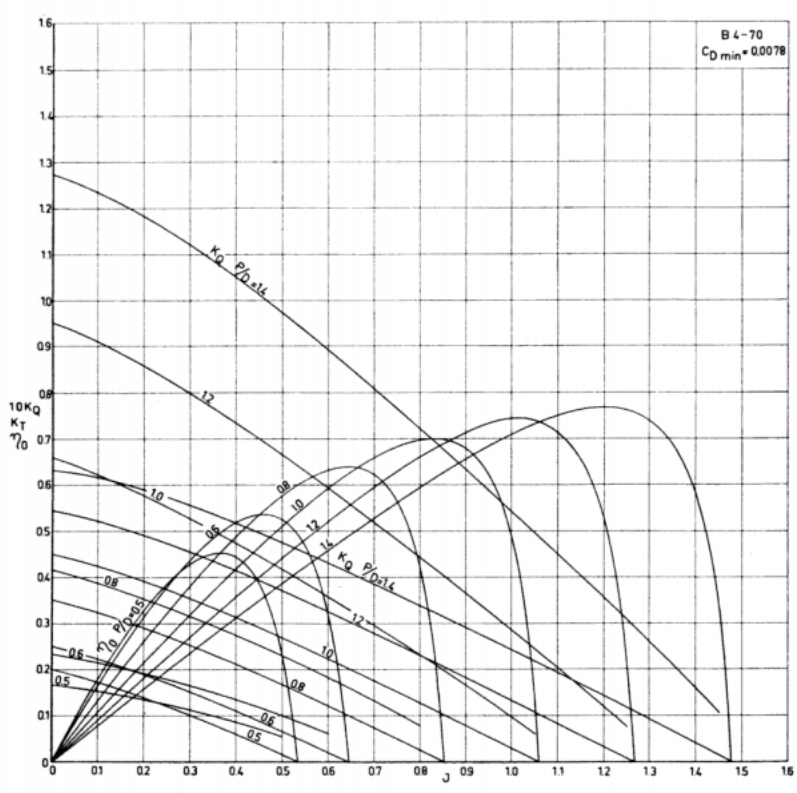


**Figure 11.4 Characteristics for Wageningen B-Screw Series B4-70 Propellers [9]**

**Figure 46.** *$K_T$-$K_Q$-diagram for a B4-70 Wageningen Series propeller [94].*

Attention should be paid here regarding the density used in the calculation of $K_T$ and subsequently the torque $Q_P$. As the bulk carrier is sailing along the channel in these simulations, the density of the water is only equal to $1,000\ kg/m^3$. Another note is that the wake fraction $w$ changes when sailing in shallow water. Therefore, Formula 29 is used here:

$$\frac{w}{w_\infty} = 1 + a(\frac{T}{h} - 0.02)^b \tag{45}$$

with $a$ and $b$ parameters depending on the block coefficient $C_B$ of the vessel, and $w_\infty = 0.37$ as calculated in Section 3. Besides this, the thrust deduction factor is related to the wake fraction by Formula 21

$$t = 0.6 \cdot w \tag{46}$$

The torque coefficient $K_Q$ can be extrapolated from the propeller diagram for each corresponding advance number $J$. After this, the torque $Q_P$ along the trajectory can be determined. The propulsive efficiency $\eta_D$ is calculated with Formula 31.

In the shaft line, the procedure from Chapter III Section 5 is followed. The delivered power available at the propeller $P_D$ may be calculated from the torque $Q_P$ used to rotate the propeller. From this power,

the brake power $P_B$ at the crankshaft can be calculated by taking into account the efficiency of the shaft line $\eta_{shaft}$ , which is equal to:

$$\eta_{shaft} = \eta_{gearbox} \cdot \eta_{shaft} \cdot \eta_{bearings} = 1 \cdot 0.99 \cdot 0.99 = 0.98 \quad (47)$$

With the brake power known, the model can work back through the engine to calculate the fuel consumption and the emissions of the vessel. Before this is possible, some coefficients are identified:

**Table 11.** *Engine coefficients of the G50 ME-C9.5 engine used in this case study.*

| **Engine coefficients** | |
|---|---|
| $\chi$ | 1 |
| $n_c$ | 9 |
| $D_b$ | $0.5\ m$ |
| $s$ | $2.5\ m$ |
| $\eta_{mech}$ | 0.85 [104] |
| $V_s = s \cdot D_b^2 \cdot \pi/4$ | $0.491\ m$ |

In order to make a more thorough comparison, MDO and HFO are both investigated. Due to their different lower heating value and chemical content, the engine efficiency, fuel consumption and emissions will be different as well. The temperature of the cold source $T_C$ for the Carnot efficiency, i.e. the air temperature, is taken to be 288 K. During combustion, the temperature inside the engine may rise to values above 1,500 K [105]. This temperature is taken as the standard hot source temperature $T_H$. The brake specific fuel consumption is made available by the engine manufacturer through *CEAS Engine Calculations* [106]. At lower loads, the combustion temperature will be lower as well, resulting in incomplete combustion. However, as the Carnot efficiency is only a theoretical optimum of the engine efficiency, the assumption is made to keep the temperatures of the hot and cold source the same as in the "normal" load case.

The fuel mass can be calculated following the same methodology as determined in Section 5, Chapter III for a 2-stroke engine. The brake specific fuel consumption used to calculate this mass changes with the load of the engine and follows the curve plotted in Figure 47. Due to the low-load operation, the BSFC in shallow water will be situated in the left part of the curve. The load diagram of the engine is plotted in Figure 48 together with the point at which the ship operates for the majority of the time (i.e. at 51 rpm).

The effective efficiency of the engine and the total ship efficiency are calculated according to the model of Chapter III.

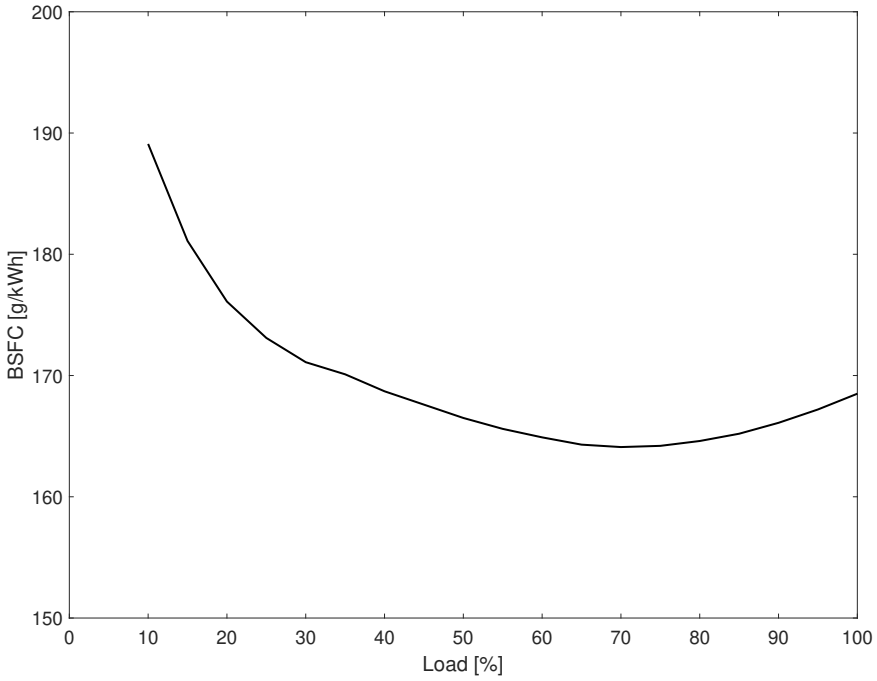


**Figure 47.** *Brake specific fuel consumption vs. load for the marine engine G50ME-C9.5 [106].*

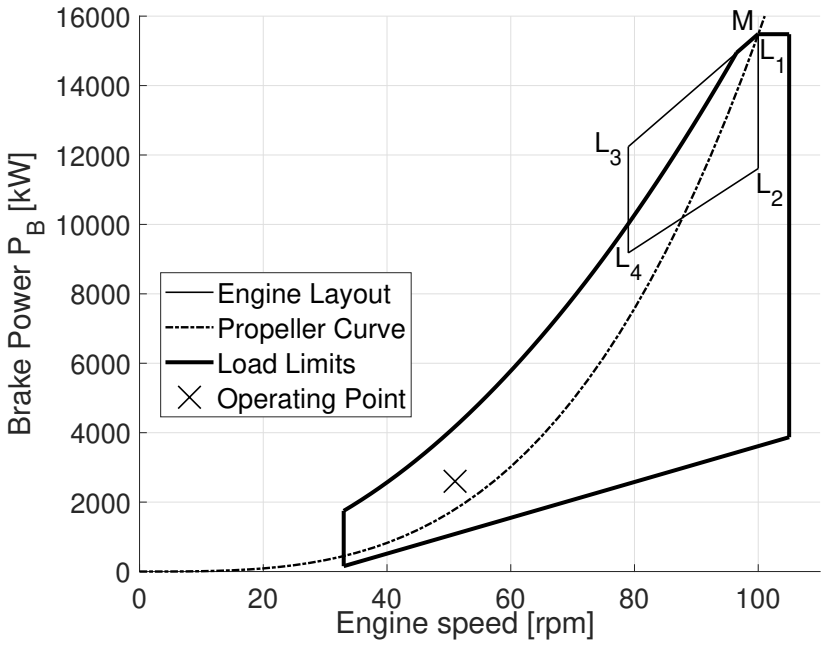


**Figure 48.** *The load diagram for the case study with the ship's operating point at 51 rpm*

**Emissions**

The emissions that the ship discharges are calculated according to the methodology of Chapter III with the help of the emission factors summarized in Table 5. These remain constant over a large load range, until $20\%$ of the maximum load. Due to the inefficient operation of the engine below this point, additional correction factors will be necessary for certain emissions. The *U.S. Environmental Protection Agency (EPA)* [107] proposes these correction factors ranging from $1\%$ to $20\%$ load. Incomplete combustion at these loads causes an increase in the emissions of particulate matter (PM), hydrocarbons (HC) and carbon monoxide (CO) [108]–[110]. Besides this, the lower combustion temperatures at low-load operation may lead to a decrease in the $NO_x$-emissions [108]. The correction factor proposed by *EPA* actually gives a multiplicative value larger than 1, which may be explained due to the fact that the calculation of $NO_x$-emissions is underestimated at low loads. The increase in $CO_2$ and $SO_2$ may be explained due to the increase in BSFC.
Along the trajectory of the ship in the channel, the engine is running at an average load of 13.5%. This results in the adjustment factors given in Table 12. According to the $EPA$, the adjustment factor for $CH_4$ may be assumed the same as for the hydrocarbons.

**Table 12.** *Calculated low load multiplicative adjustment factors [107].*

| **Load** | **$CO_2$** | **CO** | **$CH_4$** | **$NO_x$** | **$SO_2$** | **PM** |
|---|---|---|---|---|---|---|
| 13.5% | 1.125 | 1.465 | 1.535 | 1.095 | 1.125 | 1.17 |

## 3 Deep Water

The mathematical model described in Section 5 of Chapter III is used to obtain the results in this section. The bulk carrier in deep and unrestricted water is sailing at a constant load of 13.5% and a constant engine speed of 51 rpm, which corresponds to a vessel speed of 5.9 kn. This situation comes closest to an accurate comparison with the actual measurements along the channel for shallow water. Because of the constant values, each of the calculated values in the mathematical model will remain constant as well and can thus be given in this section. Although the online generator for the propeller gives some standard values for thrust and propeller efficiency for the ideal case, it was chosen to calculate these values. The calculation will still be done with the help of the $K_T - K_Q$ propeller diagram of a $B4 - 70$ Wageningen propeller.

The values obtained from the propeller calculations are summarized in Table 13. For the wake fraction and thrust deduction coefficient, a block coefficient $C_B$ is necessary. This is based on the data found on MarineTraffic [100]. With a summer displacement of $108,021\ t$ and a summer freeboard of $5.77\ m$, a draft of $14.73\ m$ is attained, which gives a block coefficient of 0.84. The values obtained from the propeller diagram are calculated according to a $\frac{P}{D}$-ratio of 0.62 (given in Table 10). A water density of $\rho = 1,025\ kg/m^3$ is used.

**Table 13.** *Calculated parameters for the propeller part of the drivetrain model.*

| Parameter | Value |
|---|---|
| $w$ | 0.37 |
| $t$ | 0.243 |
| $J$ | 0.2810 |
| $K_T$ | 0.1576 |
| $T_P$ | 478.055 kN |
| $K_Q$ | 0.0176 |
| $Q_P$ | 426.35 kNm |
| $\eta_{prop}$ | 0.4012 |
| $\eta_{hull}$ | 1.202 |
| $\eta_{rot}$ | 1 |
| $\eta_D$ | 0.4821 |

The torque originates from the shaft which is an extension of the engine driven power. The delivered power at the propeller is calculated with the help of the torque:

$$P_D = Q_P \cdot 2 \cdot \pi \cdot n = 13,213\ kW$$

The brake power available at the engine crankshaft can be determined as well:

$$P_B = \frac{P_D}{\eta_{shaft}} = 13,482\ kW$$

With the shaft efficiency $\eta_{shaft}$ still equal to 0.98.

Again, a comparison will be made between MDO and HFO. The parameters determined in Section 2 remain the same. The different values for the calculations performed in the engine part of the model are summarized in Table 14. The brake specific fuel consumption is made available by the engine manufacturer through *CEAS Engine Calculations* [106]. For the case of deep and unrestricted water, a constant value of 183.6 g/kWh is assumed, corresponding to a load of 13.5%.

**Table 14.** *Calculated parameters for the engine part of the drivetrain model.*

| Parameter | Value |
|---|---|
| $bmep$ | 6.06 bar |
| $W_{eff}$ | 2,679 kJ |
| $\eta_{Carnot}$ | 0.801 |
| $\dot{m}_{fuel}$ | 0.118 kg/s |
| $\eta_{eff,MDO}$ | 0.45 |
| $\eta_{eff,HFO}$ | 0.478 |
| $\eta_{tot,MDO}$ | 0.213 |
| $\eta_{tot,HFO}$ | 0.226 |

**Emissions**

As was already determined in the mathematical model, the emissions are calculated with the help of the emission factors summarized in Table 5. The emissions rate is obtained when this factor is multiplied with the mass fuel rate, while the total amount of emissions can be obtained from the total amount of fuel used during the trajectory. Since the comparison between shallow and deep water needs to be as realistic as possible, it is opted to compare the ships over the same distance, not the same time frame. The measurements began when the bulk carrier left the locks at Terneuzen and ended somewhere near berthing site 5350. This results in a travelled distance of 16,541.7 m, which is thus implemented in the deep and unrestricted water case as well. At an average ship speed of 5.9 kn, the ship needs 5,450.4 s to overcome this length. This is less than the time needed by the ship when sailing along the channel. A short calculation is required to calculate the total fuel used along this trajectory:

$$\dot{m}_{fuel} = 0.118\ kg/s$$

$$m_{fuel} = \dot{m}_{fuel} \cdot t = 645.82\ kg$$

From this, the emissions and their rates may easily be calculated.

**Table 15.** *Bulk carrier emissions in deep and unrestricted water.*

| | **MDO** | **HFO** |
|---|---|---|
| $\dot{\mathbf{m}}_{\mathbf{CO_2}}$ | $0.380\ kg/s$ | $0.369\ kg/s$ |
| $\dot{\mathbf{m}}_{\mathbf{CO}}$ | $0.328 \cdot 10^{-3}\ kg/s$ | $0.328 \cdot 10^{-3}\ kg/s$ |
| $\dot{\mathbf{m}}_{\mathbf{CH_4}}$ | $0.007 \cdot 10^{-3}\ kg/s$ | $0.007 \cdot 10^{-3}\ kg/s$ |
| $\dot{\mathbf{m}}_{\mathbf{NO_x}}$ | $11.39 \cdot 10^{-3}\ kg/s$ | $10.70 \cdot 10^{-3}\ kg/s$ |
| $\dot{\mathbf{m}}_{\mathbf{SO_2}}$ | $1.185 \cdot 10^{-3}\ kg/s$ | $2.96 \cdot 10^{-3}\ kg/s$ |
| $\dot{\mathbf{m}}_{\mathbf{PM}}$ | $0.115 \cdot 10^{-3}\ kg/s$ | $0.863 \cdot 10^{-3}\ kg/s$ |
| $\mathbf{m}_{\mathbf{CO_2}}$ | $2.07 \cdot 10^{3}\ kg$ | $2.01 \cdot 10^{3}\ kg$ |
| $\mathbf{m}_{\mathbf{CO}}$ | $1.79\ kg$ | $1.79\ kg$ |
| $\mathbf{m}_{\mathbf{CH_4}}$ | $0.0387\ kg$ | $0.0387\ kg$ |
| $\mathbf{m}_{\mathbf{NO_x}}$ | $62.06\ kg$ | $58.32\ kg$ |
| $\mathbf{m}_{\mathbf{SO_2}}$ | $6.46\ kg$ | $16.15\ kg$ |
| $\mathbf{m}_{\mathbf{PM}}$ | $0.626\ kg$ | $4.70\ kg$ |

# 4 Discussion

## 4.1 Shallow Water

This section will only discuss the efficiencies, fuel consumption and emissions of the bulk carrier sailing on MDO. In the next sections, a comparison between MDO and HFO will be made.

**Efficiencies**

The mathematical model of Chapter III used a reversed-calculation procedure starting from the propeller

thrust to calculate the ship's efficiency and emissions. The propeller thrust $T_P$ and its corresponding torque $Q_P$ are plotted in Figure 49. Following the model, the brake power $P_B$ can be calculated through the shaft line, while the engine load can be obtained from the rotational speed of the propeller with the help of the *CEAS* calculations [106]. These are also plotted in Figure 49.

The total ship efficiency $\eta_{tot}$, starting from the fuel tank and ending at the propeller thrust, is one of the most important parameters. This efficiency, plotted in Figure 50, consists of 3 parts: the propulsive efficiency $\eta_D$, the shaft line efficiency $\eta_{shaft}$ and the effective engine efficiency $\eta_{eff}$. The shaft line efficiency $\eta_{shaft} = 0.98$ is constant and independent of the type of sailing area. The propulsive efficiency $\eta_D$ and effective engine efficiency $\eta_{eff}$ are plotted in Figure 51.

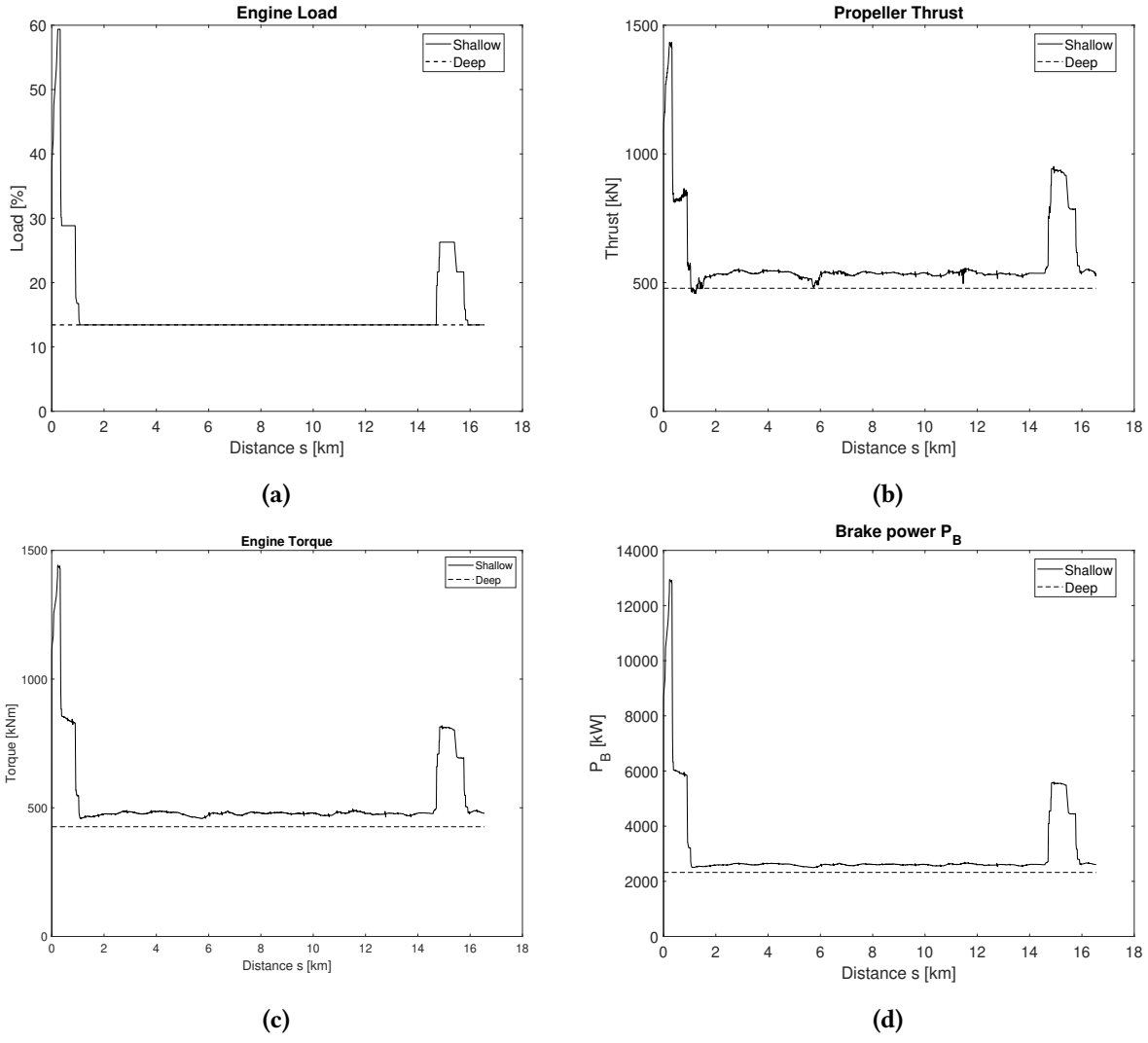


**Figure 49.** *Comparison of the propeller thrust, engine torque and engine brake power for shallow and confined water versus deep and unrestricted water, at an engine speed of 51 rpm and with MDO as fuel.*

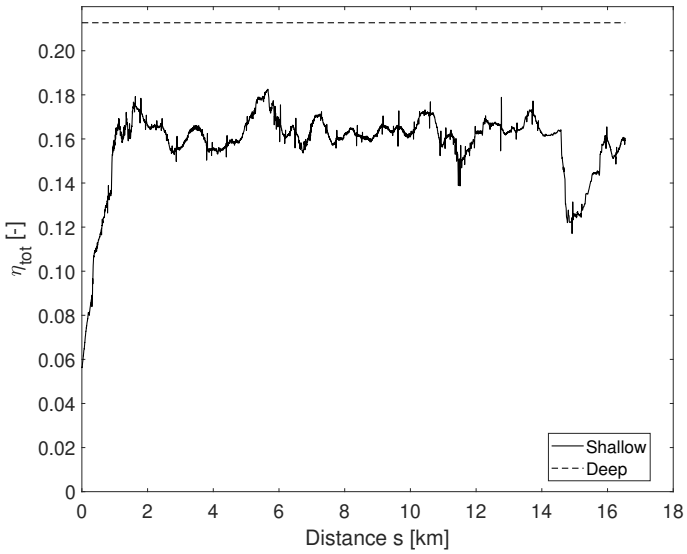


**Figure 50.** *Comparison of the total ship efficiency $\eta_{tot}$ for shallow and confined water versus deep and unrestricted water, at an engine speed of 51 rpm and with MDO as fuel.*

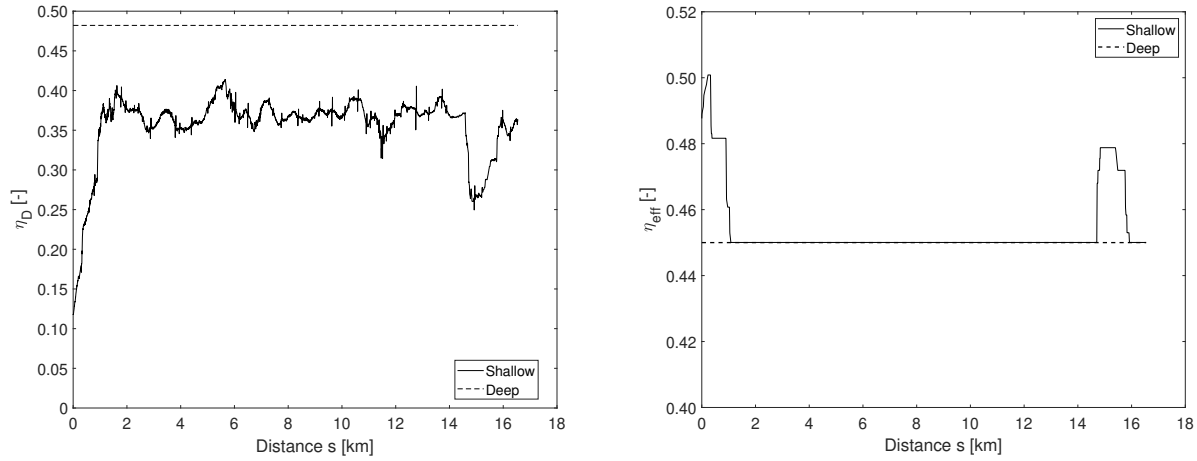


**(a)** **(b)**

**Figure 51.** *Comparison of the propulsive efficiency $\eta_D$ (left) and effective engine efficiency $\eta_{eff}$ (right) for shallow and confined water versus deep and unrestricted water, at an engine speed of 51 rpm and with MDO as fuel.*

An observation which is immediately clear is that all these plots follow a similar path over the distance of the trajectory along the channel Ghent-Terneuzen. The exception to this is the propulsive efficiency $\eta_D$, and thus the total efficiency $\eta_{tot}$ as well. While most of the parameters here mainly depend on the engine load and the engine rotational speed, the propulsive efficiency $\eta_D$ is a function of the wake fraction $w$ and thrust deduction factor $t$. These factors change throughout the trajectory depending on the depth-to-draft ratio $\frac{h}{T}$ according to Formula 29. The fluctuations of this efficiency are thus more severe and will influence

the total efficiency $\eta_{tot}$.

The other parameters such as the engine brake power $P_B$ and effective engine efficiency $\eta_{eff}$ follow a similar path as the thrust plot. The initial peak at the start of the simulations may be explained due to the high engine load when leaving the lock at a very low speed. The ship has to accelerate to sail along the channel and does this at a noticeably higher load than the rest of the trajectory. Once a quasi-constant vessel speed has been established, the engine speed drops to a constant 51 rpm for a very long time. This is also visible in the plots of Figure 45. After almost 15 km, the load and engine speed are increased once more to 64 rpm for a short period of time. This causes the emissions of all pollutants to increase drastically for this period as well. The explanation here is fairly simple: after 15 km of sailing along the channel, starting from the locks in Terneuzen, the ship passes the city Zelzate. As can be seen on Figure 52, the ship has to cross a bridge at this section of the channel. The passage here is extremely narrow and the propeller speed has to increase in order to increase the manoeuvrability of the ship while sailing past this bridge. The blockage increases to a local maximum while the h/T-ratio is quite low, as is clear from Figure 45. These severe detrimental conditions cause the increase in engine load, but also in effective engine efficiency since the engine is working back at a more optimal point. Once the bridge is passed, the danger for lack of manoeuvrability subsides and the ship can regain its initial engine speed of 51 rpm.

**Figure 52.** *Bridge on the channel Ghent-Terneuzen at Zelzate [111].*

The increase in engine speed at the bridge causes an increase in propeller thrust $T_P$ as well. This increase is easily the largest along the trajectory, but it is not the only one. Figure 53 zooms in on 2 different sections along the trajectory. These sections, respectively at around 5.5 km and 11.5 km, have some very large thrust fluctuations at that moment, while the propeller speed does not change. If the trajectory of the bulk carrier along the channel is consulted, it is found that these fluctuations happen at the exact moment that the ship needs to follow a bend in the channel for the first section, while the second section occurs when

sailing past the turning bridge at Sas van Gent, which was shown on Figure 37. These fluctuations are also represented, be it less severe, in the other parameters and efficiencies.

If the propulsive efficiency $\eta_D$ of Figure 51 is consulted, quite the opposite can be seen. Where the effective efficiency $\eta_{eff}$ increased when sailing past the bridge due to the increased engine load, the propulsive efficiency $\eta_D$ decreases drastically. If this section is enlarged on the propulsive efficiency plot, visible in Figure 54, a drop of 10-15% can be seen. This translates itself into the total efficiency of the ship being decreased by 4-5% as well, to a minimum value of 11.71%.

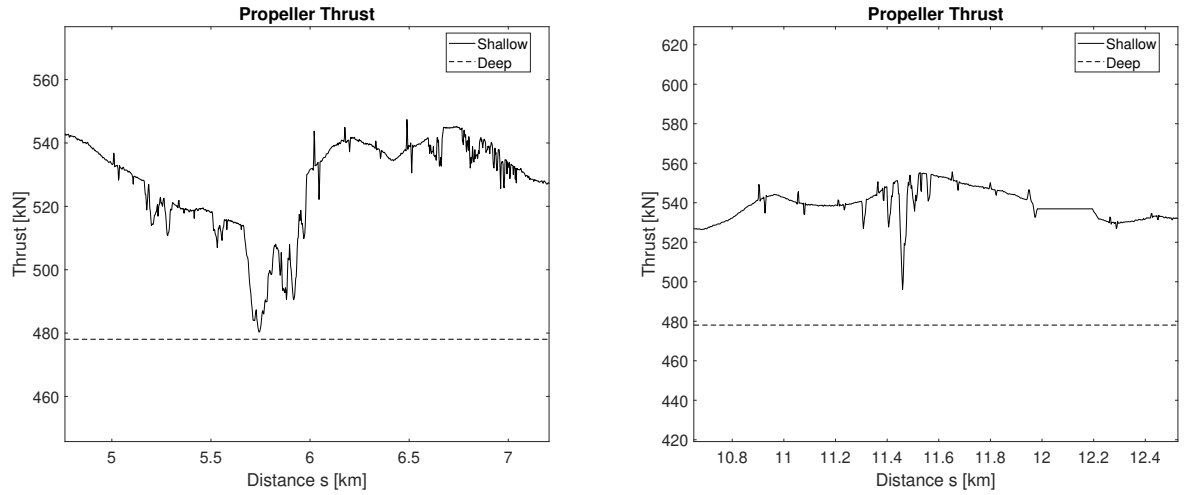


**(a)** **(b)**

**Figure 53.** *Zoomed in sections of the propeller thrust plot along the trajectory for 2 different sailing situations, at 51 rpm with MDO as fuel.*

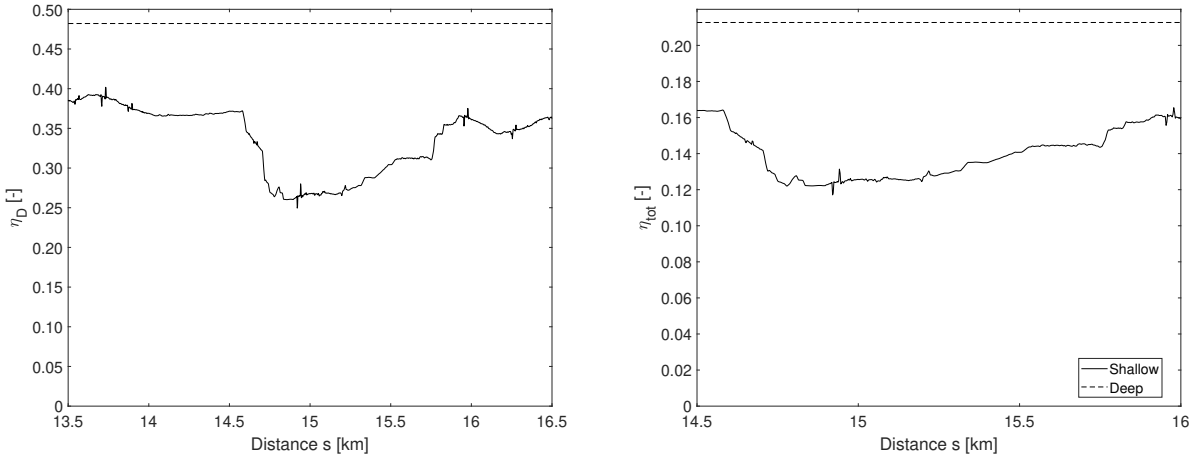


**(a)** **(b)**

**Figure 54.** *Zoomed in sections of the propulsive efficiency $\eta_D$ (left) and total ship efficiency $\eta_{tot}$ plot (right) along the trajectory for 2 different sailing situations, at 51 rpm with MDO as fuel.*

**Emissions**

When sailing along the channel Ghent-Terneuzen, the ship must comply to several regulations regarding the emissions of the engine. The fuel consumption $\dot{m}_{fuel}$ is given in Figure 55, while the emissions rates of several pollutants are given in Figure 56. More specifically, the pollutants treated here are $CO$, $CO_2$, $CH_4$, $NO_x$, $PM$ and $SO_2$.

The calculated fuel consumption and emissions in shallow and confined water fluctuate with each change in the underwater environment. The same fluctuations were visible in the effective engine efficiency plot of Figure 51, with again a severe increase when sailing past the bridge at Zelzate. This confirms the fact that these emissions are mainly dependent on the rotational engine speed, load and thus specific fuel consumption of the engine, while the small constant fluctuations originate due to the ever-changing $\frac{h}{T}$-ratio.

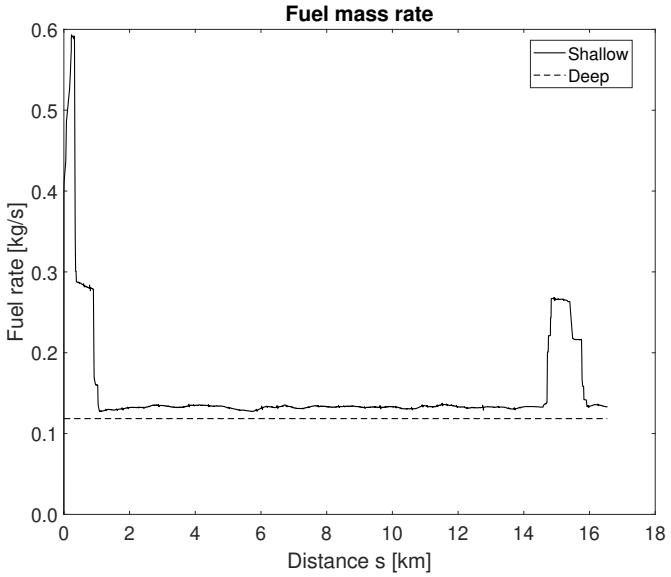


**Figure 55.** *The rate of fuel consumption over the trajectory for shallow and confined water versus deep and unrestricted water, at an engine speed of 51 rpm and with MDO as fuel.*

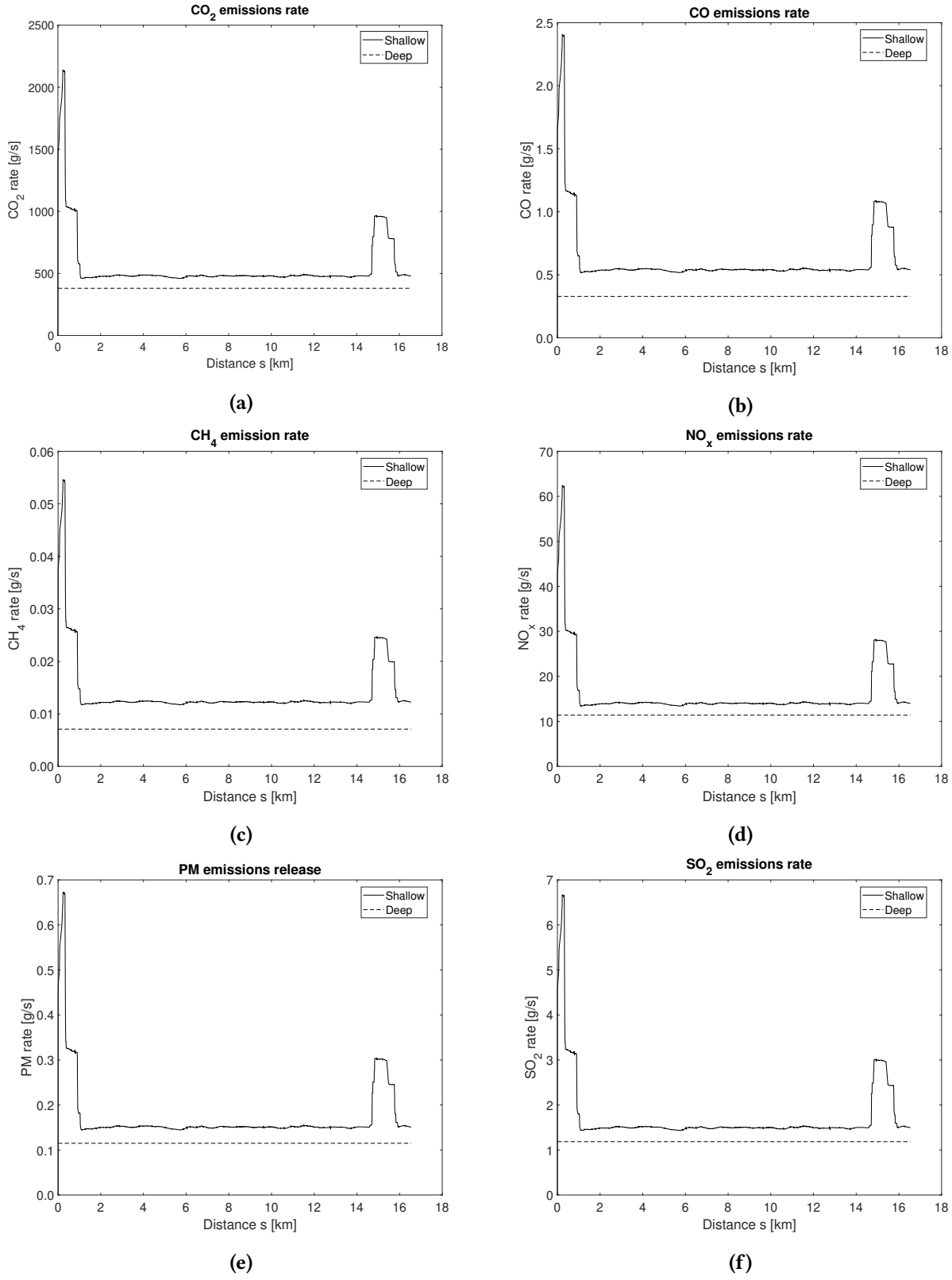


**Figure 56.** *Comparison of the release rate of emissions for shallow and confined water versus deep and unrestricted water, at an engine speed of 51 rpm and with MDO as fuel.*

**Comparison with deep and unrestricted water**

In order to assess the influence of shallow and confined water, this case study will be compared with the same bulk carrier sailing the same trajectory in deep and unrestricted water. The same distance is sailed. Due to the lack of accurate measurements for the situation in deep and unrestricted water, an important assumption was made. An accurate comparison of the efficiencies and emissions is only relevant when the marine diesel engine is working at the same load in both cases. As is visible in Figure 45, the ship maintains a rotational engine speed of 51 rpm for most of the time. Therefore, this average value is taken as a constant in deep and unrestricted water. The load is then also assumed constant at about 13.43%. This causes the rest of the values in the calculations to maintain a constant value as well throughout the entire trajectory. Moreover, due to a small speed difference attributed to the influence of shallow and confined water, the ship in deep water will accomplish this in a shorter time frame. Another assumption is that the measurements of the bulk carrier in deep and unrestricted water neglect wind and waves, as well as other external parameters. The engine load is plotted in Figure 49 as well, together with the propeller thrust $T_P$, torque $Q_P$ and engine brake power $P_B$.

The efficiencies are plotted in Figure 50 and 51 as well, represented by dashed lines. The increased propulsive efficiency $\eta_D$ and total ship efficiency $\eta_{tot}$ are very clear. This proves that the situation in shallow water is more detrimental, even when both sailing at an inefficient load. The largest difference occurs when sailing past the bridge of Zelzate. The total ship efficiency $\eta_{tot}$ in deep water keeps a constant value of 21.3%, while this efficiency along the channel Ghent-Terneuzen drops to a minimum of 11.71%, a difference of almost 10%.

Just like with the efficiencies, the fuel consumption and emissions rates for deep water are plotted together with those in shallow water in Figure 55 and 56. With these rates, the total mass released for each of these contaminants is calculated as well and shown in Figure 57.

As mentioned before, the engine speed in deep and unrestricted water is assumed to have a constant value of 51 rpm, while environmental forces are neglected. Because of this, not only the propeller thrust remains constant, but the fuel consumption and the rate of emissions as well. The increase of these parameters in shallow and confined water is instantly noticeable.

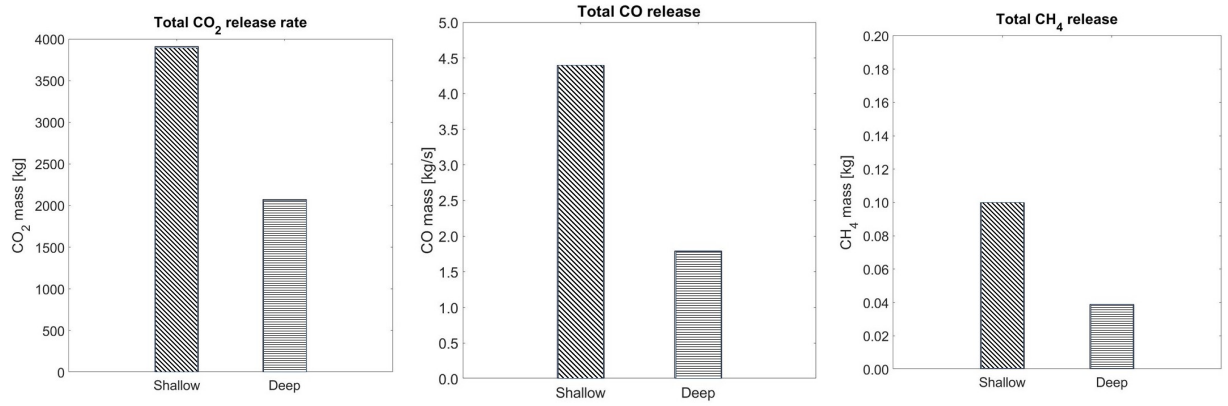


**(a)** **(b)** **(c)**

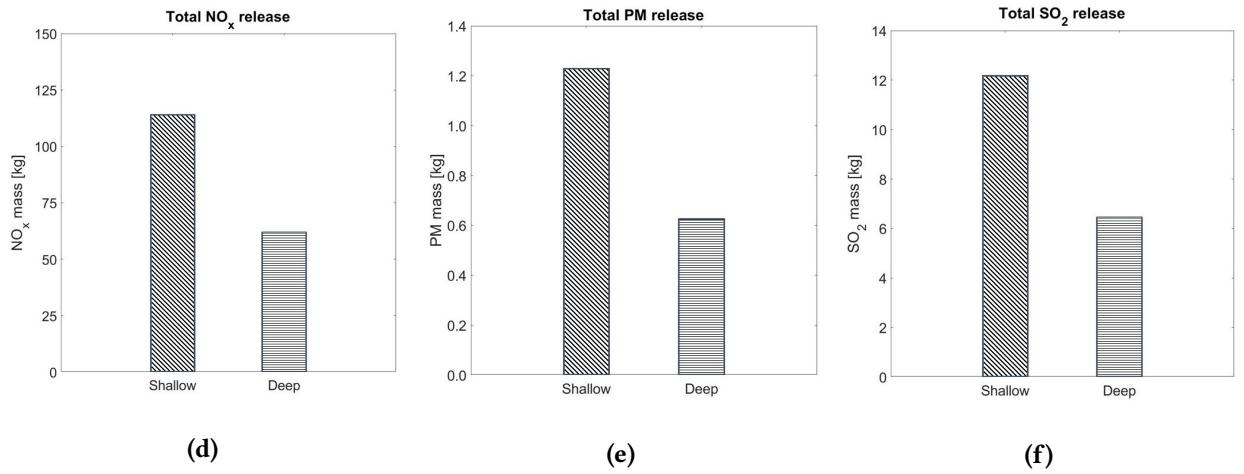


**(d)** **(e)** **(f)**

**Figure 57.** *Comparison of the total release of emissions for shallow and confined water versus deep and unrestricted water, at an engine speed of 51 rpm and with MDO as fuel.*

When the bar graphs of Figure 57 are consulted, the results are significant. Due to the shallow and confined waterway, some of the pollutants released along the trajectory are even more than doubled compared to the case of deep and unrestricted water. The difference between these two cases is defined as a ratio in Table 16. These ratios vary among the different pollutants. This increase originates from the detrimental sailing waters along the channel Ghent-Terneuzen. The shallow and confined waterway causes the thrust of the propeller to increase compared to the "normal" deep and unrestricted water case. This factor already causes an increase since the engine needs to produce more power. Besides this, the low load of the engine is a large factor as well. The inefficient combustion inside the engine changes the content of the exhaust gases significantly, with a large increase of $CO$, $CH_4$ and $PM$, which thrive in these poor conditions. The lower ratios of $CO_2$ and $SO_2$ can be explained due to the fact that they are only dependent on the fuel consumption of the engine, not on the combustion itself. The $NO_x$-multiplicative factor is the lowest as the combustion inside the chamber probably happens at lower temperatures for lower loads. Therefore, less $NO_x$ emissions are to be expected compared to a nominal load case. Nonetheless, the increased thrust still causes a significant increase. Even though the ship is sailing at the same load and engine rotational speed, the speed of the ship is larger when compared to the situation along the channel Ghent-Terneuzen, meaning that the time to travel the same distance will be shorter. This is also of importance for the total emissions.

**Table 16.** *Emissions ratio of shallow and confined water to deep and unrestricted water.*

| Pollutant | Factor |
|---|---|
| $\mathbf{CO_2}$ | 1.89 |
| **CO** | 2.46 |
| $\mathbf{CH_4}$ | 2.57 |
| $\mathbf{NO_x}$ | 1.84 |
| **PM** | 1.96 |
| $\mathbf{SO_2}$ | 1.89 |

## 4.2 MDO vs. HFO: Deep Water

The next comparison which is made concerns the emissions and efficiency of the bulk carrier sailing the same trajectory in deep and unrestricted water for heavy fuel oil and marine diesel oil. This is calculated at an inefficient engine speed of 51 rpm, as was done in the previous sections.

The different emissions are compared in the plots of Figure 58. The first thing to notice is that HFO and MDO emit the same amount of $CO$- and $CH_4$-particles. This is due to the equivalent emissions factors from Table 5. $CO$-emissions mainly exist when incomplete combustion occurs due to a shortage of air supply, as may be expected at lower loads. The $CH_4$ emission factor is extremely low since the main cause is a very small amount of methane slip. Besides this, the $CO_2$-emissions are slightly higher for MDO, resulting in 2,070.5 kg emitted versus 2,011.1 kg over the same trajectory with the same amount of fuel burned. Besides the dependency on fuel consumption, these emissions solely depend on the carbon content of the fuel, which is slightly higher for MDO.

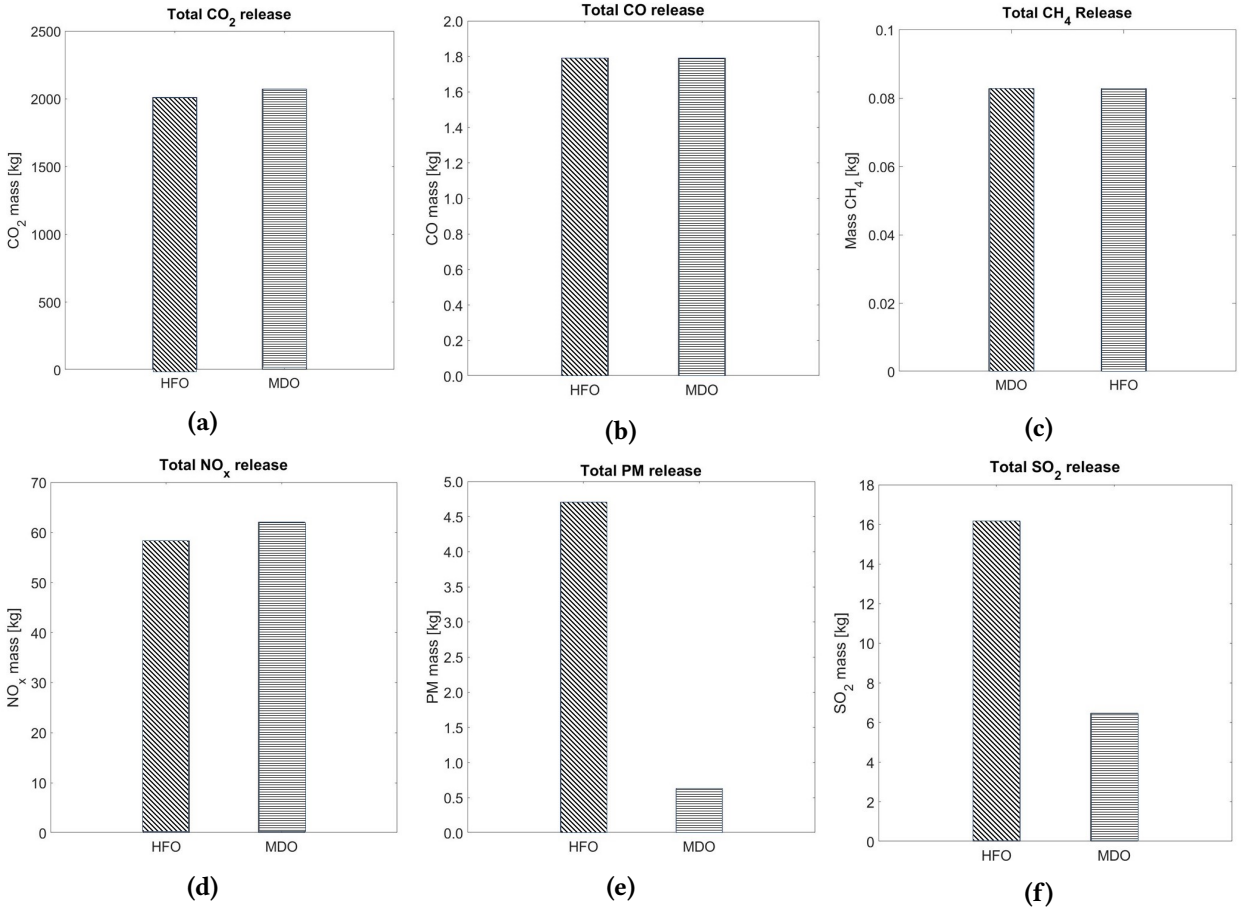


**Figure 58.** *Comparison of the total release of emissions in deep and unrestricted water for HFO and MDO, at an engine speed of 51 rpm.*

The nitrous oxides which are released during this short voyage are slightly higher for MDO than for HFO. A possible explanation for this is the fact that MDO's lower heating value is higher than that of HFO. This causes a larger amount of heat to be produced during the combustion of the fuel, which may result in an

increased amount of $NO_x$-emissions. If the emissions would be compared to the $NO_x$-limit by MARPOL (Figure 3), Figure 59 is obtained. At an engine speed of 51 rpm, the ship does not even comply with the Tier I limit. This makes sense due to the increased nitrous oxides at inefficient combustion of the fuel. If the emission rate is checked at an engine speed of 96.5 rpm, i.e. normal continuous load operation at 90%, the Tier II limit is easily obtained for MDO, and thus also for HFO in this engine. If a $NO_x$ ECA must be entered, the use of selective catalytic reduction and exhaust gas recirculation are the most promising options to comply to the standards at the moment.

The difference between the amount of $SO_2$-emissions released is quite large, with HFO emitting 2.5 times as much as MDO. This isn't hard to comprehend since the sulphur content of HFO is assumed to be 2.5%, while that of MDO is 1%. Both of these fuels would not apply to the Sulphur Cap 2020. Besides this, the North Sea and inland rivers of Belgium are compliant to the regulations of an Emission Control Area, meaning that even more stringent sulphur reduction is necessary. Luckily, it is not assumed that all these emissions are released into the air, since most of them will be captured by a scrubber which will be necessary on the ship. If this is not possible, another option is the usage of ultra-low sulphur fuel oil, which has a sulphur content below 0.1%. If no sulphur content at all is wanted, LNG may be used. However, this will lead to an increase of the $CH_4$ emissions due to the methane slip.

The last pollutant discussed here is particulate matter. These particles are a large variety of small, harmful substances such as carbon, soot, ash, sulphates, nitrates and carbonates. Therefore, it should not be too surprising that the PM release along the trajectory is far greater with HFO than MDO, since HFO may also be defined as the remnant from the distillation and cracking process of crude oil. These particles are less important at sea as they only have a limited impact on climate change, but a much more harmful impact on the human health. Therefore, it is important to prevent the use of HFO near high-populated areas and switch to even cleaner fuels. An example is LNG, which has an emissions factor 5 times lower than MDO [95]. EGR could also be used to reduce these emissions substantially.

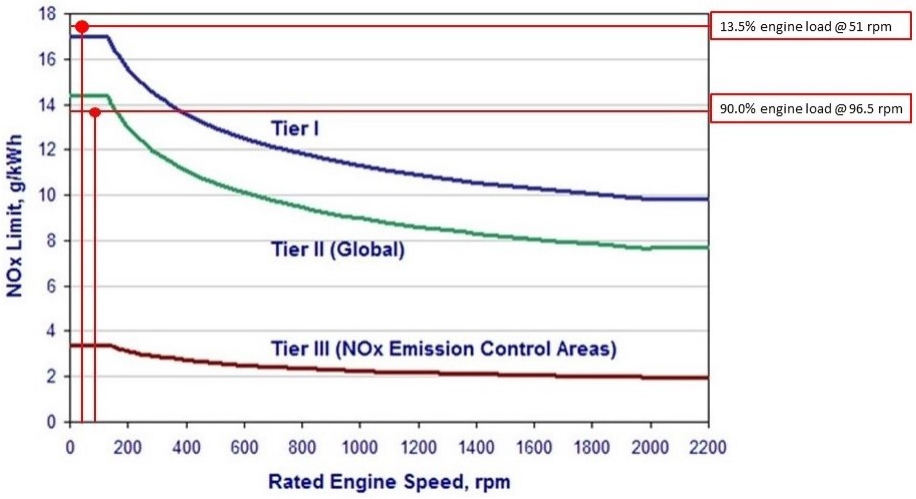


**Figure 59.** *$NO_x$ Tier II limit (non)-compliance by MDO in deep water, for low and for nominal load.*

The effective efficiency, calculated with Formula 38, is affected by the type of fuel used. Due to the lower LHV of heavy fuel oil, a slight increase of 2.8% efficiency is visible in Figure 60 at an engine load of 13.5%. This translates itself as well into the total ship efficiency, which is noticeably lower for marine diesel oil.

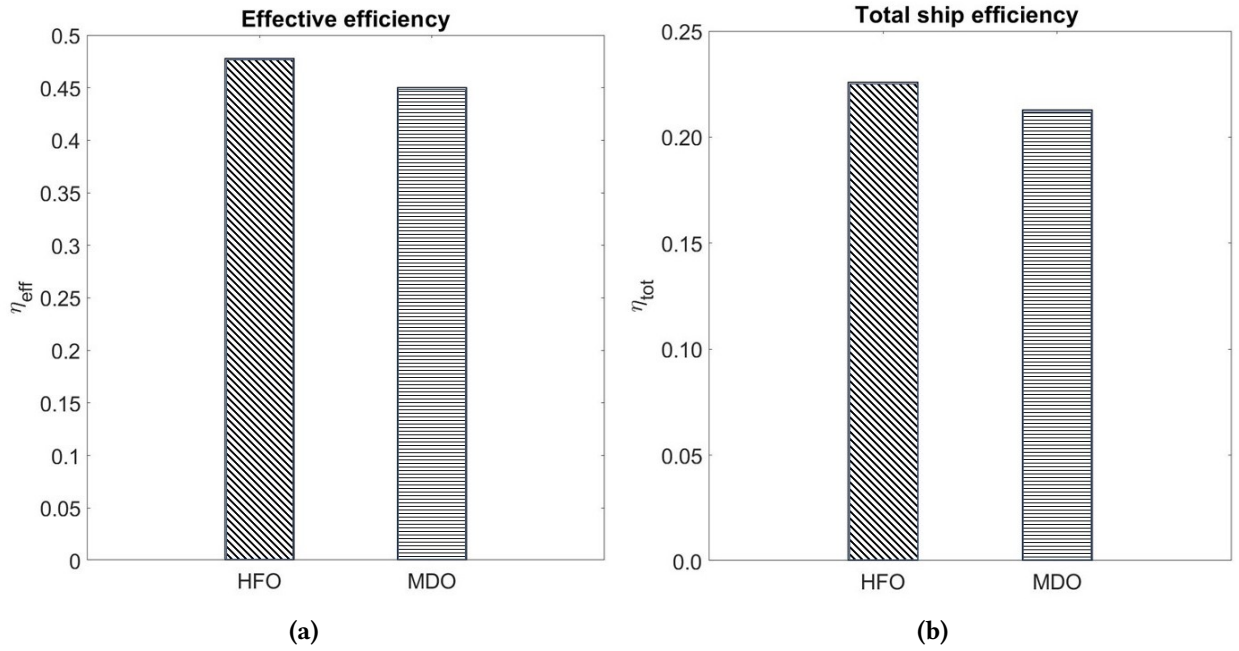


**Figure 60.** *Comparison of the effective engine efficiency $\eta_{eff}$ and total ship efficiency $\eta_{tot}$ in deep and unrestricted water for HFO and MDO, at an engine speed of 51 rpm.*

### 4.3 MDO vs. HFO: Shallow Water

A last short comparison which is made concerns the difference in emissions and efficiency between MDO and HFO when sailing in shallow and confined water, more specifically along the channel Ghent-Terneuzen. The measurements used are the same which were defined in the previous section on shallow water. The bulk carrier sails the same voyage along the channel for both fuels. Note that this is only a simulation, since the use of HFO without extra measures along the Belgian inland rivers is not allowed due to the high contamination and sulphur content.

Some of the emission rates are plotted and compared in Figure 61. The emissions of $CH_4$ and $CO$ are omitted due to the fact that they are exactly the same along the trajectory for both fuels. This may be attributed to the same reasons as explained previously for deep and unrestricted water. The total mass emitted over the trajectory for each pollutant is presented in Figure 62. Once again, the $CO_2$-emissions are slightly higher for marine diesel oil. Since these emissions depend solely on the carbon content and fuel consumption, a total release of 3,907.2 kg and 3,795.1 kg respectively for MDO and HFO can be seen.

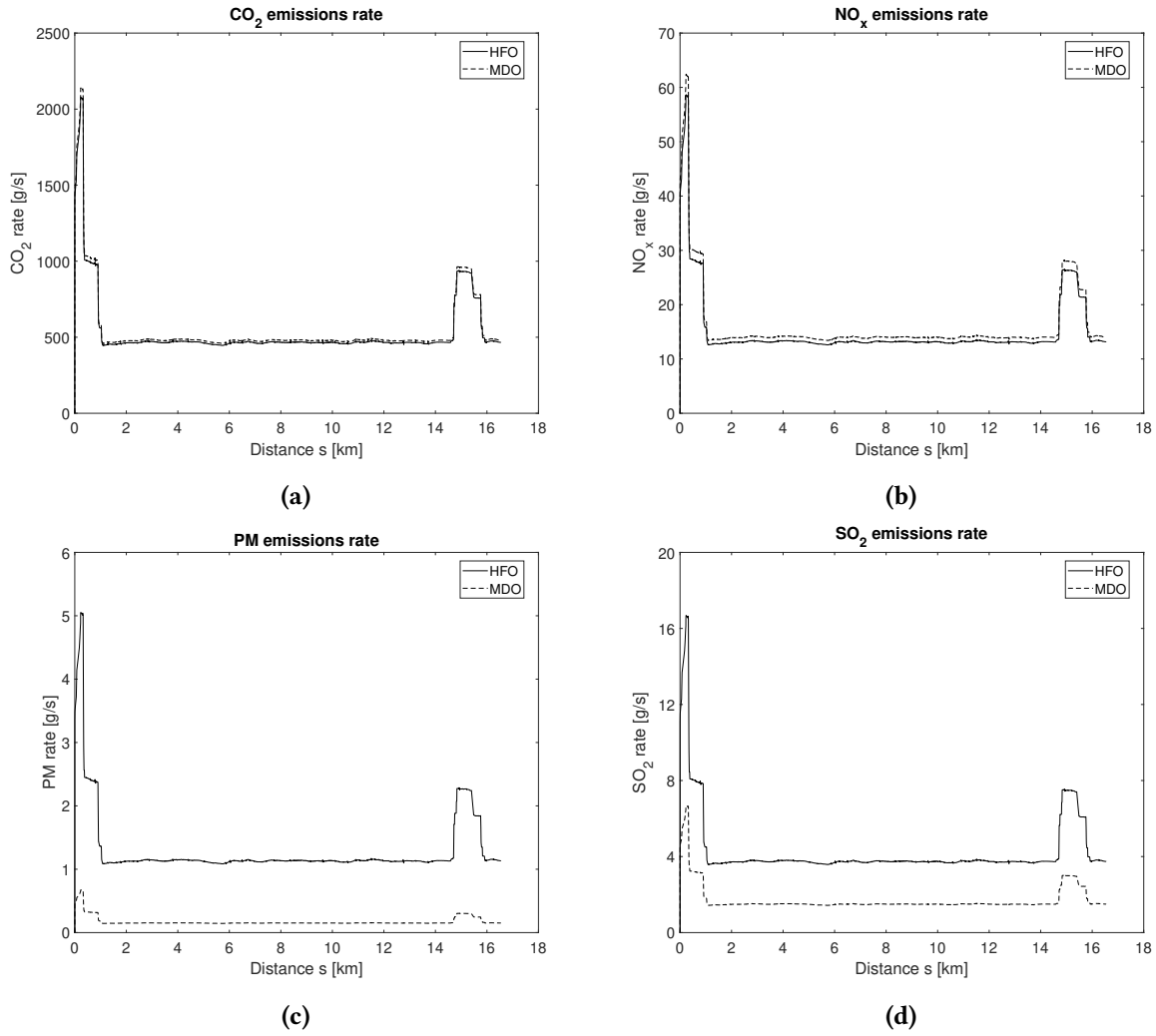


**Figure 61.** *Comparison of the emission rates in shallow and confined water for HFO and MDO, at an engine speed of 51 rpm.*

The same conclusions from the comparison in deep water could be drawn here for $NO_x$-emissions as well. When these emission rates and their total emitted amount are compared with the *MARPOL* limits for $NO_x$, Figure 63 is obtained. At an engine speed of 51 rpm, the original graph is even to small to contain the $NO_x$ emissions along the channel for MDO. Luckily, this is only the value which would be obtained without the use of selective catalytic reduction. If this would be used, a reduction of $NO_x$-emissions up to 90% is possible.

Once again, the difference between the $SO_2$-emissions is substantial, attributed to the difference in sulphur content of the different fuels. The same reasoning applies here, that a sulphur reduction will be necessary with the help of a scrubber or changing of the fuel oil to a cleaner fuel.

The last pollutant, PM, has much larger emission rates for HFO than for MDO. This may be attributed to the increased amount of pollutants and sulphur in HFO. Since this is only a theoretical value as HFO is not used in the inland waterways of Belgium without the use of extra technological measures, this result

is only of limited value.

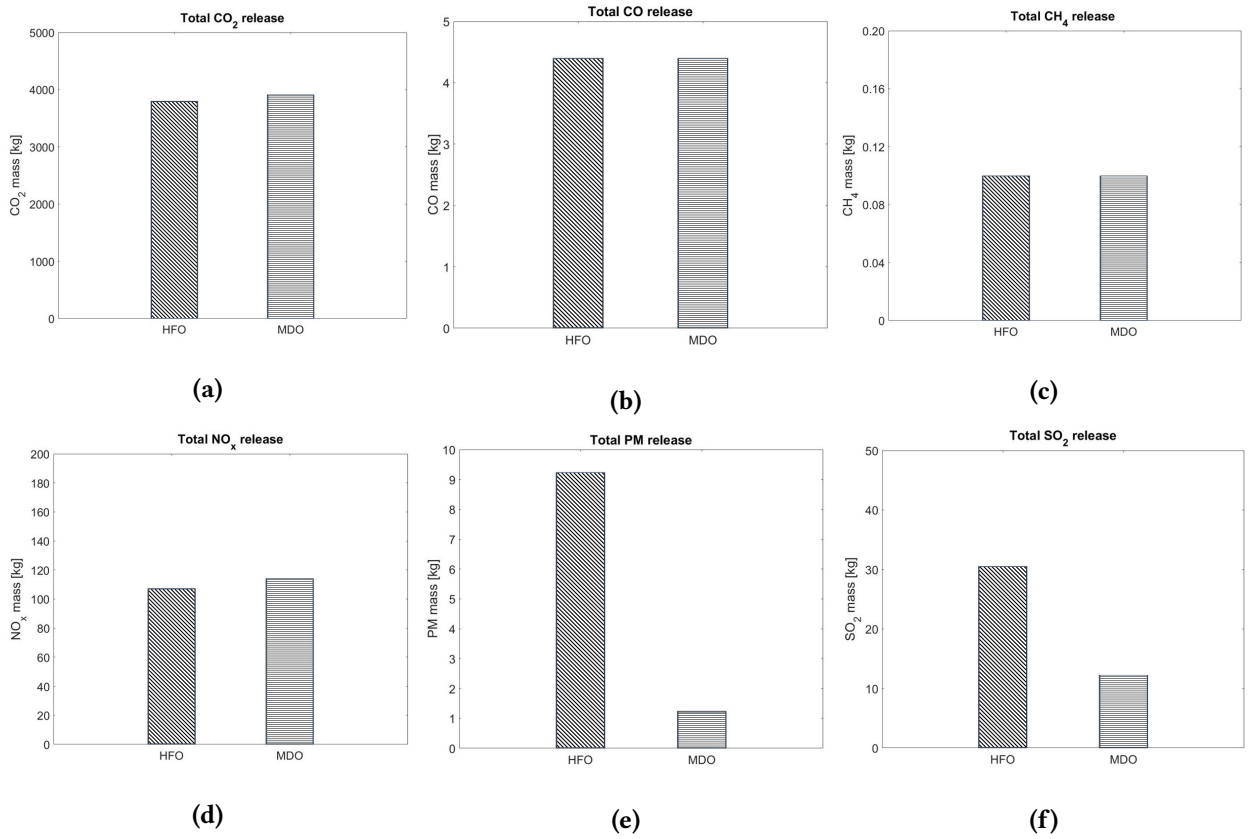


**Figure 62.** *Comparison of the total release of emissions in shallow and confined water for HFO and MDO, at an engine speed of 51 rpm.*

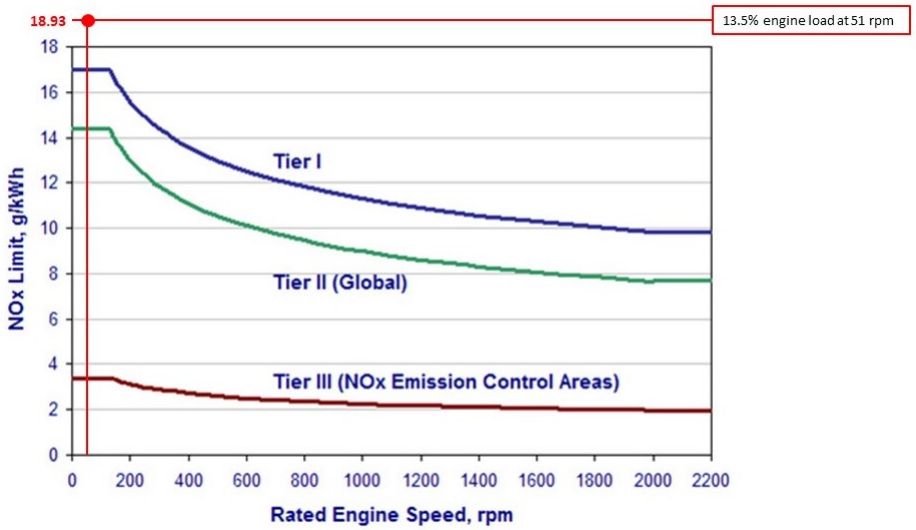


**Figure 63.** *$NO_x$ Tier II limit non-compliance by MDO in shallow water along channel Ghent-Terneuzen.*

# Chapter VI

# Conclusion and Future Research

This Master's dissertation opted to create a generic mathematical model for the calculation of a ship's fuel consumption and emissions when sailing along a shallow and confined waterway. Due to the increasing attention towards climate change and the dangers for human health, this dissertation tries to give an answer on the impact of sailing in shallow and confined water near densely populated areas. This impact would then be compared with a "normal" case of the same trajectory in deep and unrestricted water.

- At first, an extensive study on literature was performed, starting from the already existing regulations by the IMO. The technological and operational measures on how to mitigate several types of emissions were thoroughly investigated and a range of options was discussed, divided over 4 main categories: power and propulsion, alternative fuels and energy sources, hull design and operational measures. These measures consisted of mature and new technologies. None of these technologies is currently able to reduce emissions significantly to comply with the ambitious goal of IMO to reduce emissions by at least 50% by 2050. While operational measures are still applicable to current operating vessels, the three remaining alternatives require new technologies and large changes. A combination of these categories could prove to be very beneficial towards reducing the emissions, but large investment costs spook the ship owners and operators.
- Next, a mathematical model was developed for the calculation of a ship's emissions in shallow and confined water. This model, following a reverse-calculation procedure starting from the thrust and vessel speed, was designed as generic as possible. The model incorporates the influence of shallow and confined water if necessary. Based on several parameters such as the properties of the propeller and the engine as well as the emissions factors for the different types of fuel, the ship's efficiency, fuel consumption and emissions of harmful pollutants were estimated.
- The FHR provided full scale measurements and simulations regarding a bulk carrier sailing along the channel Ghent-Terneuzen. The application of the mathematical model on this case study of the bulk carrier in shallow and confined water revealed:
  - All emissions follow the same path when plotted against the trajectory. This plot resembles with the fuel consumption and brake power of the engine.
  - Near the end of the trajectory, a very significant increase was noticed. This increase was caused by the bridge of Zelzate, where the ship had to increase its propeller speed in order to maintain manoeuvrability during passage.

- Additionally, the effective engine efficiency $\eta_{eff}$ increased due to the increased load necessary at a higher rotational speed. The propulsive efficiency $\eta_D$ dropped significantly at this narrow passage, which caused the total ship efficiency $\eta_{tot}$ to drop as well to a minimum of 11.7%.
- When comparing HFO and MDO, HFO was more severe with the emission of harmful pollutants. The most significant part was that, even with MDO, the $NO_x$ Tier I limit was not attained at the low engine load on which the ship continuously sails along the channel.

When comparing the results of this case study with a similar situation in open water, the following observations were made:

- The emissions of all pollutants increased significantly for the shallow water case. The total $CO_2$ emissions over the same distance increased 1.89 times. For $CH_4$, this was even 2.57 times.
- With an average total ship efficiency $\eta_{tot}$ of 21.3% in deep water, the bulk carrier sailing along the channel performed noticeably worse with an average of 16-18% and a minimum of 11.7% when sailing past the bridge of Zelzate. This could mainly be accounted to the improved propulsive efficiency $\eta_D$ in deep water.
- Although less severe, even the $NO_x$ emissions for MDO in deep water surpassed the Tier I limit at this low load. When looking at the nominal load of 90% at which these ships usually sail, the Tier II limit was easily complied with.

These conclusions validate the need for further research on this topic with the help of more advanced models.

# 1 Future Research

As a final closure of this Master's dissertation, some ideas are included to extend the current model and to give some suggestions towards further research on this topic. First, the shortcomings of this model are addressed. These are comprised of:

- The comparison with the case of deep and unrestricted water is based on a lot of assumptions. These could be relaxed by e.g. measuring the actual thrust when sailing at this engine load, incorporating the effects of wind and waves, etc., leading to more realistic results.
- A large simplification which was made in the mathematical model was neglecting the rotational acceleration of the shaft. This way, the propeller torque and engine torque would be the same throughout the entire simulation. Incorporating this could lead to more accurate results.
- Instead of creating a model to calculate the emissions based on emissions factors, measurements of the actual emissions generated by the vessel would be preferred to obtain a better understanding.
- Investigate the effect of other fuels on pollution in shallow and confined water. A good example would be the implementation of LNG, since this fuel is gaining increased attention and will probably continue to do so.
- The model was based on the emissions of the main engine. However, auxiliary engines also exist on a ship and should be implemented as well.

- During the voyage along the channel, especially when entering and leaving the lock, tugboats will be inserted as well to ensure the manoeuvrability of the vessel. An electric transition is currently going on in this niche sector, but until completed, the emissions of tugboats should still be taken into account.

The measurements obtained ranged from the moment when the ship leaves the lock until it starts to decelerate in order to berth near the quay wall. The berthing of the vessel is not included in these measurements. The harmful pollutant emission during berthing seems like an interesting topic towards future research, especially given the fact that the ship is still near some densely populated areas. A comparison could be made with a ship being powered by batteries onboard or with power supplied by cold ironing.

A future where ships remain sailing on bunker fuels becomes more unrealistic with each passing day. Therefore, extensive research should be performed towards other, especially 'green' alternatives. For an industry that presently accounts 2-3% of the global carbon emissions, it must be innovative in its search towards cleaner options and continuously strive for improvement. The regulations imposed by different institutions will only become more stringent, and eventually everyone will have to adapt. How ship owners and operators choose to comply should be their choice, but clear rules and restrictions should be established to prevent fraudulent attempts of avoiding them. Besides this, an investigation should start towards the economic implications of reducing the fuel consumption of ships worldwide. This might serve as an extra boost or, if the cost for ship owners would be too high, start the process of financially supporting measures originating from the governments in order to gain green alternatives. The transition towards these alternatives is already in progress, but will happen gradually and take some years, even decades. Although a lot is already being done, lots of potential is still left unexploited. The maritime sector still has a long way to go, but it is getting there, step by step.

# Bibliography


[1] T.W.P. Smith et al., "Third IMO greenhous gas study 2014", IMO, 2014.

[2] K. Anderson and G. Peters, "The trouble with negative emissions", *Science 354*, pp. 182–183, 2016.

[3] E. Bouman, E. Lindstad, A. Rialland, and A. Stromman, "State-of-the-art technologies, measures, and potential for reducing GHG emissions from shipping - A review", *Transportation Research Part D 52*, pp. 408–421, 2017.

[4] IMO. (2019). Introduction to IMO, [Online]. Available: http://www.imo.org (visited on October 28, 2019).

[5] MEPC, "Report Of The Marine Environment Protection Committee On Its 58th Session", 2008.

[6] MEPC, "Report Of The Marine Environment Protection Committee On Its 58th Session: Annex 13", 2008.

[7] T. M. Trading. (2019). Thor Marine Trading: Map of (Future) ECAs., [Online]. Available: https://www.thormarinetrading.com/bunker-trading/seca-eca/ (visited on October 28, 2019).

[8] L. Zhen, M. Li, Z. Hu, W. Lv, and X. Zhao, "The Effects Of Emission Control Area Regulations On Cruise Shipping", *Transportation Research Part D 62*, pp. 47–63, 2018.

[9] L. Chen, T. Yip, and J. Mou, "Provision Of Emission Control Area And The Impact On Shipping Route Choice And Ship Emissions.", *Transportation Research Part D 58*, pp. 280–291, 2017.

[10] Wärtsila. (2019). $NO_x$ Technical Code, [Online]. Available: https://www.wartsila.com/encyclopedia/term/nox-technical-code (visited on November 18, 2019).

[11] IMO. (2019). Nitrogen Oxides ($NO_x$ - Regulation 13), [Online]. Available: http://www.imo.org/en/OurWork/Environment/PollutionPrevention/AirPollution/Pages/Nitrogen-oxides-(NOx)-%E2%80%93-Regulation-13.aspx (visited on November 18, 2019).

[12] DNV-GL. (2015). Upcoming environmental regulations for emissions to air - IMO $NO_x$ Tier III, [Online]. Available: https://www.dnvgl.com/news/upcoming-environmental-regulations-for-emissions-to-air-imo-nox-tier-iii-45479 (visited on November 18, 2019).

[13] MARPOL. (2019). EEDI & SEEMP, [Online]. Available: https://www.marpol-annex-vi.com/eedi-seemp/ (visited on November 17, 2019).

[14] MEPC, *2018 Guidelines on the method of calculation of the attained EEDI for new ships*. 2018.

[15] M. E. P. Committee, "Guidelines for voluntary use of the ship energy efficiency operational indicator (EEOI)", International Maritime Organization, 2009.

[16] M. E. P. Committee, "Guidance for the development of a ship energy efficiency management plan (SEEMP)", International Maritime Organization, 2009.

[17] "Understanding exhaust gas treatment systems: Guidance for shipowners and operators.", Lloyd's register, 2012.

[18] EGCSA. (2014). $NO_x$ Reduction by Exhaust Gas Recirculation – MAN explains, [Online]. Available: https://www.egcsa.com/exhaust-gas-recirculation-explained/ (visited on May 12, 2020).

[19] E. Zhang, X. Liang, F. Zhang, P. Yang, X. Cao, X. Wang, and H. Yu, "Evaluation of exhaust gas recirculation and fuel injection strategies for emission performance in marine two-stroke engine", *Energy Procedia 158*, pp. 4523–4528, 2018.

[20] M. Pan, Z. Zheng, R. Huang, X. Zhou, H. Huang, J. Pan, and Z. Chen, "Reduction in $pm$ and $no_x$ of a diesel engine integrated with n-octanol fuel addition and exhaust gas recirculation", *Energy 187*, 2019.

[21] J. Sai Kumar, T. Sharma, K. Murthy, and G. Prasad Rao, "Effect of reformed EGR on the performance and emissions of a diesel engine: A numerical study", *Alexandria Engineering Journal 57*, pp. 517–525, 2018.

[22] (2020). Volkswagen emissions scandal, [Online]. Available: https://en.wikipedia.org/wiki/Volkswagen_emissions_scandal (visited on May 14, 2020).

[23] F. Cattaneo, "Selective catalytic reduction system for marine applications: Dynamic modelling and system integration", TU Delft, 2018.

[24] Wärtsilä, *Wärtsilä $NO_x$ reducer (NOR): Product Leaflet*, 2017.

[25] M. Magnusson, E. Fridell, and H. Ingelsten, "The influence of sulfur dioxide and water on the performance of a marine SCR catalyst", *Applied Catalysis B: Environmental 111-112*, pp. 20–26, 2012.

[26] DNV-GL. (2018). Scrubbers at a glance, [Online]. Available: https://www.dnvgl.com/expert-story/maritime-impact/Scrubbers-at-a-glance.html (visited on May 12, 2020).

[27] S. Sethi. (2020). A guide to scrubber system on ship, [Online]. Available: https://www.marineinsight.com/tech/scrubber-system-on-ship/ (visited on May 12, 2020).

[28] YaraMarine. (2020). Yara Marine Technologies: $SO_x$ scrubbers, [Online]. Available: https://yaramarine.com/ (visited on May 12, 2020).

[29] L. Abadie, N. Goicoechea, and I. Galarraga, "Adapting the shipping sector to stricter emissions regulations: Fuel switching or installing a scrubber?", *Transportation Research Part D 57*, pp. 237–250, 2017.

[30] L. Jiang, J. Kronbak, and L. Christensen, "The costs and benefits of sulphur reduction measures: Sulphur scrubbers versus marine gas oil", *Transportation Research Part D 28*, pp. 19–27, 2014.

[31] MAN, "Waste Heat Recovery System for reduction of fuel consumption, emissions and EEDI", MAN Diesel & Turbo, 2012.

[32] ABB, "Infographic: Decreasing energy consumption with ABB waste heat recovery system", 2020.

[33] K. Senary, A. Tawfik, E. Hebazy, and A. Ali, "Development of a waste heat recovery system onboard LNG carrier to meet IMO regulations", *Alexandria Engineering Journal 55*, pp. 1951–1960, 2016.

[34] S. Suarez de la Fuente, D. Roberge, and A. Greig, "Safety and $CO_2$ emissions: Implications of using organic fluids in a ship's waste heat recovery system", *Marine Policy 75*, pp. 191–203, 2017.

[35] D. Bryant. (2012). Kort nozzle: Application of aeronautical engineering to ship propulsion, [Online]. Available: https://www.maritimeprofessional.com/blogs/post/kort-nozzle-13450 (visited on May 14, 2020).

[36] G. Gennaro and J. Gonzalez-Adalid, "Improving the propulsion efficiency by means of contracted and loaded tip (CLT) propellers", 2012.

[37] C. Hsieh and C. Felby, "Biofuels for the marine shipping sector: An overview and analysis of sector infrastructure, fuel technologies and regulations", IEA Bioenergy, 2017.

[38] P. Gilbert, C. Walsh, M. Traut, U. Kesieme, K. Pazouki, and A. Murphy, "Assessment of full life-cycle air emissions of alternative shipping fuels", *Journal of Cleaner Production 172*, pp. 855–866, 2018.

[39] F. Hossain, T. Rainey, Z. Ristovski, and R. Brown, "Performance and exhaust emissions of diesel engines using microalgae fame and the prospects for microalgae HTL biocrude", *Renewable and sustainable energy reviews 82*, pp. 4269–4278, 2018.

[40] J. Nielsen and D. Stenersen, "Emission factors for $CH_4$, $NO_x$, particulates and black carbon for domestic shipping in norway", Marintek, 2010.

[41] O. Schinas and M. Butler, "Feasibility and commercial considerations of LNG-fueled ships", *Ocean Engineering 122*, pp. 84–96, 2016.

[42] A. Milner, "Liquefied natural gas: A marine fuel for Canada's West Coast", Canadian Natural Gas Vehicle Alliance, 2014.

[43] R. Khurmi, *Material Science*. S. Chand & Company, 2014.

[44] C. Deniz and B. Zincir, "Environmental and economical assessment of alternative marine fuels", *Journal of Cleaner Production 113*, pp. 438–449, 2015.

[45] FCHEA. (2020). Fuel cell & hydrogen energy basics, [Online]. Available: http://www.fchea.org/h2-day-2019-events-activities/2019/8/1/fuel-cell-amp-hydrogen-energy-basics (visited on May 11, 2020).

[46] (2020). Hydroville, [Online]. Available: http://www.hydroville.be/ (visited on May 11, 2020).

[47] M. De Roo, "Saverys (CEO van CMB): 'Waterstof is onze toekomst als rederij'", *De Tijd*, 2020.

[48] U.S. Maritime Administration. (2007). NS Savannah, [Online]. Available: https://web.archive.org/web/20070623210106/https://voa.marad.dot.gov/programs/ns_savannah/index.asp (visited on November 17, 2019).

[49] C. S. Info. (2019). NS Savannah Cruise Ship Tour 2019, [Online]. Available: https://www.youtube.com/watch?v=rJXs2bJHUcg (visited on November 17, 2019).

[50] World Nuclear News. (2019). Russia's floating plant heads for final destination, [Online]. Available: http://www.world-nuclear-news.org/Articles/Russias-floating-plant-heads-for-final-destination (visited on November 17, 2019).

[51] J. Kim, M. Song, and S. Alameri, "Emerging areas of nuclear power applications", *Nuclear Engineering and Design 354*, 2019.

[52] SkySails Group GmBH. (2019). Skysails Website, [Online]. Available: https://www.skysails.info (visited on November 1, 2019).

[53] The Editors of Encyclopaedia Britannica. (2019). Magnus Effect, [Online]. Available: https://www.britannica.com/science/Magnus-effect (visited on November 1, 2019).

[54] L. Talluri, D. Nalianda, K. Kyprianidis, T. Nikolaidis, and P. Pilidis, "Techno-Economic and Environmental Assessment of Flettner Rotors for Marine Propulsion", *Ocean Engineering 121*, pp. 301–311, 2017.

[55] T. Perkins, G. Dijkstra, and D. Roberts, "The Maltese Falcon: The Realisation", *Hiswa Symposium 2004*, 2004.

[56] Eco Marine Power Co. Ltd. (2018). EnergySail, [Online]. Available: https://www.ecomarinepower.com/en/energysail (visited on November 1, 2019).

[57] J. Prestien. (2019). Marine Traffic: E-Ship 1 Photo, [Online]. Available: https://www.marinetraffic.com/nl/ais/details/ships/218108000 (visited on October 28, 2019).

[58] OCEANCO. (2020). OCEANCO delivers the 106.7 m Black Pearl, the largest dynarig sailing yacht in the world, [Online]. Available: https://www.oceancoyacht.com/en/press/press-releases/342-oceanco-delivers-the-106-7m-black-pearl-the-largest-dynarig-sailing-yacht-in-the-world (visited on December 5, 2019).

[59] W. Yu, P. Zhou, and H. Wang, "Evaluation on the Energy Efficiency and Emissions Reduction of a Short-Route Hybrid Sightseeing Ship.", *Ocean Engineering 162*, pp. 34–42, 2018.

[60] A. Glykas, G. Papaioannou, and S. Perissakis, "Application and Cost–Benefit Analysis of Solar Hybrid Power Installation on Merchant Marine Vessels", *Ocean Engineering 37*, pp. 592–602, 2010.

[61] European Council and Parliament, "Directive 2008/1/EC concerning integrated pollution prevention and control", *Official Journal of the European Union*, 2008.

[62] P. Kohli. (2009). Cold ironing schematic, [Online]. Available: https://en.wikipedia.org/wiki/Cold_ironing#/media/File:PxKohliColdIron.jpg (visited on May 11, 2020).

[63] T. Zis, "Prospects of cold ironing as an emissions reduction option", *Transportation Research part A 119*, pp. 82–95, 2019.

[64] European Council and Parliament, "Directive 2014/94/EU on the deployment of alternative fuels infrastructure", *Official Journal of the European Union*, 2014.

[65] F. Ballini and R. Bozzo, "Air pollution from ships in ports: The socio-economic benefit of cold-ironing technology", *Research in Transportation Business & Management 117*, pp. 92–98, 2015.

[66] H. Lindstad, B. Asbjornslett, and A. Stromman, "The importance of economies of scale for reductions in greenhouse gas emissions from shipping", *Energy Policy 46*, 2012.

[67] H. Psaraftis, "Green maritime logistics", National Technical University of Athens, Greece, 2009.

[68] H. Lindstad, E. Jullumstro, and I. Sandaas, "Reductions in cost and greenhouse gas emissions with new bulk ship designs enabled by the panama canal expansion", *Energy Policy 59*, pp. 341–349, 2013.

[69] H. Wang, J. Faber, D. Nelissen, B. Russell, and D. St Amand, "Reduction of GHG emissions from ships: Marginal abatement costs and cost effectiveness of energy-efficiency measures", MEPC (IMO), 2011.

[70] O. Buhaug et al., "Second IMO greenhous gas study 2014", IMO, 2009.

[71] ABS, "Air lubrication technology", American Bureau of Shipping, 2019.

[72] Reuters. (2014). High Fuel Costs and New Emissions Regs are Pushing the Boundaries of Naval Architecture, [Online]. Available: https://gcaptain.com/high-fuel-costs-new-emissions-regs-pushing-boundaries-naval-architecture/ (visited on May 14, 2020).

[73] G. Delefortrie and M. Candries, *Hydrostatics and Propulsion of Maritime Constructions*, 2019.

[74] D. Kane, "Technical fuel conservation: Hull and propeller performance", Propulsion Dynamics Inc., 2014.

[75] C.-C. Chang and C.-H. Chang, "Energy conservation for international dry bulk carriers via vessel speed reduction", *Energy Policy 59*, pp. 710–715, 2013.

[76] T. Tezdogan, A. Incecik, O. Turan, and P. Kellett, "Assessing the impact of a slow steaming approach on reducing the fuel consumption of a container ship advancing in head seas", *Transportation Research Procedia 14*, pp. 1659–1668, 2016.

[77] IMO. (2020). Ship's routeing and weather routeing, [Online]. Available: http://www.imo.org/en/OurWork/Safety/Navigation/Pages/ShipsRouteing.aspx (visited on May 11, 2020).

[78] DNV-GL. (2020). Glomeep: Weather routing, [Online]. Available: https://glomeep.imo.org/technology/weather-routing/ (visited on May 11, 2020).

[79] DNV-GL. (2019). Efficiency Finder - Trim & Ballast optimisation, [Online]. Available: https://www.dnvgl.com/maritime/energy-efficiency/efficiency-finder.html (visited on November 18, 2019).

[80] Y. Du, M. Qiang, W. Shuaian, and K. Haibo, "Two-phase optimal solutions for ship speed and trim optimisation over a voyage using voyage report data", *Transportation Research Part B 122*, pp. 88–114, 2019.

[81] Machinery Spaces. (2016). Ship's propeller shaft: Thrust blocks and bearings, [Online]. Available: http://www.machineryspaces.com/propeller-shaft.html (visited on May 23, 2020).

[82] J.S. Carlton, *Marine Propellers and Propulsion: 4th Edition*. Elsevier, 2018.

[83] MAN B&W, "Basic principles of ship propulsion", *MAN Diesel & Turbo*, 2011.

[84] MAN, "MAN B&W G50ME-C9.5-TII Project Guide", MAN B&W, 2014.

[85] M. Leduc. (2001). The marine diesel engine, [Online]. Available: http://www.machineryspaces.com/propeller-shaft.html (visited on May 23, 2020).

[86] United States Naval Academy, *Resistance and powering of ships*, 2020.

[87] J. Holtrop and G. Mennen, "An approximate power prediction method", *International Shipbuilding Progress 29*, pp. 166–170, 1982.

[88] "Capability of ship manoeuvring simulation models for approach channels and fairways in harbours: Report of working group no. 20 of permanent technical committee ii, supplement to pianc bulletin, no. 77.", PIANC, 1992.

[89] G. Delefortrie, *Ship Behaviour in Shallow and Confined Water*, 2020.

[90] G. Hughes, "Friction and form resistance in turbulent flow and a proposed formulation for use in model and ship correlation.", *Transactions of the Royal Institution of Naval Archtiects 96*, pp. 314–376, 1954.

[91] T. Havelock. (1921). The Effect of Shallow Water on Wave Resistance, [Online]. Available: https://royalsocietypublishing.org/doi/pdf/10.1098/rspa.1922.0013 (visited on February 4, 2020).

[92] D.W. Taylor, *The speed and power of ships*, 1943.

[93] H. Yasukawa, "Computation of effective rudder forces of a ship in shallow water", *Symposium of forces acting on a manoeuvring vessel*, pp. 125–133, 1998.

[94] G. Kuiper, *The Wageningen propeller series*. Maritiem Research Instituut Nederland, 1992.

[95] EPA. (2020). Basic information of air emissions factors and quantification, [Online]. Available: https://www.epa.gov/air-emissions-factors-and-quantification/basic-information-air-emissions-factors-and-quantification (visited on April 25, 2020).

[96] Sassevaart and Vlaams-Nederlandse Scheldecommissie. (2019). Nieuwe Sluis Terneuzen, [Online]. Available: https://nieuwesluisterneuzen.eu/. (visited on December 3, 2019).

[97] (2020). Draaibrug Sas van Gent, [Online]. Available: https://beeldbank.rws.nl/MediaObject/Details/Over_het_kanaal_Gent__Terneuzen_te_Sas_van_Gent_ligt_een_draaibrug_die_gebouwd_is_tussen_1965_en_1969_en_vormt_de_320_meter_lange_oeververbinding_tussen_de_Westelijke_en_405551 (visited on May 10, 2020).

[98] SOLAS. (1999). Maritime Safety Committee's 70th Session, [Online]. Available: https://web.archive.org/web/20070904190443/http://www.eagle.org/regulatory/regupdate/msc70/bulk.html (visited on November 24, 2019).

[99] "The World Merchant Fleet in 2018: Statistics from Equasis", Equasis, 2018.

[100] MarineTraffic. (2019). KMAX VISION Vessel Particulars, [Online]. Available: https://www.marinetraffic.com/en/ais/details/ships/shipid:194054/mmsi:209995000/imo:9436654/vessel:KMAX_VISION (visited on November 24, 2019).

[101] MAN B&W, "Propulsion Trends in Bulk Carriers", *MAN Diesel & Turbo*, 2019.

[102] (2020). B-Series Propeller Generator, [Online]. Available: https://www.wageningen-b-series-propeller.com/ (visited on April 28, 2020).

[103] E. Lataire, M. Vantorre, M. Candries, K. Eloot, J. Verwilligen, G. Delefortrie, C. Chen, and M. Mansuy, "Systematic techniques for fairway evaluation based on ship manoeuvring simulations", *34th PIANC-World Congress Panama City*, 2018.

[104] M. Vedran, Z. Bozica, and P.-O. Jasna, "Marine slow speed two-stroke diesel engine: Numerical analysis of efficiencies and important operating parameters", *International Scientific Jorunal "Machines. Technologies. Materials" 10*, pp. 481–484, 2017.

[105] X. Sun and X. Liang, "Influence on different fuels physical properties for marine diesel engine", *Energy Procedia 142*, pp. 1159–1165, 2017.

[106] (2020). CEAS Engine Calculations, [Online]. Available: https://marine.man-es.com/two-stroke/ceas (visited on March 30, 2020).

[107] I. International, "Current methodologies in preparing mobile source port-related emission inventories", U.S. Environmental Protection Agency, 2009.

[108] S. Verhelst, *Displacement Pumps, Compressors and IC Engine Fundamentals*, 2019.

[109] A. Shirneshan, "$HC$, $CO$, $CO_2$ and $NO_x$ Emission evaluation of a diesel engine fueled with waste frying oil methyl ester", *Procedia - Social and Behavioral Sciences 75*, pp. 292–297, 2013.

[110] T. Ogawa, K. Nakakita, M. Yamamoto, M. Okada, and Y. Fujimoto, "Fuel effects on particulate emissions from d.i. engine - relationship among diesel fuel, exhaust gas and particulates", pp. 1683–1696, 1997.

[111] (2017). Scheepvaart op Gent even onderbroken door probleem met Zelzatebrug, [Online]. Available: https://www.flows.be/nl/shipping/scheepvaart-op-gent-even-onderbroken-door-probleem-met-zelzatebrug (visited on May 10, 2020).

# Appendices

# Appendix A

# CEAS Engine Data Report

# MAN Energy Solutions

## CEAS Engine Data report
## 9G50ME-C9.5 HL with scrubber

**DISCLAIMER: This engine has been replaced by a newer and more efficient engine. Data from replaced engines should only be used for comparison and processing existing or repeat orders. For new projects, the latest version of the engine catalogue must be used.**

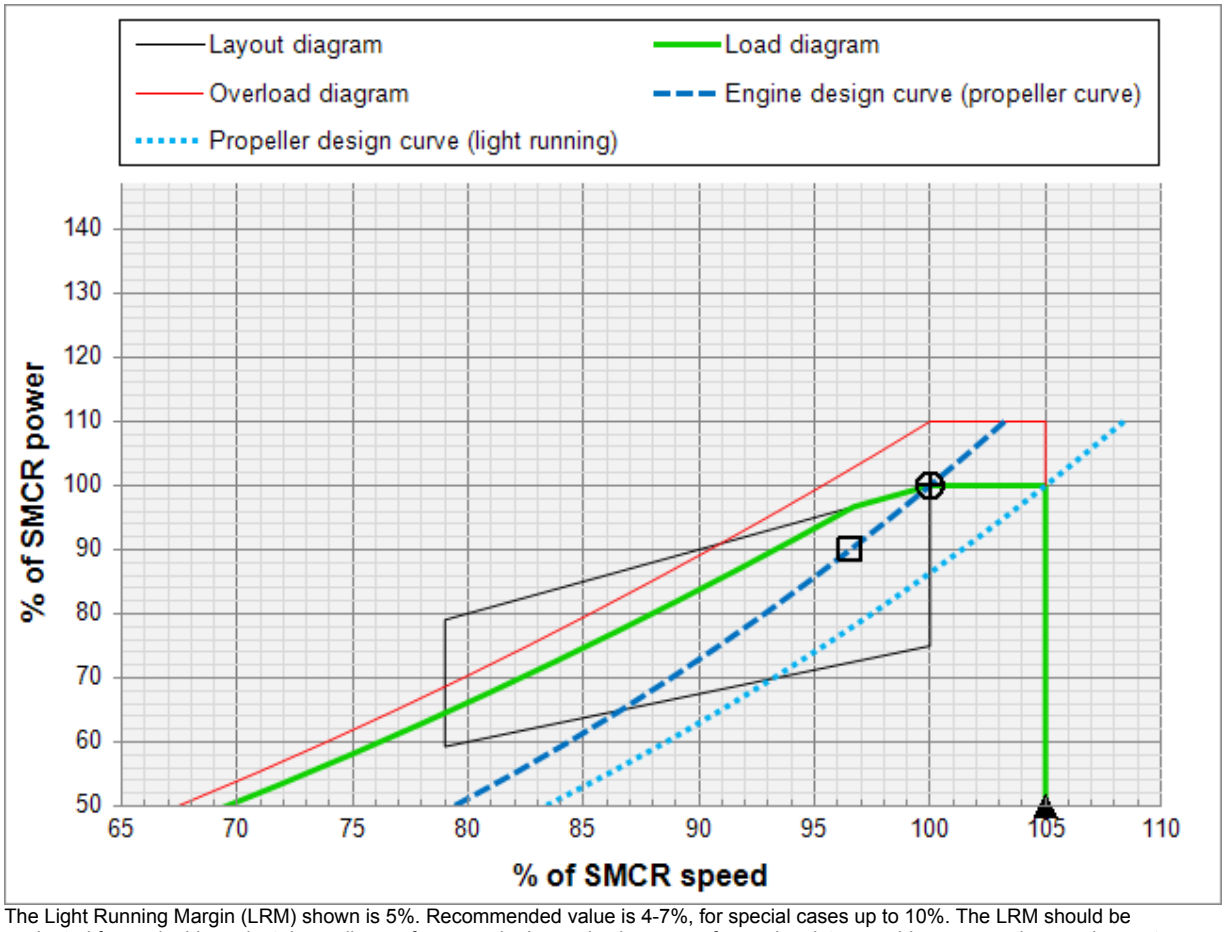


The Light Running Margin (LRM) shown is 5%. Recommended value is 4-7%, for special cases up to 10%. The LRM should be evaluated for each ship project depending on for example: In-service increase of vessel resistance, ship manoeuvring requirements, additional engine load due to power take-out (PTO) and possible requirements related to a barred speed range (short passing time).

| Point | | Power kW | Speed r/min | MEP Bar |
|---|---|---|---|---|
| + | SMCR: Specified Maximum Continuous Rating (100.0% of NMCR) | 15,480 | 100.0 | 21.0 |
| □ | NCR: Normal Continuous Rating (90.00% of SMCR) | 13,932 | 96.5 | 19.6 |
| | Maximum over load (110% of SMCR) | 17,028 | - | - |
| ▲ | Maximum speed limit (105% of SMCR) | - | 105.0 | - |
| ○ | L1, NMCR: Nominal Maximum Continuous Rating | 15,480 | 100.0 | 21.0 |

Further reading: Basic principles of ship propulsion

## Specified main engine and other parameters

| Specified parameters | |
|---|---|
| Type of propeller | Fixed pitch propeller |
| Cooling system | Central water cooling system |
| Hydraulic control oil system | Common (system oil) |
| Hydraulic power supply | Mechanical |
| Cylinder oil lubricator type | Alpha lubricator |
| Fuel sulphur content for engine design | High sulphur |
| Sulphur in fuel (Tier II) | max 3.5% sulphur |
| NOx emission compliance | Tier II |

| Turbocharger specifications | |
|---|---|
| Turbocharger efficiency | High efficiency |
| Number of turbochargers and make/type | 1 x MAN TCA77-21 |
| Turbocharger lubrication | Common (system oil) |
| Exhaust gas scrubber for high sulphur | Standard |
| Exhaust back pressure (Tier II) | 60 mbar |

## Fuel consumption and gas figures

| | Tier II | |
|---|---|---|
| **SFOC** | **SMCR** g/kWh | **NCR** g/kWh |
| ISO | 168.5 | 166.1 |
| Tropical | 170.2 | 167.9 |
| Specified | 166.4 | 164.1 |

SFOC: Specific Fuel Oil Consumption (LCV: 42,700 kJ/kg)

| | Tier II | |
|---|---|---|
| **Exhaust gas amount** | **SMCR** kg/s | **NCR** kg/s |
| ISO | 32.7 | 30.4 |
| Tropical | 30.3 | 28.2 |
| Specified | 34.0 | 31.7 |

| | Tier II | |
|---|---|---|
| **Exhaust gas temperature** | **SMCR** °C | **NCR** °C |
| ISO | 245 | 232 |
| Tropical | 278 | 265 |
| Specified | 220 | 207 |

| | Tier II | |
|---|---|---|
| **Turbocharger air consumption** | **SMCR** kg/s | **NCR** kg/s |
| ISO | 32.0 | 29.8 |
| Tropical | 29.6 | 27.6 |
| Specified | 33.3 | 31.0 |

ISO, tropical and specified conditions are listed in the References and tolerances section.

## Expected lubrication oil consumption

| Fuel sulphur | Cylinder oil consumption | Lube oil consumption |
|---|---|---|
| 2.1%-3.5% | typically 0.63-1.05 g/kWh* | 41 kg/24h |

*) Using 100 BN cylinder oil.

## Capacities of pumps and coolers

| Pump | Flow capacity $m^3/h$ | Pump head bar |
|---|---|---|
| Fuel oil circulation | 7.3 | 6.0 |
| Fuel oil supply | 4.2 | 4.0 |
| Jacket cooling water | 130 | 3.0 |
| Central fresh water | 340 | 2.0 |
| Sea water for central cooling | 460 | 2.5 |
| Lubrication oil | 350 | 4.0 |

| Capacities of cooler(s) on engine | No. of coolers | Central water flow $m^3/h$ | Heat dissipation kW |
|---|---|---|---|
| Scavenge air cooler(s) – data per cooler | 1 | 200 | 5,630 |
| Scavenge air cooler(s) – total | | 200 | 5,630 |

| Capacities of auxiliary heat exchangers | | $m^3/h$ | Central water flow $m^3/h$ | Heat dissipation kW |
|---|---|---|---|---|
| Central cooler | Sea water flow | 460 | 340 | 9,380 |
| Jacket water cooler | Jacket water flow | 130 | 140 | 2,410 |
| Lubricating oil cooler | Oil flow | 350 | 140 | 1,260 |

All flows are stated as minimum required flows.
The pump heads stated are for guidance only, and depend on the actual pressure drop across coolers, filters, etc. in the systems. The capacities do not account for any components other than the engine itself.
Pertaining cooling water flow diagram, temperatures, viscosities and pressures for pumps and coolers, see “Engine Project Guide”.

## Capacities of auxiliary systems

| Air cooler cleaning unit | |
|---|---|
| Air cooler cleaning tank | 0.60 $m^3$ |
| Capacity of pump | 2.0 $m^3/h$ |

| Cylinder oil system | |
|---|---|
| Storage tanks | 2 x 27 $m^3$ |
| Service tanks | 2.1 $m^3$ |

| Fuel oil system | |
|---|---|
| Distillate marine fuel service tank, 12 h | 36.5 $m^3$ |
| Residual marine fuel settling tanks, 2 x 12 h | 2 x 34.2 $m^3$ |
| Residual marine fuel service tank, 12 h/95 °C | 35 $m^3$ |
| Residual marine fuel separator, 98 °C | 3,560 l/h |
| Fuel oil pre-heater | 121 kW |

| Lubrication oil system | |
|---|---|
| Storage tanks (2 x 3 months) | 2 x 4.9 $m^3$ |
| Separator, 95 °C | 2,110 l/h |
| Recommended lube oil bottom tank | 21 $m^3$ |

| Miscellaneous | |
|---|---|
| Jacket water expansion tank*) | 10 % |
| Motor rating, auxiliary blowers | 2 x 48 kW |

*) Jacket water expansion tank volume given in percent of the total jacket water volume.

| Starting air system, 30 bar***) | |
|---|---|
| Receiver volume (12 starts) | 2 x 6.0 $m^3$ |
| Compressors (total) | 360 $m^3/h$ |

***) Starting air system capacities do not include air consumption for ventilation of double wall pipe or Tier III air consumers. An assessment is to be performed to determine whether the above needs to be increased.

| Various drain tanks | |
|---|---|
| Stuffing box drain tank | 0.30 $m^3$ |
| Scavenge air drain tank | 0.40 $m^3$ |

# Engine dimensions, masses and overhaul heights

| Dimensions | |
|---|---|
| A: Cylinder distance | 872 mm |
| B1: Width of bedplate at foot flange | 3,776 mm |
| B2: Width of bedplate at top flange | 3,652 mm |
| C: Distance from foot to crankshaft | 1,205 mm |
| L min: Minimum length of engine | 9,748 mm |

| Overhaul heights | |
|---|---|
| H1: Normal lifting procedure | 10,775 mm |
| H2: Reduced height lifting procedure | 10,075 mm |
| H3: Tilted lifting with double jib crane | 9,775 mm |

| Crane capacities | |
|---|---|
| Normal lifting procedure | 3.2 t |
| With electrical double jib crane | 2 x 1.6 t |

| Masses | |
|---|---|
| Mass of main engine, dry | 345 t |
| Mass of water and oil in engine | 2.0 t |

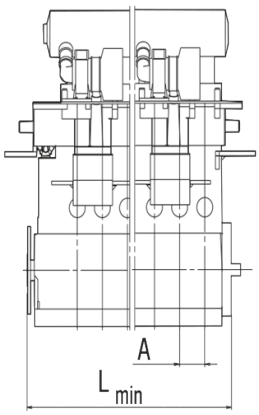


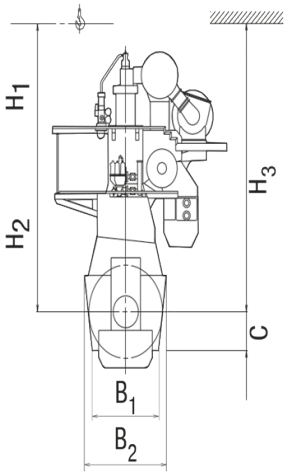


The real engine length at crankshaft centreline level may be larger than the minimum length of the engine, as it depends on the vibration conditions of the main engine and shaft system, i.e. on whether a vibration damper and/or moment compensator needs to be installed. Indicated values are for guidance only and are not binding.

## Fuel consumption and exhaust gas data
## Fuel Oil, Tier II mode

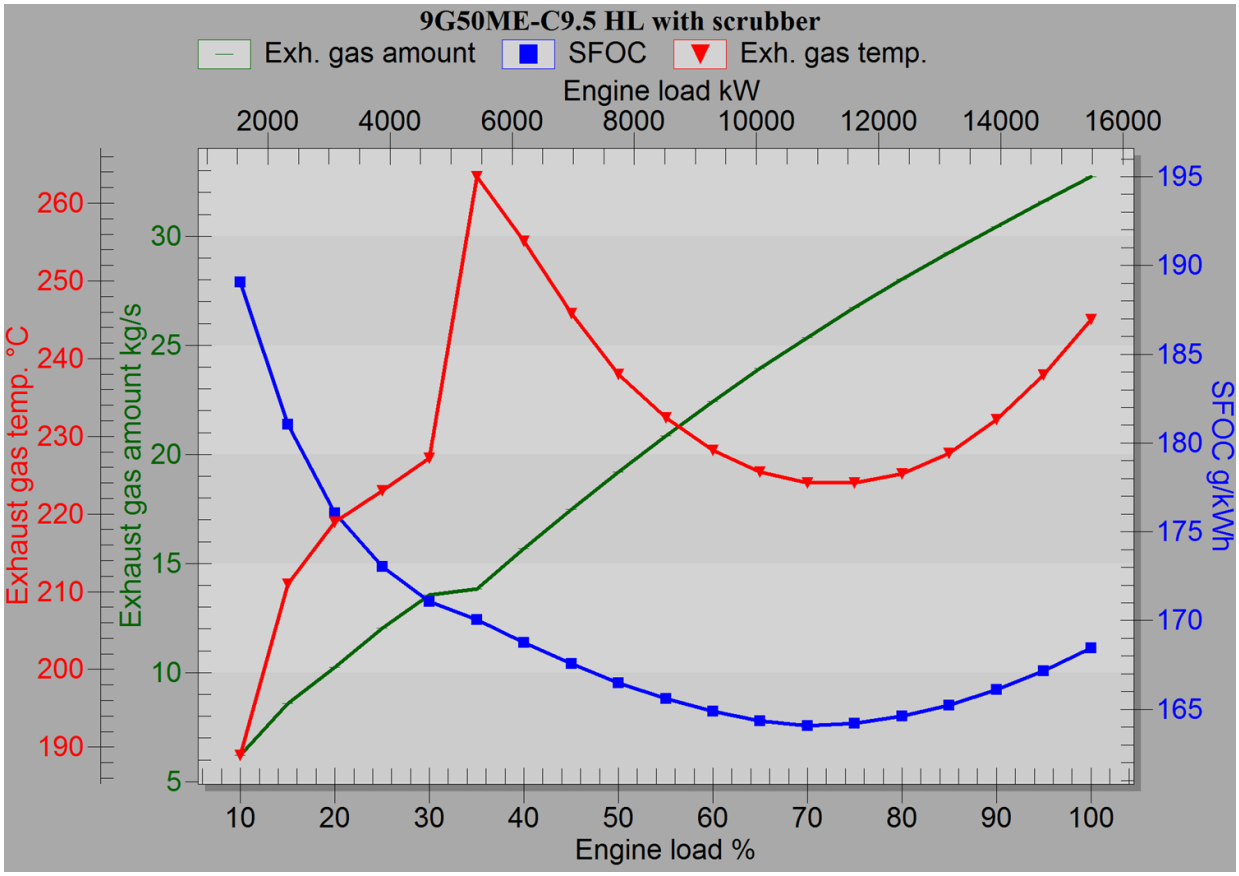


### ISO ambient conditions (ambient air: 25 °C, scavenge air coolant: 25 °C)

| Load<br>% SMCR | Power<br>kW | Speed<br>r/min | SFOC<br>g/kWh | Exh. gas<br>kg/s | Exh. gas*)<br>°C | Steam**)<br>kg/h |
|---|---|---|---|---|---|---|
| 100 | 15,480 | 100.0 | 168.5 | 32.7 | 245 | 2,930 |
| 95 | 14,706 | 98.3 | 167.2 | 31.6 | 238 | 2,590 |
| 90 | 13,932 | 96.5 | 166.1 | 30.4 | 232 | 2,310 |
| 85 | 13,158 | 94.7 | 165.2 | 29.3 | 228 | 2,090 |
| 80 | 12,384 | 92.8 | 164.6 | 28.0 | 225 | 1,930 |
| 75 | 11,610 | 90.9 | 164.2 | 26.7 | 224 | 1,820 |
| 70 | 10,836 | 88.8 | 164.1 | 25.4 | 224 | 1,750 |
| 65 | 10,062 | 86.6 | 164.3 | 23.9 | 225 | 1,710 |
| 60 | 9,288 | 84.3 | 164.9 | 22.4 | 228 | 1,700 |
| 55 | 8,514 | 81.9 | 165.6 | 20.9 | 232 | 1,720 |
| 50 | 7,740 | 79.4 | 166.5 | 19.2 | 238 | 1,750 |
| 45 | 6,966 | 76.6 | 167.6 | 17.5 | 246 | 1,800 |
| 40 | 6,192 | 73.7 | 168.7 | 15.7 | 255 | 1,840 |
| 35 | 5,418 | 70.5 | 170.1 | 13.8 | 263 | 1,810 |
| 30 | 4,644 | 66.9 | 171.1 | 13.6 | 227 | 1,100 |
| 25 | 3,870 | 63.0 | 173.1 | 12.0 | 223 | 910 |
| 20 | 3,096 | 58.5 | 176.1 | 10.2 | 219 | 710 |
| 15 | 2,322 | 53.1 | 181.1 | 8.6 | 211 | 460 |
| 10 | 1,548 | 46.4 | 189.1 | 6.2 | 189 | 0 |

# Fuel consumption and exhaust gas data
# Fuel Oil, Tier II mode

## Tropical ambient conditions (ambient air: 45 °C, scavenge air coolant: 36 °C)

| Load % SMCR | Power kW | Speed r/min | SFOC g/kWh | Exh. gas kg/s | Exh. gas*) °C | Steam**) kg/h |
|---|---|---|---|---|---|---|
| 100 | 15,480 | 100.0 | 170.2 | 30.3 | 278 | 3,910 |
| 95 | 14,706 | 98.3 | 168.9 | 29.3 | 271 | 3,570 |
| 90 | 13,932 | 96.5 | 167.9 | 28.2 | 265 | 3,270 |
| 85 | 13,158 | 94.7 | 167.0 | 27.1 | 260 | 3,020 |
| 80 | 12,384 | 92.8 | 166.4 | 26.0 | 257 | 2,840 |
| 75 | 11,610 | 90.9 | 166.0 | 24.8 | 256 | 2,690 |
| 70 | 10,836 | 88.8 | 165.8 | 23.5 | 256 | 2,590 |
| 65 | 10,062 | 86.6 | 166.1 | 22.2 | 257 | 2,510 |
| 60 | 9,288 | 84.3 | 166.6 | 20.8 | 260 | 2,460 |
| 55 | 8,514 | 81.9 | 167.4 | 19.3 | 265 | 2,430 |
| 50 | 7,740 | 79.4 | 168.3 | 17.8 | 271 | 2,420 |
| 45 | 6,966 | 76.6 | 169.3 | 16.2 | 279 | 2,420 |
| 40 | 6,192 | 73.7 | 170.5 | 14.5 | 289 | 2,410 |
| 35 | 5,418 | 70.5 | 171.9 | 12.8 | 298 | 2,320 |
| 30 | 4,644 | 66.9 | 172.9 | 12.5 | 259 | 1,600 |
| 25 | 3,870 | 63.0 | 174.9 | 11.1 | 255 | 1,370 |
| 20 | 3,096 | 58.5 | 177.9 | 9.5 | 251 | 1,120 |
| 15 | 2,322 | 53.1 | 183.0 | 7.9 | 242 | 830 |
| 10 | 1,548 | 46.4 | 191.1 | 5.8 | 219 | 0 |

## Specified ambient conditions (ambient air: 10 °C, scavenge air coolant: 10 °C)

| Load % SMCR | Power kW | Speed r/min | SFOC g/kWh | Exh. gas kg/s | Exh. gas*) °C | Steam**) kg/h |
|---|---|---|---|---|---|---|
| 100 | 15,480 | 100.0 | 166.4 | 34.0 | 220 | 2,020 |
| 95 | 14,706 | 98.3 | 165.2 | 32.9 | 213 | 1,710 |
| 90 | 13,932 | 96.5 | 164.1 | 31.7 | 207 | 1,460 |
| 85 | 13,158 | 94.7 | 163.3 | 30.4 | 203 | 1,260 |
| 80 | 12,384 | 92.8 | 162.7 | 29.2 | 201 | 1,130 |
| 75 | 11,610 | 90.9 | 162.3 | 27.8 | 200 | 1,050 |
| 70 | 10,836 | 88.8 | 162.1 | 26.4 | 199 | 1,010 |
| 65 | 10,062 | 86.6 | 162.4 | 24.9 | 201 | 1,000 |
| 60 | 9,288 | 84.3 | 162.9 | 23.3 | 203 | 1,030 |
| 55 | 8,514 | 81.9 | 163.6 | 21.7 | 207 | 1,080 |
| 50 | 7,740 | 79.4 | 164.5 | 20.0 | 213 | 1,150 |
| 45 | 6,966 | 76.6 | 165.5 | 18.2 | 220 | 1,240 |
| 40 | 6,192 | 73.7 | 166.7 | 16.3 | 229 | 1,330 |
| 35 | 5,418 | 70.5 | 168.0 | 14.4 | 237 | 1,350 |
| 30 | 4,644 | 66.9 | 169.0 | 14.1 | 202 | 630 |
| 25 | 3,870 | 63.0 | 171.0 | 12.5 | 198 | 470 |
| 20 | 3,096 | 58.5 | 173.9 | 10.6 | 195 | 300 |
| 15 | 2,322 | 53.1 | 178.9 | 8.9 | 187 | 0 |
| 10 | 1,548 | 46.4 | 186.8 | 6.5 | 166 | 0 |

Comments / details:
SFOC: Specific Fuel Oil Consumption (LCV: 42,700 kJ/kg)
Loads below 50% are associated with larger tolerances.

*) Mixed exhaust gas temperature after turbocharger.
**) Guiding steam production capacity at 7.0 bara with variable pinch point temperature, matched to 15°C at 85% load in Tier II and ISO. Contact boiler maker for actual steam production.

# Tables of cooler capacities - Tier II

| | | | | | |
|---|---|---|---|---|---|
| 1 | Engine load (% SMCR) | 4 | Scavenge air receiver temp. (°C) | 7 | Main lubrication oil heat (kW) |
| 2 | TC air consumption (kg/s) +/-5% | 5 | Scavenge air cooler heat (kW) | 8 | Condensed water (t/24h) |
| 3 | Scavenge air pressure (bara) | 6 | Jacket water cooler heat (kW) +0/-15% | | |

Loads below 50% are associated with larger tolerances.

| 1 | 2 | 3 | 4 | 5 | 6 | 7 | 8 |
|---|---|---|---|---|---|---|---|
| **ISO condition** | | Ambient air: 25.0 °C | | | Scavenge air coolant: 25.0 °C | | |
| 100 | 32.0 | 4.20 | 37 | 5,630 | 1,880 | 1,120 | 0.0 |
| 95 | 30.9 | 4.01 | 36 | 5,220 | 1,810 | 1,110 | 0.0 |
| 90 | 29.8 | 3.82 | 35 | 4,810 | 1,740 | 1,090 | 0.0 |
| 85 | 28.7 | 3.63 | 34 | 4,410 | 1,670 | 1,070 | 0.0 |
| 80 | 27.5 | 3.48 | 33 | 4,060 | 1,600 | 1,050 | 0.0 |
| 75 | 26.2 | 3.33 | 32 | 3,720 | 1,530 | 1,030 | 0.0 |
| 70 | 24.9 | 3.12 | 31 | 3,310 | 1,460 | 1,000 | 0.0 |
| 65 | 23.5 | 2.91 | 30 | 2,910 | 1,390 | 970 | 0.0 |
| 60 | 22.0 | 2.70 | 30 | 2,520 | 1,320 | 940 | 0.0 |
| 55 | 20.5 | 2.49 | 29 | 2,140 | 1,250 | 910 | 0.0 |
| 50 | 18.8 | 2.29 | 28 | 1,770 | 1,180 | 870 | 0.0 |
| 45 | 17.2 | 2.10 | 27 | 1,440 | 1,110 | 830 | 0.0 |
| 40 | 15.4 | 1.92 | 26 | 1,130 | 1,050 | 790 | 0.0 |
| 35 | 13.6 | 1.76 | 33 | 860 | 980 | 740 | 0.0 |
| 30 | 13.3 | 1.61 | 32 | 710 | 910 | 690 | 0.0 |
| 25 | 11.8 | 1.47 | 32 | 510 | 840 | 630 | 0.0 |
| **Tropical condition** | | Ambient air: 45.0 °C | | | Scavenge air coolant: 36.0 °C | | |
| 100 | 29.6 | 4.00 | 48 | 5,600 | 1,900 | 1,130 | 54.7 |
| 95 | 28.6 | 3.81 | 47 | 5,190 | 1,830 | 1,120 | 53.3 |
| 90 | 27.6 | 3.63 | 46 | 4,790 | 1,760 | 1,100 | 51.4 |
| 85 | 26.5 | 3.45 | 45 | 4,390 | 1,690 | 1,080 | 49.2 |
| 80 | 25.4 | 3.31 | 44 | 4,050 | 1,620 | 1,060 | 47.1 |
| 75 | 24.2 | 3.17 | 43 | 3,720 | 1,550 | 1,040 | 44.7 |
| 70 | 23.0 | 2.97 | 42 | 3,320 | 1,480 | 1,010 | 41.5 |
| 65 | 21.7 | 2.77 | 41 | 2,920 | 1,410 | 980 | 38.1 |
| 60 | 20.3 | 2.57 | 41 | 2,530 | 1,340 | 950 | 34.5 |
| 55 | 18.9 | 2.37 | 40 | 2,150 | 1,270 | 920 | 30.8 |
| 50 | 17.4 | 2.17 | 39 | 1,790 | 1,200 | 880 | 26.9 |
| 45 | 15.9 | 2.00 | 38 | 1,460 | 1,130 | 840 | 23.1 |
| 40 | 14.2 | 1.83 | 37 | 1,160 | 1,060 | 800 | 19.3 |
| 35 | 12.6 | 1.68 | 44 | 880 | 990 | 750 | 15.6 |
| 30 | 12.3 | 1.53 | 43 | 740 | 910 | 700 | 13.6 |
| 25 | 11.0 | 1.40 | 43 | 540 | 840 | 640 | 10.2 |
| **Specified condition** | | Ambient air: 10.0 °C | | | Scavenge air coolant: 10.0 °C | | |
| 100 | 33.3 | 4.28 | 22 | 5,650 | 1,860 | 1,110 | 3.8 |
| 95 | 32.2 | 4.08 | 21 | 5,230 | 1,790 | 1,100 | 3.8 |
| 90 | 31.0 | 3.89 | 20 | 4,830 | 1,720 | 1,080 | 3.7 |
| 85 | 29.8 | 3.69 | 19 | 4,430 | 1,650 | 1,060 | 3.6 |
| 80 | 28.6 | 3.54 | 18 | 4,080 | 1,580 | 1,040 | 3.4 |
| 75 | 27.3 | 3.40 | 17 | 3,740 | 1,520 | 1,020 | 3.3 |
| 70 | 25.9 | 3.18 | 16 | 3,340 | 1,450 | 990 | 2.9 |
| 65 | 24.4 | 2.97 | 15 | 2,940 | 1,380 | 960 | 2.5 |
| 60 | 22.9 | 2.75 | 15 | 2,540 | 1,310 | 930 | 2.1 |
| 55 | 21.3 | 2.54 | 14 | 2,160 | 1,240 | 900 | 1.7 |
| 50 | 19.6 | 2.33 | 13 | 1,790 | 1,170 | 860 | 1.3 |
| 45 | 17.9 | 2.14 | 12 | 1,460 | 1,100 | 820 | 0.9 |
| 40 | 16.0 | 1.96 | 11 | 1,160 | 1,030 | 780 | 0.5 |
| 35 | 14.1 | 1.79 | 18 | 880 | 960 | 730 | 0.2 |
| 30 | 13.9 | 1.64 | 17 | 730 | 890 | 680 | 0.0 |
| 25 | 12.3 | 1.50 | 17 | 530 | 830 | 620 | 0.0 |

—

# Typical noise and vibration levels

SMCR

| Octave band centre freq. in Hz | 31.5 | 63 | 125 | 250 | 500 | 1k | 2k | 4k | 8k | dB(lin) | dB(A) | Max |
|---|---|---|---|---|---|---|---|---|---|---|---|---|
| A) Exhaust gas noise | 125.8 | 120.5 | 112.7 | 107.6 | 106.2 | 102.4 | 91.4 | 81.4 | 72.8 | 127.2 | 107.4 | - |
| B) Spatial noise, standard NR | 98.4 | 97.1 | 98.1 | 97.5 | 97.6 | 98.9 | 99.9 | 95.0 | 86.8 | 107.1 | 104.6 | 109.8 |
| C) Spatial noise, additional NR | 98.4 | 96.4 | 95.6 | 95.9 | 95.7 | 97.0 | 97.9 | 90.3 | 83.0 | 105.4 | 102.3 | 106.6 |
| D) Structure borne vibrations | 78.2 | 76.3 | 73.5 | 71.4 | 69.6 | 63.9 | 57.8 | 49.6 | 42.9 | - | - | - |

NCR (90.00% of SMCR)

| Octave band centre freq. in Hz | 31.5 | 63 | 125 | 250 | 500 | 1k | 2k | 4k | 8k | dB(lin) | dB(A) | Max |
|---|---|---|---|---|---|---|---|---|---|---|---|---|
| A) Exhaust gas noise | 124.7 | 119.3 | 111.5 | 106.7 | 105.1 | 101.1 | 90.1 | 80.2 | 71.7 | 126.0 | 106.2 | - |
| B) Spatial noise, standard NR | 97.5 | 96.4 | 97.3 | 96.7 | 96.7 | 97.8 | 98.1 | 92.8 | 85.5 | 106.0 | 103.0 | 107.7 |
| C) Spatial noise, additional NR | 97.5 | 95.6 | 94.8 | 95.0 | 94.8 | 95.9 | 96.0 | 88.2 | 81.7 | 104.3 | 100.8 | 104.6 |
| D) Structure borne vibrations | 77.4 | 75.4 | 72.5 | 70.6 | 68.5 | 62.9 | 56.7 | 48.5 | 41.9 | - | - | - |

**A) Sound pressure levels from exhaust gas system ($2x10^{-5}$ Pa).**
The expected sound pressure level at 1 metre from the edge of the exhaust gas pipe opening at an angle of 30 degrees to the direction of the gas flow and valid for a normal exhaust gas system - but without a boiler and silencer.

**B) Airborne sound pressure levels - with standard noise reduction (NR) countermeasures ($2x10^{-5}$ Pa).**
Expected mean sound pressure octave spectrum levels, i.e. the average spatial noise values at a distance of 1 metre from the engine. Prescribed measuring surface area is 376.9 m².

**C) Air-borne sound pressure levels - with additional noise reduction (NR) countermeasures ($2x10^{-5}$ Pa).**
Expected mean sound pressure octave spectrum levels, i.e. the average spatial noise values at a distance of 1 metre from the engine. Prescribed measuring surface area is 376.9 m².

Additional noise reduction countermeasures, e.g.:
Extra good turbocharger air intake silencer(s)
External sound insulation of scavenge air receiver
External sound insulation of scavenge air cooler(s).

Supplementary reduction of 0.0 dB is needed.

Other additional noise reduction countermeasures are also available. The noise figures given are in accordance with the CIMAC recommendations for measurements of the overall noise for reciprocating engines. The average levels will, depending on the actual engine room configuration, be 1-5 dB higher when the engine is installed in the engine room.

**D) Structure borne vibration levels ($5x10^{-8}$ Pa).**
Expected mean velocity octave spectrum levels at the engine base plate as installed on board the ship. Based on an average engine foundation of a ship, and may only be used as a rough estimate as the velocity levels will depend on the actual foundation used. If the vibration velocity levels are referred to $10^{-9}$ m/s instead of $5x10^{-8}$ m/s, the calculated dB figures will be 34.0 dB higher than above stated.

## Reference data

| Ambient condition | Scavenge air coolant temp.*) °C | Ambient air temp. °C | Rel. air humidity % | Barometric pressure mbar |
|---|---|---|---|---|
| ISO**) | 25 | 25 | 30 | 1,000 |
| Tropical | 36 | 45 | 60 | 1,000 |
| Specified | 10 | 10 | 60 | 1,000 |

*) With a central cooling system, the sea water will be 4 °C lower than these temperatures.
**) Refers to ISO 3046-1 2002(E) and ISO 15550:2002(E).

| Tolerances | |
|---|---|
| Specific fuel consumption tolerance (SMCR) | +/- 5 % |
| Exhaust gas amount tolerance | +/- 5 % |
| Exhaust gas temperature tolerance | +/- 15 °C |

| Values for EEDI | |
|---|---|
| Engine type | 9G50ME-C9.5 HL with scrubber |
| SMCR power | 15,480 kW |
| SMCR RPM | 100.0 r/min |
| Ambient condition | ISO |
| Reference LCV of fuel oil | 42,700 kJ/kg |
| SFOC (SMCR) | 168.5 g/kWh |
| SFOC (75% of SMCR) | 164.2 g/kWh |
| **SFOC incl. 6% tolerance** | **174.1 g/kWh** |

| Report ID for Design Specification Order (DSO) |
|---|
| 7224f928-1bac-49f5-b883-df1b7ed09752 |

This ID must be used by an MAN-ES licensee when creating a DSO.

# Appendix B

# Bulk carrier data from MarineTraffic

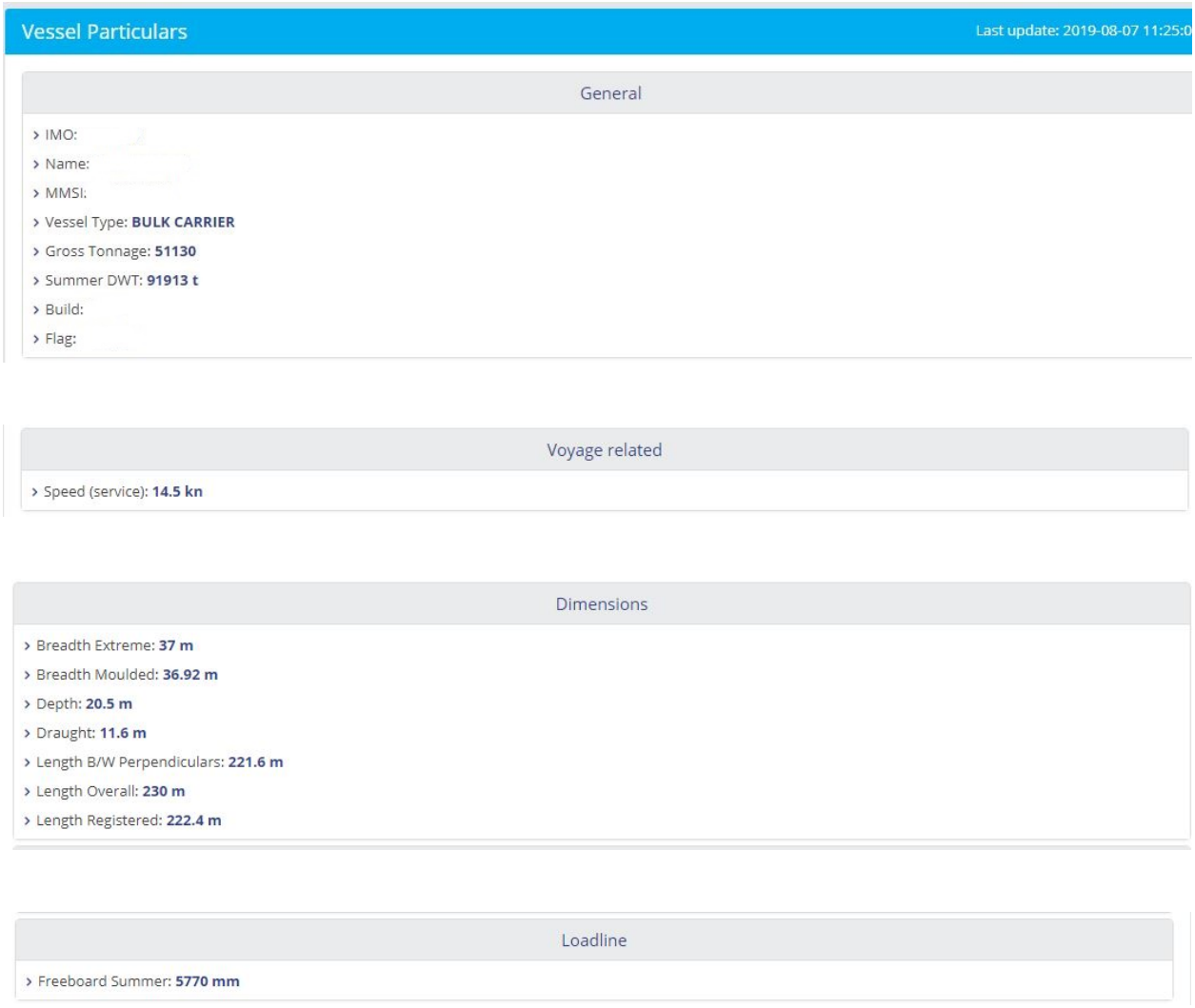

Vessel Particulars

Last update: 2019-08-07 11:25:0

General

- IMO:
- Name:
- MMSI:
- Vessel Type: **BULK CARRIER**
- Gross Tonnage: **51130**
- Summer DWT: **91913 t**
- Build:
- Flag:

Voyage related

- Speed (service): **14.5 kn**

Dimensions

- Breadth Extreme: **37 m**
- Breadth Moulded: **36.92 m**
- Depth: **20.5 m**
- Draught: **11.6 m**
- Length B/W Perpendiculars: **221.6 m**
- Length Overall: **230 m**
- Length Registered: **222.4 m**

Loadline

- Freeboard Summer: **5770 mm**

[H]


Tonnage/Capacity
Net Tonnage: 30678 t
Displacement - Lightship: 16108 t
Displacement Summer: 108021 t
Bale: 103631 m3
Grain: 109085 m3
Structure
Decks Number: 1
Hull Material: STEEL
Hull Type: SINGLE HULL

# Appendix C

# Matlab Code

## General

```
format compact

%-------------------------------------------------------------%
close all
clear variables
clc
%-------------------------------------------------------------%

%***
value=0; %value = 0 means open water, value = 1 means shallow water
for the calculation.
%***

if value == 0

    %Open water calculations are done at 100% SMCR load
    %Known data
    %-------------------------------------------------------%
    n = 51; %[rpm], rotational speed of engine
    Thrust = 478.055; %[kN], propeller thrust
    u = 0.5144*5.9; % [m/s], calculated from 15 knots

    %-------------------------------------------------------%

    %Calculations
    %-------------------------------------------------------%
    [KQ, J, Torque,etaprop, etahull, etarot, etaD]
        = OpenPropeller(u,n,Thrust);
    [PD, etashaft, PS] = ShaftLine(Torque,n);
```

```
    [etacarnot, etaind, etaeff, etatot, BSFC, mdotfuel, mfuel, bmep,
        Peff ] = OpenEngine(PS, etaD, etashaft, n, u, Torque);
    [CO2, mCO2, CO, mCO, CH4, mCH4, NOx, mNOx, PM, mPM, SO2, mSO2]
        =OpenEmissions(mdotfuel, mfuel);


    %-------------------------------------------------------%


elseif value ==1
    %Known data
    %-------------------------------------------------------%

    t = xlsread('C:“Users“jordy“Documents“Masterproef“MATLAB“KGT
        koutalianoscaptivetrackFSyesKOC.csv','A13:A6912'); % [s]
        time duration of the simulation
    u = xlsread('C:“Users“jordy“Documents“Masterproef“MATLAB“KGT
        koutalianoscaptivetrackFSyesKOC.csv','H13:H6912'); % [m/s]
        longitudinal speed of the vessel
    Thrust = xlsread('C:“Users“jordy“Documents“Masterproef“MATLAB“KGT
        koutalianoscaptivetrackFSyesKOC.csv','AV13:AV6912');
        % [ton] torque produced by the propeller in simulation
    n = xlsread('C:“Users“jordy“Documents“Masterproef“MATLAB“KGT
        koutalianoscaptivetrackFSyesKOC.csv','P13:P6912')*60;
    s = xlsread('C:“Users“jordy“Documents“Masterproef“MATLAB“KGT
        koutalianoscaptivetrackFSyesKOC.csv','B13:B6912');
    s = (s-2201.8)/1000;


    %-------------------------------------------------------%

    %Calculations
    %-------------------------------------------------------%

    [KQ, J, Torque, etaprop, etahull, etarot, etaD]
        = ShallowPropeller(u,n,Thrust);
    [PD, etashaft, PS] = ShaftLine(Torque,n);
    [etacarnot, etaind, etaeff, etatot, BSFC, Load, mdotfuel, mfuel,
         bmep, Peff ] = ShallowEngine(PS, etaD, etashaft, n, t, Torque);
    [CO2, mCO2, CO, mCO, CH4, mCH4, NOx, mNOx, PM, mPM, SO2, mSO2]
        = ShallowEmissions(mdotfuel, mfuel);

    %-------------------------------------------------------%
```

```
else
    fprintf('wrong entry')
end
```

## Deep Water

### Propeller

```
function [KQ, J, Torque, etaprop, etahull, etarot, etaD]
        = OpenPropeller(longspeed,propspeed,thrust)

%KT-KQ diagrams are from a B4-70 Wageningen Series

%DATA
%-------------------------------------------------------------%
CB = 0.8407; % [-], Block coefficient
rho = 1025; %[kg/m3], sea water during ocean travel
D = 8; % [m], propeller diameter
wake = 0.5*CB-0.05; % [-] wake fraction, Taylor's formula
thr = 0.23*CB+0.05; % [-] thrust deduction factor, Taylor's formula
advspeed = longspeed*(1-wake);
etaprop = 0; % [-], propeller efficiency
etahull = (1-thr)/(1-wake); % [-], hull efficiency
etarot = 1; % [-], rotative efficiency
%-------------------------------------------------------------%

%Calculations
%-------------------------------------------------------------%

J = advspeed/(propspeed/60*D);
KT = 0.1576;
if J¡0
    fprintf('Error, J smaller than 0')
elseif J¿=0 && J¡0.025
    KQ = 0.025 + (0.02425-0.025)/(0.025-0)*(J-0);
elseif J¿=0.025 && J¡0.05
    KQ = 0.02425 + (0.0235-0.02425)/(0.025)*(J-0.025);
elseif J¿=0.05 && J¡0.075
    KQ = 0.0235 + (0.023-0.0235)/(0.025)*(J-0.05);
elseif J¿=0.075 && J¡0.1
    KQ = 0.023 + (0.0225-0.0235)/(0.025)*(J-0.075);
elseif J¿=0.1 && J¡0.125
    KQ = 0.0225 + (0.022-0.0225)/(0.025)*(J-0.1);
```

```
elseif J¿=0.125 && J¡0.15
    KQ = 0.022 + (0.0215-0.022)/(0.025)*(J-0.125);
elseif J¿=0.15 && J¡0.175
    KQ = 0.0215 + (0.02075-0.0215)/(0.025)*(J-0.15);
elseif J¿=0.175 && J¡0.2
    KQ = 0.02075 + (0.02-0.02075)/(0.025)*(J-0.175);
elseif J¿=0.2 && J¡0.225
    KQ = 0.02 + (0.01925-0.02)/(0.025)*(J-0.2);
elseif J¿=0.225 && J¡0.25
    KQ = 0.01925 + (0.0185-0.01925)/(0.025)*(J-0.225);
elseif J¿=0.25 && J¡0.275
    KQ = 0.01925 + (0.01775-0.01925)/(0.025)*(J-0.25);
elseif J¿=0.275 && J¡0.3
    KQ = 0.01775 + (0.017-0.01775)/(0.025)*(J-0.275);
elseif J¿=0.3 && J¡0.325
    KQ = 0.017 + (0.01625-0.017)/(0.025)*(J-0.3);
elseif J¿=0.325 && J¡0.35
    KQ = 0.01625 + (0.0155-0.01625)/(0.025)*(J-0.325);
elseif J¿=0.35 && J¡0.375
    KQ = 0.0155 + (0.01475-0.0155)/(0.025)*(J-0.35);
elseif J¿=0.375 && J¡0.4
    KQ = 0.01475 + (0.014-0.01475)/(0.025)*(J-0.375);
elseif J¿=0.4 && J¡0.425
    KQ = 0.014 + (0.013-0.014)/(0.025)*(J-0.4);
elseif J¿=0.425 && J¡0.45
    KQ = 0.013 + (0.012-0.013)/(0.025)*(J-0.425);
elseif J¿=0.45 && J¡0.475
    KQ = 0.012 + (0.011-0.012)/(0.025)*(J-0.45);
elseif J¿=0.475 && J¡0.5
    KQ = 0.011 + (0.01-0.011)/(0.025)*(J-0.475);
elseif J¿=0.5 && J¡0.525
    KQ = 0.01 + (0.00925-0.01)/(0.025)*(J-0.5);
elseif J¿=0.525 && J¡0.55
    KQ = 0.00925 + (0.0085-0.00925)/(0.025)*(J-0.525);
elseif J¿=0.55 && J¡0.575
    KQ = 0.0085 + (0.0075-0.0085)/(0.025)*(J-0.55);
elseif J¿=0.575 && J¡0.6
    KQ = 0.0075 + (0.0065-0.0075)/(0.025)*(J-0.575);
elseif J¿=0.6 && J¡0.625
    KQ = 0.0065 + (0.00575-0.0065)/(0.025)*(J-0.6);
elseif J¿=0.625 && J¡0.65
    KQ = 0.00575 + (0.005-0.00575)/(0.025)*(J-0.625);
elseif J¿=0.65 && J¡0.675
```

```
    KQ = 0.005 + (0-0.005)/(0.025)*(J-0.65);
else
    fprintf('Wrong Entry, J larger than limit')
end
etaprop=KT/KQ*J/2/pi
Torque = KQ*(rho*(propspeed/60).2*D5)/1000; %[kNm]
etaD = etaprop*etahull*etarot; % [-] propulsive efficiency
%--------------------------------------------------------------%
end
```

**Shaft line**

```
function [PD, etashaft, PS] = ShaftLine(Torque, propspeed)


%The Shaft Line part stays the same in open as in shallow water

%DATA
%--------------------------------------------------------------%
etagbox = 1; %no gearbox, direct drive
etabearings = 0.99; % 1% loss due to bearings
etalength = 0.99; % 1% loss due to shaft length
%--------------------------------------------------------------%

%Calculations
%--------------------------------------------------------------%
etashaft = etagbox*etabearings*etalength; % shaft efficiency
PD = Torque*2*pi.*propspeed/60;  % [kW] Delivered power at propeller
PS = PD/etashaft;  % [kW] Service Power
%--------------------------------------------------------------%

end
```

**Engine**

```
function [etacarnot, etaind, etaeff, etatot, BSFC, mdotfuel, mfuel,
        bmep, Peff ] = OpenEngine(PS, etaD, etashaft, n, u, Torque)

%DATA
%--------------------------------------------------------------%
D = 0.5; % [m] bore diameter
s = 2.5; % [m] stroke
chi = 1; % [-] 2 stroke engine
nc = 9; % [-] number of cylinders
```

```
TC = 298; % [K] cold T for Carnot
TH = 1500; % [K] hot T for Carnot
etam = 0.85; % [-] mechanical efficiency
l = 16541.7; % [m] length of the trajectory on canal GT
t = l/u % [s] time spend travelling same distance
%-------------------------------------------------------------%

%Fuel Type
%-------------------------------------------------------------%
f = 0; % fuel type: MDO = 0, HFO = 1
if f==0
     LHV = 42.7; % [MJ/kg] lower heating value
elseif f==1
     LHV = 40.2; % [MJ/kg] lower heating value
else
    fprintf('Wrong fuel type entry');
end
%-------------------------------------------------------------%

%Calculations
%-------------------------------------------------------------%
Vs = D2*pi/4*s; % [m³] swept volume
Peff = PS; % [kW] total engine brake power
bmep = 2*pi*Torque/(chi*nc*Vs);% [kPa] brake mean effective pressure,
        L1 of 21 bar according to engine file
Weff = bmep*Vs*nc % [kJ] work available at crankshaft
etacarnot = 1-TC/TH; % Carnot efficiency
BSFC = 183.6075; % [g/kWh] brake specific fuel consumption

mdotfuel=BSFC*Peff/3600; %[g/s]
mfuel = mdotfuel*t; %[g]
etaeff = Weff/(mdotfuel/(n/60)*LHV); % effective efficiency
etaind = etaeff/etam; % indicative efficiency
etatot = etaD*etashaft*etaeff; % total efficiency drivetrain
%-------------------------------------------------------------%


end
```

**Emissions**

```
function [CO2, mCO2, CO, mCO, CH4, mCH4, NOx, mNOx, PM, mPM, SO2, mSO2]
        = OpenEmissions(mdotfuel, mfuel)
%DATA
```

```
%-------------------------------------------------------------%
f=0;

if f==0
FCO2=3.206; %[kg CO2/kg fuel]
FCO = 0.00277;
FCH4 = 0.00006;
FNOx = 0.0961;
FPM = 0.00097;
FSO2 = 0.01;

elseif f==1
FCO2=3.114; %[kg CO2/kg fuel]
FCO = 0.00277;
FCH4 = 0.00006;
FNOx = 0.0903;
FPM = 0.00728;
FSO2 = 0.025;
else
    fprintf('Wrong fuel type entry');
end

%-------------------------------------------------------------%

%Calculations
%-------------------------------------------------------------%
CO2 = mdotfuel*FCO2;
mCO2 = mfuel * FCO2;
CO=mdotfuel*FCO;
mCO=mfuel*FCO;
CH4=mdotfuel*FCH4;
mCH4=mfuel*FCH4;
NOx=mdotfuel*FNOx;
mNOx=mfuel*FNOx;
PM=mdotfuel*FPM;
mPM=mfuel*FPM;
SO2=mdotfuel*FSO2;
mSO2=mfuel*FSO2;
%-------------------------------------------------------------%


end
```

## Confined Water

### Propeller

```
function [KQ, J, Torque,etaprop, etahull, etarot, etaD]
        = ShallowPropeller(longspeed,propspeed,thrust)

%KT-KQ diagrams are from a B4-70 Wageningen Series
%DATA
%-----------------------------------------------------------%
rho = 1000; %[kg/m3], fresh water in canal GT
D = 8; % [m], propeller diameter
CB=0.864; % [-] block coefficient
wake0 = 0.5*CB-0.05; % [-] wake fraction in open water, Taylor's formula
T = xlsread('C:"Users"jordy"Documents"Masterproef"MATLAB"KGTkoutalianos
        captivetrackFSyesKOC.csv','AG13:AG6912'); % [m] draft
h = xlsread('C:"Users"jordy"Documents"Masterproef"MATLAB"KGTkoutalianos
        captivetrackFSyesKOC.csv','EJ13:EJ6912'); % [m] water depth
a = 6.6-7.0*CB; % [-] factor for wake fraction calculation
b = 5.4*CB-2.2; % [-] factor for wake fraction calculation
wake = wake0*(1+a.*(T./h-0.2).b); % [-] Wake fraction in shallow water
thr = 0.6*wake; % [-] Thrust deduction factor in shallow water
advspeed = longspeed.*(1-wake); % [m/s] advance speed
etahull = (1-thr)./(1-wake); % [-], hull efficiency
etarot = 1; % [-], rotative efficiency
%-----------------------------------------------------------%

%Calculations
%-----------------------------------------------------------%
KT = thrust*1000*9.81./(rho*(propspeed/60).2*D4);
J = advspeed./(propspeed/60*D);
for i = 1:length(J)
   if J(i)¡0
    fprintf('Error, J smaller than 0')
    elseif J(i)¿=0 && J(i)¡0.025
        KQ(i) = 0.025 + (0.02425-0.025)/(0.025-0)*(J(i)-0);
    elseif J(i)¿=0.025 && J(i)¡0.05
        KQ(i) = 0.02425 + (0.0235-0.02425)/(0.025)*(J(i)-0.025);
    elseif J(i)¿=0.05 && J(i)¡0.075
        KQ(i) = 0.0235 + (0.023-0.0235)/(0.025)*(J(i)-0.05);
    elseif J(i)¿=0.075 && J(i)¡0.1
        KQ(i) = 0.023 + (0.0225-0.0235)/(0.025)*(J(i)-0.075);
    elseif J(i)¿=0.1 && J(i)¡0.125
        KQ(i) = 0.0225 + (0.022-0.0225)/(0.025)*(J(i)-0.1);
```

```
elseif J(i)¿=0.125 && J(i)¡0.15
    KQ(i) = 0.022 + (0.0215-0.022)/(0.025)*(J(i)-0.125);
elseif J(i)¿=0.15 && J(i)¡0.175
    KQ(i) = 0.0215 + (0.02075-0.0215)/(0.025)*(J(i)-0.15);
elseif J(i)¿=0.175 && J(i)¡0.2
    KQ(i) = 0.02075 + (0.02-0.02075)/(0.025)*(J(i)-0.175);
elseif J(i)¿=0.2 && J(i)¡0.225
    KQ(i) = 0.02 + (0.01925-0.02)/(0.025)*(J(i)-0.2);
elseif J(i)¿=0.225 && J(i)¡0.25
    KQ(i) = 0.01925 + (0.0185-0.01925)/(0.025)*(J(i)-0.225);
elseif J(i)¿=0.25 && J(i)¡0.275
    KQ(i) = 0.01925 + (0.01775-0.01925)/(0.025)*(J(i)-0.25);
elseif J(i)¿=0.275 && J(i)¡0.3
    KQ(i) = 0.01775 + (0.017-0.01775)/(0.025)*(J(i)-0.275);
elseif J(i)¿=0.3 && J(i)¡0.325
    KQ(i) = 0.017 + (0.01625-0.017)/(0.025)*(J(i)-0.3);
elseif J(i)¿=0.325 && J(i)¡0.35
    KQ(i) = 0.01625 + (0.0155-0.01625)/(0.025)*(J(i)-0.325);
elseif J(i)¿=0.35 && J(i)¡0.375
    KQ(i) = 0.0155 + (0.01475-0.0155)/(0.025)*(J(i)-0.35);
elseif J(i)¿=0.375 && J(i)¡0.4
    KQ(i) = 0.01475 + (0.014-0.01475)/(0.025)*(J(i)-0.375);
elseif J(i)¿=0.4 && J(i)¡0.425
    KQ(i) = 0.014 + (0.013-0.014)/(0.025)*(J(i)-0.4);
elseif J(i)¿=0.425 && J(i)¡0.45
    KQ(i) = 0.013 + (0.012-0.013)/(0.025)*(J(i)-0.425);
elseif J(i)¿=0.45 && J(i)¡0.475
    KQ(i) = 0.012 + (0.011-0.012)/(0.025)*(J(i)-0.45);
elseif J(i)¿=0.475 && J(i)¡0.5
    KQ(i) = 0.011 + (0.01-0.011)/(0.025)*(J(i)-0.475);
elseif J(i)¿=0.5 && J(i)¡0.525
    KQ(i) = 0.01 + (0.00925-0.01)/(0.025)*(J(i)-0.5);
elseif J(i)¿=0.525 && J(i)¡0.55
    KQ(i) = 0.00925 + (0.0085-0.00925)/(0.025)*(J(i)-0.525);
elseif J(i)¿=0.55 && J(i)¡0.575
    KQ(i) = 0.0085 + (0.0075-0.0085)/(0.025)*(J(i)-0.55);
elseif J(i)¿=0.575 && J(i)¡0.6
    KQ(i) = 0.0075 + (0.0065-0.0075)/(0.025)*(J(i)-0.575);
elseif J(i)¿=0.6 && J(i)¡0.625
    KQ(i) = 0.0065 + (0.00575-0.0065)/(0.025)*(J(i)-0.6);
elseif J(i)¿=0.625 && J(i)¡0.65
    KQ(i) = 0.00575 + (0.005-0.00575)/(0.025)*(J(i)-0.625);
elseif J(i)¿=0.65 && J(i)¡0.675
```

```
        KQ(i) = 0.005 + (0-0.005)/(0.025)*(J(i)-0.65);
    else
        fprintf('Wrong Entry, J larger than limit')
    end
end
KQ=KQ';
Torque = KQ.*(rho*(propspeed/60).2*D5)/1000; %[kNm]
etaprop = KT.*J./(KQ*2*pi);
etaD = etaprop.*etahull.*etarot; % [-] propulsive efficiency
%--------------------------------------------------------%

end
```

**Shaft line**

```
function [PD, etashaft, PS] = ShaftLine(Torque, propspeed)


%The Shaft Line part stays the same in open as in shallow water

%DATA
%--------------------------------------------------------------------%
etagbox = 1; %no gearbox, direct drive
etabearings = 0.99; % 1% loss due to bearings
etalength = 0.99; % 1% loss due to shaft length
%--------------------------------------------------------------------%

%Calculations
%--------------------------------------------------------------------%
etashaft = etagbox*etabearings*etalength; % shaft efficiency
PD = Torque*2*pi.*propspeed/60;  % [kW] Delivered power at propeller
PS = PD/etashaft;  % [kW] Service Power
%--------------------------------------------------------------------%

end
```

**Engine**

```
function [etacarnot, etaind, etaeff, etatot, BSFC, Load, mdotfuel, mfuel,
        bmep, Peff ] = ShallowEngine(PS, etaD, etashaft, n, t, Torque )

%DATA
%--------------------------------------------------------------------%
D = 0.5; % [m] bore diameter
```

```
s = 2.5; % [m] stroke
chi = 1; % [-] 2 stroke engine
nc = 9; % [-] number of cylinders
TC = 298; % **Temporary Value** [K] cold T for Carnot
TH = 1500; % **Temporary Value** [K] hot T for Carnot
etam = 0.85; % [-] mechanical efficiency
%--------------------------------------------------------------------%

%Fuel Type
%--------------------------------------------------------------------%
f = 0; % fuel type: MDO = 0, HFO = 1
if f==0
     LHV = 42.7; % [MJ/kg] lower heating value
elseif f==1
     LHV = 40.2; % [MJ/kg] lower heating value
else
    fprintf('Wrong fuel type entry');
end
%--------------------------------------------------------------------%

%Calculations
%--------------------------------------------------------------------%
Vs = D2*pi/4*s; % [m³] swept volume
Peff = PS; % [kW] total engine brake power
bmep = 2*pi*Torque./(chi*Vs*nc); % [kPa] brake mean effective pressure
Weff = bmep*Vs*nc; % [kJ] work available at crankshaft

for i=1:length(n) %BSFC, in g/kWh
    if n(i)¿100
        fprintf('wrong propeller rpm')
    elseif n(i)¡=100 && n(i)¿98.3
        BSFC(i) = 168.5 + (167.2-168.5)/(98.3-100)*(n(i)-100);
    elseif n(i)¡=98.3 && n(i)¿96.5
        BSFC(i) = 167.2 + (166.1-167.2)/(96.5-98.3)*(n(i)-98.3);
    elseif n(i)¡=96.5 && n(i)¿94.7
        BSFC(i) = 166.1 + (165.2-166.1)/(94.7-96.5)*(n(i)-96.5);
    elseif n(i)¡=94.7 && n(i)¿92.8
        BSFC(i) = 165.2 + (164.6-165.2)/(92.8-94.7)*(n(i)-94.7);
    elseif n(i)¡=92.8 && n(i)¿90.9
        BSFC(i) = 164.6 + (164.2-164.6)/(90.9-92.8)*(n(i)-92.8);
    elseif n(i)¡=90.9 && n(i)¿88.8
        BSFC(i) = 164.2 + (164.1-164.2)/(88.8-90.9)*(n(i)-90.9);
    elseif n(i)¡=88.8 && n(i)¿86.6
```

```
        BSFC(i) = 164.1 + (164.3-164.1)/(86.6-88.8)*(n(i)-88.8);
    elseif n(i)¡=86.6 && n(i)¿84.3
        BSFC(i) = 164.3 + (164.9-164.3)/(84.3-86.6)*(n(i)-86.6);
    elseif n(i)¡=84.3 && n(i)¿81.9
        BSFC(i) = 164.9 + (165.6-164.9)/(81.9-84.3)*(n(i)-84.3);
    elseif n(i)¡=81.9 && n(i)¿79.4
        BSFC(i) = 165.6 + (166.5-165.6)/(79.4-81.9)*(n(i)-81.9);
    elseif n(i)¡=79.4 && n(i)¿76.6
        BSFC(i) = 166.5 + (167.6-166.5)/(76.6-79.4)*(n(i)-79.4);
    elseif n(i)¡=76.6 && n(i)¿73.7
        BSFC(i) = 167.6 + (168.7-167.6)/(73.7-76.6)*(n(i)-76.6);
    elseif n(i)¡=73.7 && n(i)¿70.5
        BSFC(i) = 168.7 + (170.1-168.7)/(70.5-73.7)*(n(i)-73.7);
    elseif n(i)¡=70.5 && n(i)¿66.9
        BSFC(i) = 170.1 + (171.1-170.1)/(66.9-70.5)*(n(i)-70.5);
    elseif n(i)¡=66.9 && n(i)¿63
        BSFC(i) = 171.1 + (173.1-171.1)/(63-66.9)*(n(i)-66.9);
    elseif n(i)¡=63 && n(i)¿58.5
        BSFC(i) = 173.1 + (176.1-173.1)/(58.5-63)*(n(i)-63);
    elseif n(i)¡=58.5 && n(i)¿53.1
        BSFC(i) = 176.1 + (181.1-176.1)/(53.1-58.5)*(n(i)-58.5);
   elseif n(i)¡=53.1 && n(i)¿46.4
        BSFC(i) = 181.1 + (189.1-181.1)/(46.4-53.1)*(n(i)-53.1);
    elseif n(i)¡=46.4 && n(i)¿46.3
        BSFC(i) = 189.1;
    else
        fprintf('wrong propeller rpm')
    end
end

for i=1:length(n)
    if n(i)¿100
        fprintf('wrong propeller rpm')
    elseif n(i)¡=100 && n(i)¿98.3
        Load(i) = 100+(95-100)/(98.3-100)*(n(i)-100);
    elseif n(i)¡=98.3 && n(i)¿96.5
        Load(i) = 95+(90-95)/(96.5-98.3)*(n(i)-98.3);
    elseif n(i)¡=96.5 && n(i)¿94.7
        Load(i) = 90+(85-90)/(94.7-96.5)*(n(i)-96.5);
    elseif n(i)¡=94.7 && n(i)¿92.8
        Load(i) =85+(80-85)/(92.8-94.7)*(n(i)-94.7);
    elseif n(i)¡=92.8 && n(i)¿90.9
        Load(i) = 80+(75-80)/(90.9-92.8)*(n(i)-92.8);
```

```
    elseif n(i)¡=90.9 && n(i)¿88.8
        Load(i) = 75+(70-75)/(88.8-90.9)*(n(i)-90.9);
    elseif n(i)¡=88.8 && n(i)¿86.6
        Load(i) = 70+(65-70)/(86.6-88.8)*(n(i)-88.8);
    elseif n(i)¡=86.6 && n(i)¿84.3
        Load(i) = 65+(60-65)/(84.3-86.6)*(n(i)-86.6);
    elseif n(i)¡=84.3 && n(i)¿81.9
        Load(i) = 60+(55-60)/(81.9-84.3)*(n(i)-84.3);
    elseif n(i)¡=81.9 && n(i)¿79.4
        Load(i) = 55+(50-55)/(79.4-81.9)*(n(i)-81.9);
    elseif n(i)¡=79.4 && n(i)¿76.6
        Load(i) = 50+(45-50)/(76.6-79.4)*(n(i)-79.4);
    elseif n(i)¡=76.6 && n(i)¿73.7
        Load(i) = 45+(40-45)/(73.7-76.6)*(n(i)-76.6);
    elseif n(i)¡=73.7 && n(i)¿70.5
        Load(i) = 40+(35-40)/(70.5-73.7)*(n(i)-73.7);
    elseif n(i)¡=70.5 && n(i)¿66.9
        Load(i) = 35+(30-35)/(66.9-70.5)*(n(i)-70.5);
    elseif n(i)¡=66.9 && n(i)¿63
        Load(i) = 30+(25-30)/(63-66.9)*(n(i)-66.9);
    elseif n(i)¡=63 && n(i)¿58.5
        Load(i) = 25+(20-25)/(58.5-63)*(n(i)-63);
    elseif n(i)¡=58.5 && n(i)¿55.8
        Load(i) = 20+(17.5-20)/(55.8-58.5)*(n(i)-58.5);
    elseif n(i)¡=55.8 && n(i)¿53.1
        Load(i) = 17.5+(15-17.5)/(53.1-55.8)*(n(i)-55.8);
    elseif n(i)¡=53.1 && n(i)¿49.75
        Load(i) = 15+(12.5-15)/(49.75-53.1)*(n(i)-53.1);
    elseif n(i)¡=49.75 && n(i)¿46.4
        Load(i) = 12.5+(10-12.5)/(46.4-49.75)*(n(i)-49.75);
    elseif n(i)¡=46.4 && n(i)¿46.3
        Load(i) = 100;
    else
        fprintf('wrong propeller rpm')
    end
end %Load, in %SMCR

BSFC=BSFC'; % [g/kWh]
Load=Load'; % [%SMCR]
mdotfuel=BSFC.*Peff/3600; % [g/s]
mfuel = trapz(t, mdotfuel); % [g]
etacarnot = 1-TC./TH; % Carnot efficiencyùml
etaeff = Weff./(mdotfuel./(n/60)*LHV); % effective efficiency
```

```
etaind = etaeff/etam; % indicative efficiency
etatot = etaD.*etashaft.*etaeff; % total efficiency drivetrain
%-------------------------------------------------------------%


end
```

**Emissions**

```
function [CO2, mCO2, CO, mCO, CH4, mCH4, NOx, mNOx, PM, mPM, SO2, mSO2]
        = ShallowEmissions(mdotfuel, mfuel)
%DATA
%-------------------------------------------------------------%
f=0;

if f==0
FCO2=3.206; %[kg CO2/kg fuel]
FCO = 0.00277;
FCH4 = 0.00006;
FNOx = 0.0961;
FPM = 0.00097;
FSO2 = 0.01;

elseif f==1
FCO2=3.114; %[kg CO2/kg fuel]
FCO = 0.00277;
FCH4 = 0.00006;
FNOx = 0.0903;
FPM = 0.00728;
FSO2 = 0.025;
else
    fprintf('Wrong fuel type entry');
end

adjCO2 = 1.125;
adjCO = 1.465;
adjHC = 1.535;
adjNOx = 1.095;
adjSO2 = 1.125;
adjPM = 1.17;

%-------------------------------------------------------------%

%Calculations
```

```
%-------------------------------------------------------------%
CO2 = mdotfuel*FCO2*adjCO2;
mCO2 = mfuel * FCO2*adjCO2;
CO=mdotfuel*FCO*adjCO;
mCO=mfuel*FCO*adjCO;
CH4=mdotfuel*FCH4*adjHC;
mCH4=mfuel*FCH4*adjHC;
NOx=mdotfuel*FNOx*adjNOx;
mNOx=mfuel*FNOx*adjNOx;
PM=mdotfuel*FPM*adjPM;
mPM=mfuel*FPM*adjPM;
SO2=mdotfuel*FSO2*adjSO2;
mSO2=mfuel*FSO2*adjSO2;
%-------------------------------------------------------------%


end
```

FACULTY OF ENGINEERING AND ARCHITECTURE

# Air pollution by ships in close proximity to dense populated areas

Jordy Delvaeye
Student number: 01503307

Supervisors: Prof. dr. ir. Evert Lataire, Dr. ir. Manasés Tello Ruiz

Master's dissertation submitted in order to obtain the academic degree of
Master of Science in Electromechanical Engineering

Academic year 2019-2020

GHENT UNIVERSITY